Optical Fibre Measurement for Clock Tones in Telescope Networks

By

Phumla P. Dlamini

Thesis presented in partial fulfillment of the requirements for the degree of

MAGISTER SCIENTIAE

in the Faculty of Science at the Nelson Mandela Metropolitan University

April 2017

Supervisor: Professor T.B. Gibbon
Co-supervisor: Doctor R.R.G. Gamatham
Co-supervisor: Professor A.W.R Leitch

To my aunt, Ntozakhe Beauty Mkhize

ACKNOWLEDGEMENTS

My sincere thanks and gratitude is extended to:
My supervisor, Professor Timothy Gibbon, and co-supervisors, Doctor Romeo Gamatham and Professor Andrew Leitch for their support and guidance throughout this study.
The Nelson Mandela Metropolitan University Centre for Broadband Communication research partners and project funders:
African Laser Centre (ALC)
CISCO
Department of Science and Technology (DST)
Dartcom
Telkom South Africa
INGOMA communication services
South African National Research Foundation (NRF)
Technology and Human Resources for Industry Programme (THRIP)
CSIR National Laser Centre
National Metrology Institution of South Africa (NMISA)

The Square Kilometre Array (SKA), and the Nelson Mandela Metropolitan University for the financial assistance.

Finally, a special thanks to my family and friends for the continuous support and encouragement.

ABBREVIATION LIST

APD	Avalanche Photodiode
CD	Chromatic Dispersion
DFB	Distributed Feedback Laser
DGD	Differential Group Delay
DOP	Degree Of Polarization
EDFA	Erbium Doped Fibre Amplifier
ESA	Electrical Spectrum Analyzer
FFT	Fast Fourier Transform
LNA	Low Noise Amplifier
LO	Local Oscillator
NZDSF	Non-Zero Dispersion Shifted Fibre
PIN	Positive Intrinsic Negative Photodiode
PLL	Phase Lock Loop
PMD	Polarization Mode Dispersion
RF	Radio Frequency
RMS	Root Mean Square
SSB	Single Sideband
TEC	Temperature Controller
VCO	Voltage Controlled Oscillator
VCSEL	Vertical Cavity Surface Emitting Laser
WDM	Wavelength Division Multiplexing
ZDSF	Zero Dispersion Shifted Fibre

TABLE OF CONTENTS

Chapter 1

Introduction

Astronomy dates back to the early man's impression of the heavens with little information recorded including some drawings of comets, eclipse and supernovas[1]. Major progress has been made in the field of Astronomy since then. Scientific curiosity to probe the universe in attempt to answer questions such as the origin of the universe, the matter it is made of, the formation of stars, planets and galaxies, and tracking life in other solar systems has brought about the need for more advanced tools capable of detailed observations. In 1608 H. Lippershey developed the first refracting telescope[2], [3]. A year later Galileo used a similar telescope pointing skywards discovering mountains and craters on the earth's moon, the moons of Jupiter and the phases of Venus. Over the years telescopes have been developed with advancements from the optical telescope towards much larger and more sensitive radio telescopes. The first radio signal from space was detected by Karl Jansky and ever since then astronomers have been using radio telescopes to explore the universe by detecting radio waves emitted by cosmic objects[4]. The ability of radio telescopes to detect weak signals is related to the signal capture surface.

As the demand for sensitivity, transmission bandwidth and data rate increases, so does the need for telescopes with a large field of view and capability to observe different parts of the sky at once[5]. This is possible with radio telescope array, with the data from the antennas combined electronically to produce a high resolution image of the sky. The South African MeerKAT radio telescope is an array of 64 interlinked antennas each transmitting up to 160 Gbps of data to the central processing site over optical fibre which is ideal for carrying large volumes of data at high speeds. The MeerKAT telescope is a precursor to the Square kilometer Array which will have up to 50 times the sensitivity and 10000 times the survey speed than the best telescope[6]. The MeerKAT and SKA

telescope rely on the distribution of a highly stable RF clock signal from the central processing site to the remote antennas to drive a digitizer, time stamp data and signal processing (correlation).

The sinusoidal signal generated by the RF clock is not perfectly stable. Instead it exhibits noise, the signal amplitude, phase and frequency fluctuate with time. In addition to this, the signal is affected by a number of factors as it is distributed from a central point to the antenna further degrading the clock stability. These include optical fibre birefringence and polarization fluctuations which introduce phase instability to the clock tone. This brings about difficulties in the operation of the MeerKAT telescope as the clock is required to maintain a stability within several hundred femtosecond jitter. The RF clock stability and additive noise can be analyzed as random short-term instability (phase fluctuation) and long-term instability (frequency drift). The aim of this work is to accurately characterize the RF clock stability and the noise induced as the optical signal is transmitted over fibre.

Since the establishment of the Optical fibre research unit in 2001 a lot of work has been done at the Nelson Mandela Metropolitan University to investigate effects on an optical signal transmitted over fibre and to apply various measurement techniques that characterize these phenomena. These include measurement of polarization mode dispersion (PMD) on optical fibre under different environmental and deployment conditions using cross-correlation interferometric and polarimetric measuring techniques. As well as characterization of chromatic dispersion (CD) on single mode fibre using pulse delay and phase shift measurement techniques, and polarization measurements characterization of state of polarization fluctuation rates if buried and overhead fibre. The techniques were designed and constructed using modern optical fibre research equipment available in the lab. Over the years the Optical Fibre Research Unit has expanded in research projects and developed into the Centre for Broadband Communication in partnership with CISCO, Department of Science and Technology (DST) and Square Kilometre Array (SKA). This has brought new exciting research opportunities for the students with projects such as flexible spectrum optical network optimization and optical

fibre measurements for clock tones in telescope networks. In the work represented in this thesis, it is the first time that clock phase stability and frequency drift measurements of an optical signal transmitted over fibre will be investigated at the NMMU optical fibre research lab. The aim of this study is to formulate and implement a suite of measurement tools suitable for a complete characterization of clock to distribution system similar to the MeerKAT and SKA telescope network.

This was done using a direct method to analyze the random signal fluctuation in the frequency domain characterized as phase noise (reported as jitter in the time domain) and deterministic frequency drift in the time domain characterized as non-overlapping Allan deviation. This work will provide a detailed discussion of the nature of clock tones and signal instability and understanding on how optical link components affect the stability of a clock signal. It will consider the requirements and performance of the distribution system over optical fibre of different length, different types and under environmental condition fluctuations to meet these criteria of successful operation stability.

In chapter 2 the principle of light propagation through a waveguide is addressed using two different approaches. The reflection and refraction can be used to describe the propagation as in the Ray model, or light can be treated as an electromagnetic wave making use of Maxwell's equations to define propagation. The different types of fibre used for transmission are discussed along with the attenuation and signal degradation associated with each.

Chapter 3 is an introduction to telescope network design and stability requirements for successful operation of the system; the critical role of clock tones in timing and synchronization in distribution systems are also addressed. The theory of clock stability and origin of signal instability is specified in the time and frequency domains. There is a relationship between the two domains using phase noise to phase jitter conversion. This relation is demonstrated. In latter sections the different types of noise associated with clock stability of an optical signal distributed over optical fibre are discussed.

There are three common techniques used for clock signal stability characterization: phase locked loop, delay line, and the direct method. The setup complexity and calibration for each technique is unique as explained in chapter 4. There are advantages and disadvantages associated with each method such as the sensitivity level, therefore the choice of which method to use is based on the stability requirements of the distribution under test. Since the establishment of the NMMU Centre for Broadband Communication, this method is being developed and the study of stability using phase noise and Allan deviation measurements will be conducted for the first time. The simplicity of the direct method setup and sensitivity levels being above noise level of interest as per MeerKAT stability requirements make it the ideal technique for this research.

Chapter 5 gives an overview of the apparatus used to build up the direct method experiments for random short-term instability and long-term frequency drift explaining the parameters under which the measurement equipment was operated.

In chapter 6 the signal instability was characterized in the frequency domain using an electrical spectrum analyzer. The RF clock tone origin was from signal generated. The measurement results were used as a reference to investigate the noise contributed by a transmission link on a clock signal distributed over optical fibre as a function of length. Chapter 7 is a comprehensive discussion of Allan Deviation extraction from instantaneous frequency measurement of a clock signal observed over different time periods.

Chapter 8 and 9 is a representation of measurement results collected for the analysis of additive noise contribution from different components making up the transmission link of the optical clock signal distribution system. Comparison was made between different components, under different environmental conditions especially for the optical fibre and different operating conditions (gain of amplifier and position along the link). These results were analyzed using both phase noise and Allan deviation to investigate the distribution system stability over time.

The work presented in this thesis is of high relevance for measuring and analyzing the stability of RF clock tone important for the telescope design, operation and optical clock signal for the distribution system over optical fibre.

Chapter 2

Optical Fibre Waveguide Theory

In this chapter the design of basic optical fibre will be address. Optical fibre is used for transmitting light from the light source to the receiver, so it is essential that the theory describing the nature of light and its propagation through the waveguide be discussed. A brief description of the types of fibre with their advantage and disadvantages in the different windows of transmission is also addressed. The signal degradation by attenuation, chromatic dispersion and polarization mode dispersion are covered. The signal instability introduced by optical link components such as lasers, amplifiers and photodiodes is discussed. The distribution of stable RF clock tone for timing and synchronization in telescope networks depends on the transmission of light over optical fibre. The propagation of light in a waveguide can be approach in two models. The ray model that uses reflection and refraction has been approached in next section.

2.1 Optical Fibre Design

In an optical fibre telescope network system the optical fibre is used to transfer the light pulse from the transmitter to a receiver as timing signal, and scientific data from the antenna to the central processing building. Optical fibre is a cylindrical dielectric waveguide over which light is transmitted based on the principle of total internal reflection. Optical fibre is made up of core and cladding, where the core is the central cylinder of fibre with refractive index n_1. The cladding was first proposed by Holger Moeller in 1951 as a transparent material of lower refractive index layer n_2 surrounding the core[7]. The use of optical fibre as a waveguide has been developed since the first bent glass rod was used to illuminate body cavities as demonstrated in 1888 by Doctors Roth and Reuss.

If the light is incident on the optical fibre with an angle of incident θ_i greater than the critical angle θ_c then the light will be guided along the core [8]. The critical angle is defined as the angle of incidence that gives a refracted angle of 90 degrees, this occurs when the cladding to core refractive index ratio is less than one (rays of light pass through a denser medium to the surface of less dense medium) and is given as:

$$\theta_c = \sin^{-1}\left(\frac{n_2}{n_1}\right) \qquad (2.1)$$

derived from Snell's law for a wave traveling along two media. The capacity an optical fibre has to gather light is given by the Numeric Aperture (NA) expressed as:

$$NA = \sqrt{{n_1}^2 - {n_2}^2} \qquad (2.2)$$

A higher NA value reflects more light being collected to propagate in the fibre.

The fibre has two essential components namely core and cladding which are made out of different materials at different size dimensions depending on the type of fibre and the application. The optical fibre may have additional layers for protection as seen in figure 2.1.

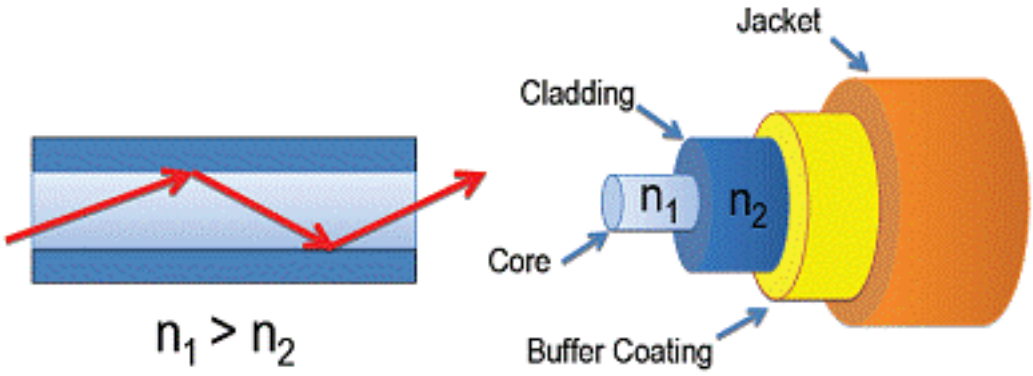

Figure 2.1: typical optical fibre structure[9]

The core diameter is typically 9, 50, 62.5 or 100 μm and that of a cladding being 125 μm or 140 μm with the size of the fibre described as 62.5/125 or 100/140. Plastic optical fibre has both essential components made of polymethyl methacrylate with the polymer

fluorinated for the cladding[10]. This type of fibre has very high attenuation and is commonly used to transmit light over short distances (tens of metres). Numeric aperture is the light gathering capacity of an optical fibre. The larger the numeric aperture/core size, the more light is collected to propagate through the fibre. An increase in the numeric aperture/core size results in an increase in the number of modes.

For a silica fibre, both core and cladding are made of glass. The refractive index requirement can be achieved by doping the core with germanium/phosphorus to increase it or decrease the cladding refractive index by doping it with boron or fluorine. Both silicon and germanium are group four elements sharing very similar chemical properties[11]. Germanium is the preferred dopant as it exhibits low absorption properties for transmission wavelengths 1310 nm and 1550 nm. Glass optical fibre has low attenuation and is suited for long distance transmission (100 to 1000 km). Other fibre can be made from a glass core surrounded by plastic cladding. Coating is a layer surrounding the cladding to strip out light rays traveling in the cladding and a buffer over coating for extra protection. The coating has a diameter of 250 μm and painted with ultraviolet cured paint, which helps with identification when handling a number of fibres in a cable. The buffered optical fibre is surrounded by Kevlar and coated to form a tight jacket or it can be laid inside a loose plastic tube for harsh environmental condition protection[12].

2.2 Signal Degradation

The light pulse propagating through the optical fibre is subject to signal degradation as it is transferred from the transmitter to the receiver. Attenuation weakens the signal intensity as the light travels through the optical fibre, limiting the transmission distance. Dispersion is the main contributing factor in signal degradation. Signal degradation causes the light pulse to broaden as it propagates along the optical fibre path length, overlapping of pulses results in errors on the detection process by receiver limiting optical fibre information carrying capacity.

2.2.1 Attenuation of the Fibre

Attenuation leads to the decrease in optical power of the signal. It may be caused by scattering associated with the fibre material and structural imperfections, and absorption related to fibre material. As the light ray travels down the fibre it is scattered and absorbed, which diminish the signal intensity. The absorption of a light pulse is caused by many different mechanisms including intrinsic absorption, extrinsic absorption and atomic defects. The intrinsic absorption is a fundamental lower limit. For silica fibre intrinsic absorption is due to the molecular composition of pure silica (SiO_2) with certain wavelengths being absorbed[13]. Wavelengths in the ultraviolet region are absorbed due to electronic resonance in silica. In the infrared region the absorption is affected by the silicon-oxygen atomic bond vibration. Extrinsic absorption occurs because of various impurities introduced during the manufacturing process of the optical fibre. These impurities can be from transition metal ions such as iron, nickel and chromium. The largest absorption arise due to hydroxyl ions (OH^-) with absorption peaks at 2700 nm, 1400 nm, 950 nm and 725 nm wavelength[14].

The absorption loss is a lower limit as opposed to the scattering loss in the transmission windows of modern optical fibres. Scattering signal loss is a result of microscopic variations in the fibre material density, molecular concentration variation, structural inhomogeneities and waveguide imperfections (defects). The effect of density and composition fluctuation gives rise to the variations of refractive index resulting in Rayleigh scattering. As the light pulse propagates down the waveguide, the photons interact with the fibre atoms (depending on the atom relative to the wavelength of light) resulting in the photons changing direction and light escaping the waveguide.

The Rayleigh scattered intensity is proportional to $\frac{1}{\lambda^4}$; this results in a drastic decrease in scattering loss with increasing wavelength[15]. At high signal power non-linear effects (Raman and Brillouin scattering) occur. During Raman scattering the photons are absorbed by the silica molecules and re-emitted at slightly shifted wavelength with some of the energy absorbed. The energy of the scattered photon is equal to the energy of the

incident photon minus the energy of vibrating molecule (Stoke scattering) or plus the energy of the vibrating molecule (anti-Stoke scattering) which cause the re-emitted photon to change direction and polarization[14]. Brillouin scattering occurs when the high optical power generated acoustic waves affect the density of fibre resulting in variation in the refractive index[14].

The power of a light pulse propagating through the fibre decreases with the distance traveled. Attenuation is one of the fibre's very important properties as it determines the maximum distance a signal can be transmitted along a fibre before it cannot be detected or amplification is required. A signal incident on a fibre with input power P_{in} and output power P_{out} at the end of the path length L in km experience a signal loss in units of decibels per kilometer given as:

$$attenuation(dB/km) = -\frac{10}{L}\log_{10}\left(\frac{P_{out}}{P_{in}}\right) \qquad (2.3)$$

The signal loss is a function of transmission wavelength as illustrated by the attenuation curve in figure 2.2

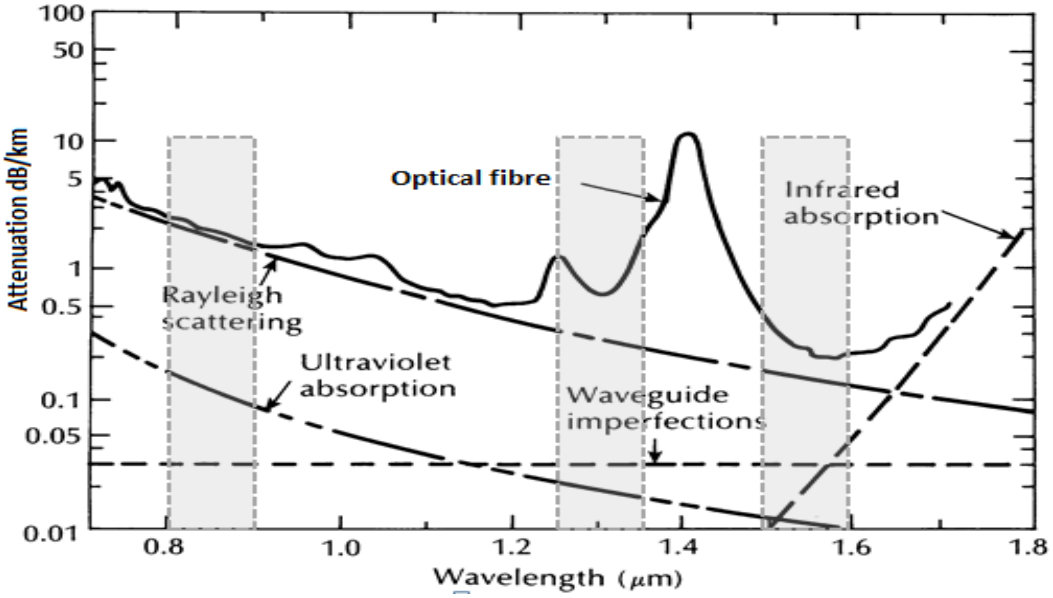

Figure 2.2: optical fibre attenuation as a function of wavelength at different windows of transmission[14]

The absorption spectrum of standard glass has 3 transmission windows. The first window of transmission 850nm has an attenuation of 3 dB/km. Its relative high attenuation limits transmission operation over optical fibre path lengths of over a few kilometres. It is useful for short-range transmission due to the availability and cost efficiency of the optical components operating at this wavelength. In the early 1980s the original band (O-band) was developed. The optical fibre attenuation as a function of wavelength at 1310 nm yields a value of 0.5 dB/km for a standard optical fibre.

This window was used when the transmitter and receiver technology for 1310 nm and 1550 nm was still under developed. The relatively wide 1550 nm window (conventional, C- band) gained recognition in the mid 1980 to early 1990s with the development of the Erbuim Doped Fibre Amplifier (EDFA) for all optical amplification in this window. The attenuation at this window of transmission is 0.3 dB/km for standard optical fibre.

2.2.2 Dispersion

Dispersion is the broadening of a light pulse as it propagates through the optical fibre. Peak broadening can lead to neighboring pulses overlapping resulting in corruption of data which causes difficulties in the detection process at the receiver end of the link. The penalties of pulse broadening are intersymbol interference and power fading effects. If the pulse broadening exceeds the dispersion of the fibre the data output is rendered undetectable. This also poses limitations in the overall bandwidth of the fibre and affects the data transmission capacity, especially for high bit rate system operation where spacing (time domain) between pulses is small. Dispersion measures the total pulse broadening per unit distances. The total pulse broadening Δt is defined as the root of the difference between the input pulse spread Δt_{in} and the output pulse spread Δt_{out} given by[15][16]:

$$\Delta t = \sqrt{\Delta t^2{}_{out} - \Delta t^2{}_{in}} = dispersion\left(\frac{ns}{km}\right) \times L(km) \qquad (2.4)$$

It is measured in time, typically nanoseconds or picoseconds. Dispersion is a function of optical fibre path length, the longer the fibre the higher the dispersion value. There are three major dispersion effects in the optical fibre: Modal dispersion, chromatic dispersion (CD), and polarization mode dispersion (PMD).

(i) Modal Dispersion

Modal dispersion is the pulse broadening caused by the time delay between rays traveling in different modes. Step index multimode fibre has light rays traveling in different directions, some travel in a straight path down the core (lower mode), whereas others zigzag as they bounce off the cladding (higher mode)[17]. Each mode travels a different distance hence they reach the end of the optical fibre path length at different times. This time delay results in pulse broadening, dispersion. The more modes present in an optical fibre the greater the effect of modal dispersion. It limits the bandwidth of a fibre. The effect of modal dispersion can be reduced by altering the refractive index profile of the fibre. For example the refractive index of fibre can be altered such that the refractive index of the core diminishes gradually from the center axis out towards the cladding. The light traveling in a straight path down the fibre propagates slower as compared to the light that curves helicaly of the periphery of the cladding[18]. The reduced path of the reflected light and high speed allows it to arrive at the receiver at the same time as the straight path light resulting in a less spread out pulse. This is referred to as graded index multimode fibre.

(ii) Chromatic Dispersion

Chromatic dispersion occurs within a single mode of propagation. It is a pulse broadening due to the different wavelengths of light propagating at slightly different velocities through the optical fibre path length. All light sources emit more than one wavelength instead of a single discrete spectral line since they have a finite number of spectral

width[19]. Chromatic dispersion is an aggregate of material dispersion and waveguide dispersion.

Material dispersion is due to the refractive index of waveguide medium dependency a the light source wavelength. The refractive index varies as a function of wavelength. Consider an optical fibre where all the modes of propagation are excited with the spectral power equally distributed with each mode. Light propagation in each of these modes is treated as an individual spectral component of the wavelength of the source. Each spectral component through the optical fibre path length encounters different interference with the refractive index of the medium and thus travels through at different velocities[7][8]. These spectral components of the wavelength have different propagation times resulting in pulse broadening. The total delay difference Δt_g for a light source with spectral width $\Delta\lambda$ propagating through a fibre of length L is given as[20]:

$$\Delta t_g = -\frac{L}{c}\frac{\Delta\lambda}{\lambda}D(\lambda) \qquad (2.5)$$

where D(λ) is the material dispersion coefficient. The material dispersion pulse broadening is proportional to optical fibre length and the source spectral width. Broadband light sources such as a light emitting diode (LED) would lead to severe signal degradation (pulse broadening and overlap). To reduce the effect of material dispersion a light source with a narrow spectral width such as laser should be used.

Waveguide dispersion is related to the ratio of mode confinement, which depends on the physical structure of the waveguide and the wavelength of light propagating within it. It results from the distribution variation of optical light power between the core and cladding[9]. Light distribution is a function of wavelength, core radius and the refractive index of the fibre. In single mode fibre, 80% of the light is confined in the core. Twenty percent of the light propagates in the cladding, traveling faster than the light confined in the core, as the cladding refractive index is relatively lower than that of the core. This results in the pulse broadening, waveguide dispersion.

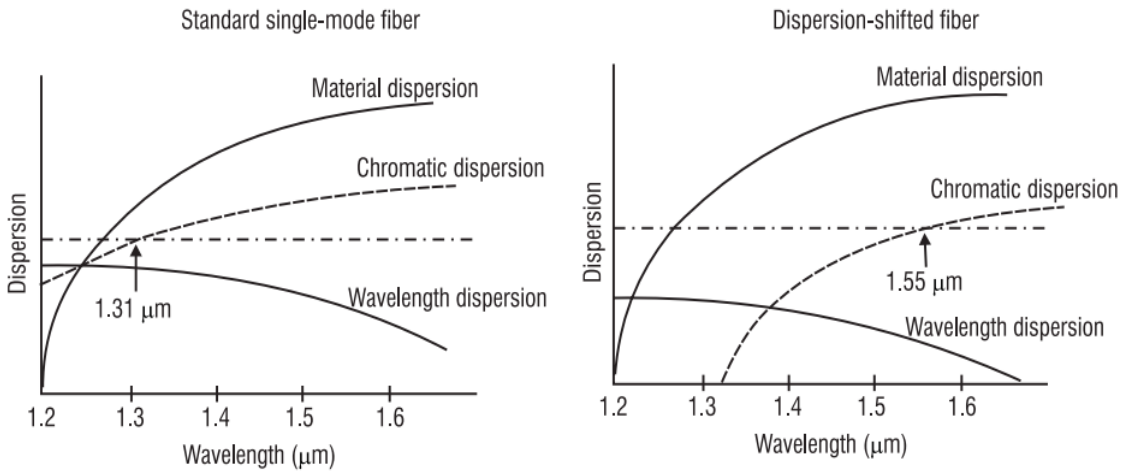

Figure 2.3: chromatic dispersion curve for standard single mode fibre and dispersion shifted fibre[14].

Material dispersion and waveguide dispersion can have opposite signs depending on the wavelength of the light source being transmitted. It is possible for these effects to cancel out yielding a chromatic dispersion of zero. This is the case for standard step index single mode fibre at 1310 nm where the material dispersion positive and the negative waveguide dispersion counteract[21] as shown in figure 2.3. Although transmission in the 1550 nm wavelength is preferred because of low attenuation, it does not posses the zero-dispersion properties seen in 1310 nm. By altering the design of the waveguide a dispersion-shifted fibre can be developed, this is achieved by increasing the waveguide dispersion such that the chromatic dispersion at 1550 nm is zero making high bandwidth and long distance communication possible[15]. Transmission of multiple closely-spaced wavelengths in the 1550 nm bands over the zero dispersion shifted fibre gives rise to severe nonlinear effects. Non-zero dispersion shifted fibre was introduced to address the nonlinearities problem. This type of fibre ensures that all the channels have different speeds as they propagate through the optical fibre, achieved by moving the dispersion wavelength to either end of the 1550 nm band[22]. Non-zero dispersion fibre has a high tolerance for non-linear distortion effect and offers minimized bending and splice loss for dense wavelength division multiplexing networks[23].

(iii) Polarization Mode Dispersion

Polarization mode dispersion is the pulse broadening that occurs because of a phase delay between two orthogonal polarization states. The light pulse orthogonal components (polarization modes) generate a phase difference changing in time as they propagate through the orthogonal axes (principle axis) of the optical fibre.
It is an aggregate of birefringence and mode coupling. The effect of PMD causes an increase in bit error rate making a limiting factor in high bit rate transmission systems. The PMD for a G.652.C optical fibre at 1550 nm transmission is 0.20 ps/$\sqrt{km}$ relative to the chromatic dispersion value of 18 ps/nm.km, PMD is a second order effect[24].

Single mode fibre supports one fundamental propagation mode consisting of two orthogonal propagation states. Ideally this optical fibre has a perfectly circular core and same refractive index for the propagation states[25]. However asymmetries in the optical fibre core geometry occur due to mechanical and thermal stress introduced during the manufacturing process. As a result of this asymmetry a small difference in the refractive index of the polarization states exists, a property known as birefringence. This creates different optical axes, one slow and the other fast. Birefringence causes the polarization states to travel with different velocities (one faster than the other) resulting in a difference in the time of arrival at the receiver end, called differential group delay (DGD) therefore an overall pulse broadening as shown in figure 2.4.

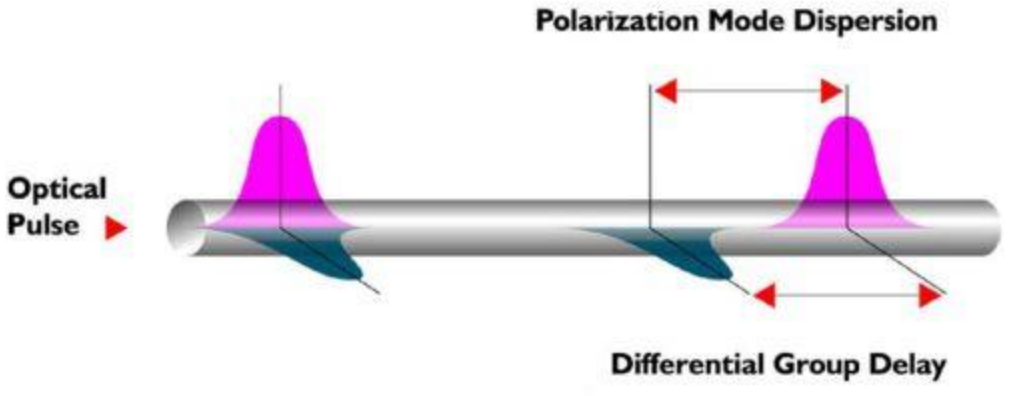

Figure 2.4: Polarization mode dispersion in a fibre[26]

The time difference is a function of wavelength. DGD is typically measured in units of picoseconds. The effect is intensified by external mechanical stress (bending and twist) and environmental condition fluctuation on the optical fibre. These random effects add up along the path length of the fibre, thus PMD is not given by a single value but it is rather described by the average of the DGD over some wavelength.

Mode coupling is the exchange in energy amongst the two polarization modes propagating along the optical fibre path length. The birefringence of an optical fibre is exacerbated by any bends or twist generating points of perturbation referred to as mode coupling sites. These points occur at random positions and with random orientation along the optical fibre length. When two states of polarization encounter the mode coupling site energy is exchange depending on the position and orientation. Mode coupling introduces multiple polarization modes splitting the input signal between the new fast and slow axes (random orientation of mode coupling site)[14]. For strong birefringence fibre there is a low degree of mode coupling as light propagates through the fibre, and the PMD increases linearly with fibre length. Mode coupling occurs easily in weak birefringence fibre, the average distance between mode coupling sites is less than the fibre length. In such cases the degree of mode coupling is high, and PMD has a square root dependence to the length of the fibre. Mode coupling mitigates the effect of PMD[27], [28]. In modern fibres mode coupling is induced intentionally during the manufacturing processes

to reduce PMD of a fibre. This is done by spinning the fibre while it is being drawn from the preform, this realigns the orientation of the axes of the fibre.

The instantaneous PMD will be different along the length of the fibre as the wavelength of laser will be different. A small change in the wavelength can have a significant impact on PMD. The clock stability budget for the MeerKAT X/Ku-band (8-14.5 GHz/ SKA phase 1 mid) is 2.2 ps for a 0.2 rad phase error. For fibre length, L, the PMD penalty is approximately $3 \times \left(19.4\ \mathrm{fm/km^{\frac{1}{2}}}\right) \times L^{\frac{1}{2}}$[29].

2.3 Optical Fibre Types

Two types of optical fibre are described in optical fibre communications, it transmits light in 1310 nm and 1550 nm wavelength. It was first suggested by Charle Kao and George Hockham that the loss of glass fibre could be reduced, this could be achieved by removing impurities. In the 1970s Corning glass work achieved a single mode fibre attenuation of less than 20dB/km by doping it with titanium[30]. This was one of the first lowest attenuation attempts.

2.3.1 Multimode Fibre

Multimode fibre is the first manufactured and commercialized fibre. It supports a number of modes that propagate simultaneously through the waveguide. The number of modes supported depends on the core size relative to the wavelength of light being transmitted and the numeric aperture. The core diameter of the multimode fibre is relatively large and supports a large number of modes. Multimode fibre can transfer light transmitted at 850, 1310 and 1550 nm wavelength. Due to the large core a number of reflections are formed as light passes through. Multimode fibre can be categorized as either step index or graded index as shown in figure 2.5.

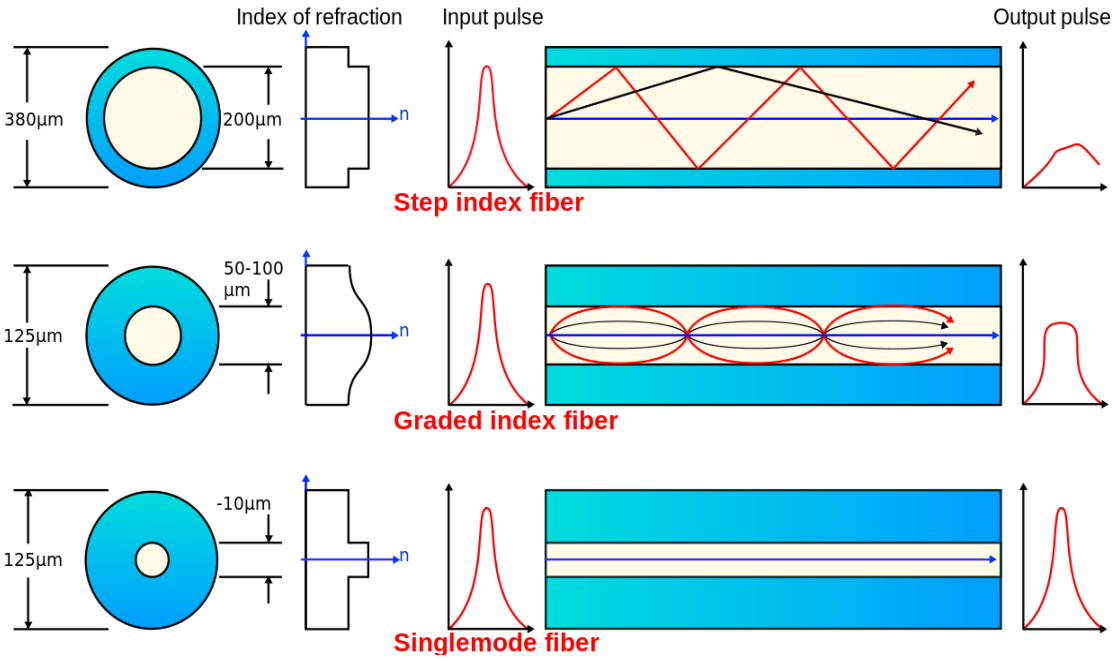

Figure 2.5: types of optical fibre[31]

Step index multimode fibre has a uniform refractive index throughout the core and changes drastically at the core-cladding interface. This type of multimode fibre has light rays of a pulse traveling in different directions, some travel in a straight path down the core which others zigzag as they bounce off the cladding. Combinations of the different modes spread out the well-defined shape of the pulse. The dispersion caused by the difference in the path length for the varies modes makes this fibre too slow for most use, it is barely used in communication systems.

Graded index multimode fibre refractive index of the core diminishes gradually from the center axis out towards the cladding. The light travels in a straight path down the fibre slowly compared to the light that curves helically of the periphery of the cladding. Variation in the refractive index of the core compensates for the different path length of the modes[32]. The reduced path of the reflected light and high speed allows it to arrive at the receiver at same time as the light that propagated along the straight path resulting in a less spread out pulse. Graded index multimode fibre offers more bandwidth than the step index multimode fibre.

Due to the large core different light sources such as LEDs and VCSELs may be suited for applications over multimode fibre depending on the transmission speed and wavelength of light. The reach over multimode fibre is limited by modal dispersion and attenuation, typically 1.5 dB/km.

2.3.2 Single Mode Fibre

Theoretical description of single mode fibre with small core carrying light in one waveguide mode came in 1961 when Elias Snitzer demonstrated it using thin glass fibre with a loss suited for medical application[1]. Single-mode fibre allows one mode of light to propagate in a straight line down its small core without any internal reflection as the refractive index is reduced as shown in figure 2.5.

To ensure no additional modes are created, the single mode fibre of core diameter d can only transmit wavelengths longer than the cut off wavelength λ_c given as[5][6]:

$$\lambda_c = \frac{\pi d}{2.405}\sqrt{{n_1}^2 - {n_2}^2} \qquad (2.6)$$

The typical core diameter of single mode fibre is 9 μm. Single mode fibre has a lower attenuation than multimode fibre and thus retains better pulse accuracy (less signal intensity weakening). Single mode fibre is characterized as step index fibre. It carries light in the second and third window of transmission where attenuation is minimized. The typical value is 0.4 and 0.25 dB/km for transmission at 1310 nm and 1550 nm respectively[16]. This means light can be transmitted over longer distances. For long reach transmission over single mode fibre, a light source with narrow spectral width should be used as the waveguide has a small core. The reach is limited by chromatic and polarization mode dispersion as single mode fibre does not exhibit modal dispersion. At 1310 nm the chromatic dispersion is zero for non-dispersion shifted fibre, the need of high bandwidth has brought about the need to operate at 1550 nm[5]. By modifying the refractive index of the step index single mode fibre such that it gradually diminished from

the center of the core into the low refractive index cladding, zero chromatic dispersion at 1550 nm could be achieve, this was the introduction to zero dispersion shifted fibre.

2.4 Mathematical Wave Description of Light

In this section the electromagnetic theory is introduced. The theory describes the best known propagation phenomena of light and begins with Maxwell's equations. The second approach uses Maxwell's equation and treats light as an electromagnetic wave.

2.4.1 Maxwell's Equation

The electromagnetic wave consists of oscillating electric fields $\bar{E}$ and magnetic fields $\bar{B}$ that are perpendicularly aligned. For a dielectric waveguide with no free charges or current the Maxwell's equations can be expressed as[33]:

$$\nabla \cdot \bar{E} = 0 \qquad (2.7)$$

$$\nabla \times \bar{E} = -\frac{\partial \bar{B}}{\partial t} \qquad (2.8)$$

$$\nabla \cdot \bar{B} = 0 \qquad (2.9)$$

$$\nabla \times \bar{B} = \mu\varepsilon \frac{\partial \bar{E}}{\partial t} \qquad (2.10)$$

where μ and ε are the permeability and permittivity of the waveguide material respectively. μ and ε, do not depend on the direction of propagation and are not a function of frequency[34]. The equations can be decoupled by taking the curl of equation 2.8 and 2.10 to give a standard wave equation for the electric and magnetic fields:

$$\nabla^2 \bar{E} = \mu\varepsilon \frac{\partial^2 \bar{E}}{\partial t^2} \qquad (2.11)$$

$$\nabla^2 \bar{B} = \mu\varepsilon \frac{\partial^2 \bar{B}}{\partial t^2} \qquad (2.12)$$

The two equations satisfy the classical wave equation with three-dimension generic form given as:

$$\nabla^2 \bar{f} = \frac{1}{v^2} \frac{\partial^2 \bar{f}}{\partial t^2} \qquad (2.13)$$

where v is the velocity of the wave and f is the wave amplitude. The electromagnetic waves propagate through the waveguide with a velocity:

$$v = \frac{1}{\sqrt{\mu\varepsilon}} = \frac{c}{n} \qquad (2.14)$$

where n is the refractive index of the material. For an electromagnetic wave propagating in the z direction the refractive index is assumed to be constant, but can vary in the x and y direction[35]. The standard wave equation of the electric fields propagating in the z direction at a given instant in time t can be expressed as:

$$\bar{E}(z,t) = \overline{E_0}(x,y) e^{i\beta z - i\omega t} \qquad (2.15)$$

where ω is the angular frequency and $\beta = \frac{\omega}{c} n$ is the propagation constant. Due to the core dimension and the fibre geometry only discrete values of β act as solutions to equation 2.15 hence only certain modes are supported.

Substituting equation 2.15 into the wave equation of the electric field gives:

$$\left(\frac{\partial^2}{\partial x^2} + \frac{\partial^2}{\partial y^2}\right) \bar{E}(x,y) + (\mu\varepsilon\omega^2 - \beta^2)\bar{E}(x,y) = 0 \qquad (2.16)$$

The solution of the electric field in equation 2.16 may either vary exponentially or sinusoidally depending on whether $(\mu\varepsilon\omega^2 - \beta^2)$ is positive or negative. For light to propagate through the optical fibre length it must be confined in the core. This is achievable when the solution of the electric field is a stable sinusoidal varying function in the core and exponentially decaying function in the cladding[18][19].

2.4.2 Polarization of Light

Light consists of a number of waves each with different orientations of the electric field depending on the direction atoms and molecules of the source to which it is radiated. A wave propagating in the z direction within an optical waveguide may be treated as a superposition of two orthogonal waves of the same frequency as shown in figure 2.6.

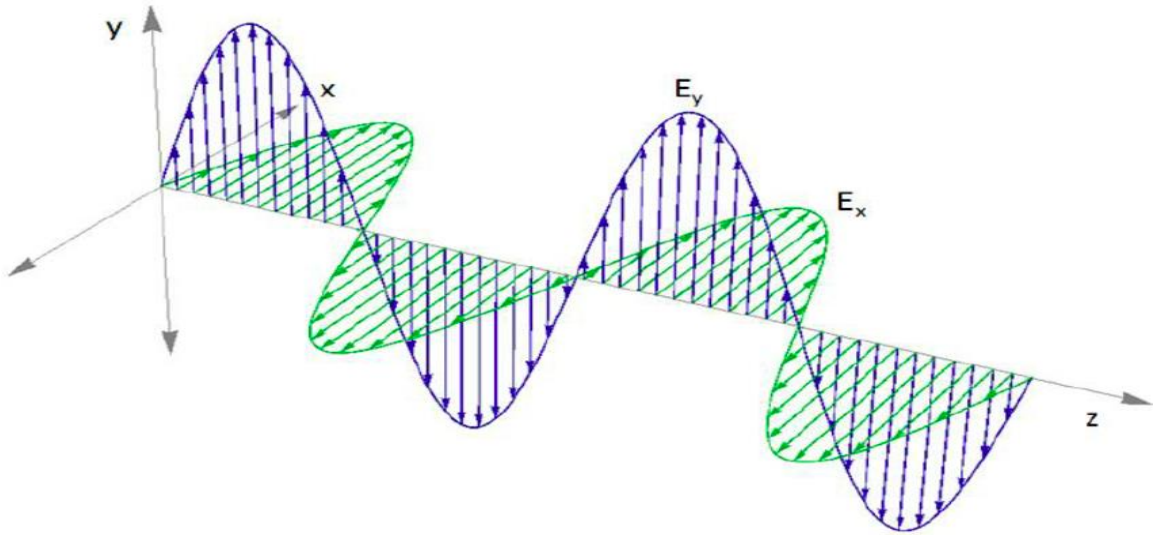

Figure 2.6: electric field propagating in the z-direction

The resultant electric field of the wave can be expressed as a superposition of the time varying orthogonal components[33]:

$$\bar{E}(z,t) = \overline{E_x}(z,t) + \overline{E_y}(z,t) \qquad (2.17)$$

$$\overline{E_x}(z,t) = E_{ox}\cos(\beta z - \omega t + \delta_1) \quad (2.18)$$

$$\overline{E_y}(z,t) = E_{oy}\cos(\beta z - \omega t + \delta_2) \quad (2.19)$$

This light will be unpolarized as the electric field orientation would vary randomly with time. For polarized light the resultant electric field variation is predictable. The magnitude and orientation of the electric field is referred to as the state of polarization obtained once the amplitude E_{oi} and phase δ_n of the orthogonal components is known[36]. Light can be either unpolarized, partially polarized or polarized depending on the degree of polarization (DOP), which gives the intensity of the polarized light relative to the total intensity. There are three states of polarization used to describe the orientation of the electric field for a propagating wave: linear, circular and elliptical. The states depend on the amplitude of the orthogonal wave components and the relative phase difference ($\delta = \delta_2 - \delta_1$) between them. In the xy plane the phase difference ranges from 0 to 2π. This also controls the direction in which light is swept. For phase difference $0 < \delta < \pi$ the electric field would trace out in a clockwise direction and light is said to be right handed polarization state. Left hand polarization occurs when the electric field traces in an anticlockwise direction for phase difference $\pi < \delta < 2\pi$[37]. Figure 2.7 shows the three states of polarization of light and the different directions.

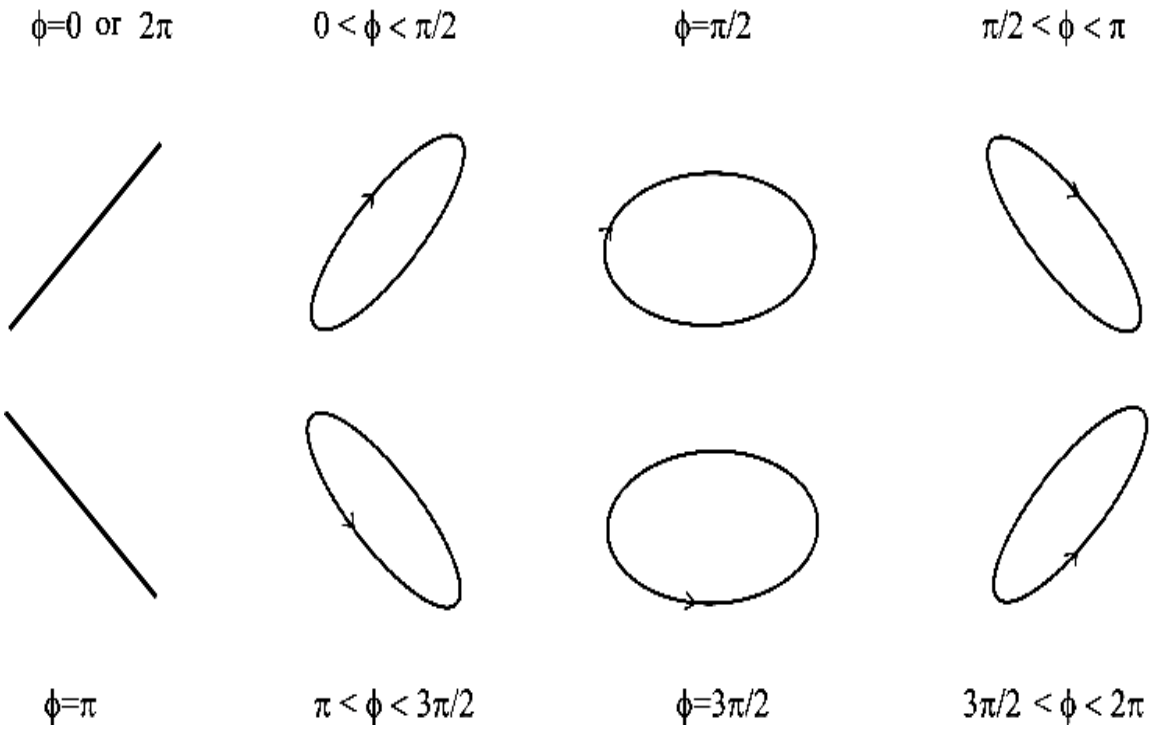

Figure 2.7 state of polarization for varies phase differences[38]

Light is linearly polarized if the phase difference between the components of the electric field is zero or an integer multiple of π.

$$\delta = n\pi$$

Light is considered to be circular polarized when the amplitude of the orthogonal wave components is equivalent and the phase difference is given by:

$$\delta = \pm\frac{\pi}{2} \pm 2n\pi$$

and depending on the sign of the first term it is either left ($-\frac{\pi}{2} \pm 2n\pi$) or right ($+\frac{\pi}{2} \pm 2n\pi$) circular polarized. Light is left circular polarized if the electric vector coming towards you appears to be rotating clockwise. If the rotation is counter clockwise, the light is right circular polarized. When the critical conditions that classify light as either linearly or circular polarized are not met, then light is said to be elliptically polarized[21].

2.4.3 Stokes Parameter and the Poincaré Sphere

Any form of complete polarization that results from a coherent light source can be analyzed using the polarization ellipse. The states of polarization of the resultant electric field may be represented by a polarization ellipse.[39] The minor and major axes of the ellipse do not correspond to the x and y axis. Instead the ellipse is tilted an angle α with respect to the x-axis as seen in figure 2.8.

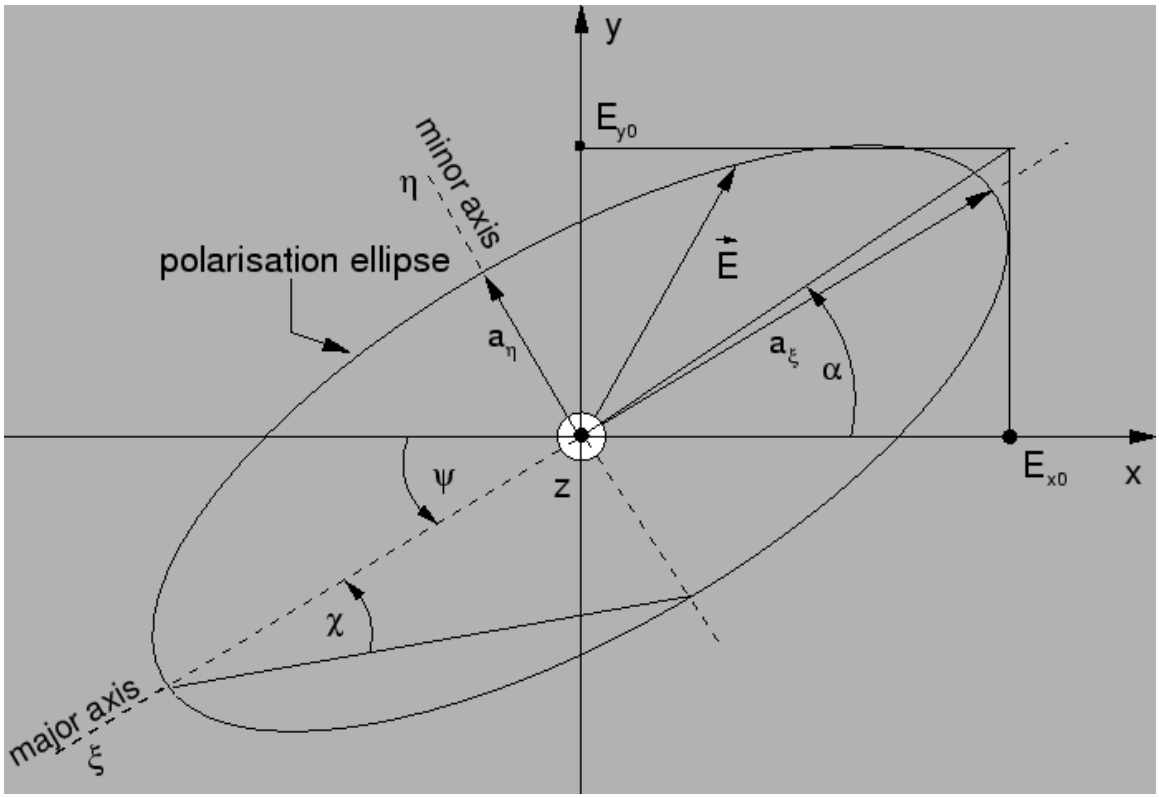

Figure 2.8: polarization ellipse for electric field propagation in the z direction[40]

Different states of polarization have a unique polarization ellipse described in terms of two angles ψ and χ. The angle ψ specifies the orientation of the ellipse. The second angle χ is the ellipticity, it specifies the points of intersection a_η and a_ξ of states of polarization with the major axis of the ellipse. The angle χ is defined in terms of the intersection point given as [39], [41]:

$$\tan\chi = \pm\frac{a_\xi}{a_\eta} \qquad (-\frac{\pi}{4} \leq \chi \leq \frac{\pi}{4})$$

The sign of $\tan\chi$ distinguishes the different directions in which light traces out an ellipse. For light in the right-handed polarization state $0 \leq \chi \leq \frac{\pi}{4}$ therefore $\tan\chi$ is positive. For light in the left-handed polarization state $-\frac{\pi}{4} \leq \chi \leq 0$ $\tan\chi$ is negative[24]. This relates to the direction the electric field traces out its path, clockwise is for left-handed polarization and counter clockwise is for right-handed polarized light.

The states of polarization of light be it unpolarized, partially polarized and polarized can be characterized by Stokes parameters. This is a more practical and convenient way to analyze light. These parameters are constructed from the orthogonal wave components of the electric field and are given as[42]:

$$S_o = {E_{ox}}^2 + {E_{oy}}^2 \qquad (2.20)$$

$$S_1 = {E_{ox}}^2 - {E_{oy}}^2 \qquad (2.21)$$

$$S_2 = 2E_{ox}E_{oy}\cos\delta \qquad (2.22)$$

$$S_3 = 2E_{ox}E_{oy}\sin\delta \qquad (2.23)$$

The four quantities were introduced by G.G Stokes in 1852. Only three of Stokes parameters are independent. S_o is dependent on the other three parameters and can be given as[24]:

$$S_o = \sqrt{{S_1}^2 + {S_2}^2 + {S_3}^2} \qquad (2.24)$$

The Stokes parameters may be used to determine the degree of polarization of partially polarized light given as[43]:

$$\mathrm{DOP} = \frac{\sqrt{S_1{}^2 + S_2{}^2 + S_3{}^2}}{S_o} \qquad (2.25)$$

S_o is proportional to the intensity of the wave. The three independent Stokes parameters can be expressed in terms of ψ and χ.

$$S_1 = S_o \cos 2\chi \cos 2\psi \qquad (2.26)$$

$$S_2 = S_o \cos 2\chi \sin 2\psi \qquad (2.27)$$

$$S_3 = S_o \sin 2\psi \qquad (2.28)$$

These parameters represent the Cartesian coordinates of a point with spherical coordinates 2χ and 2ψ on a sphere of radius S_o as shown in figure 2.9.

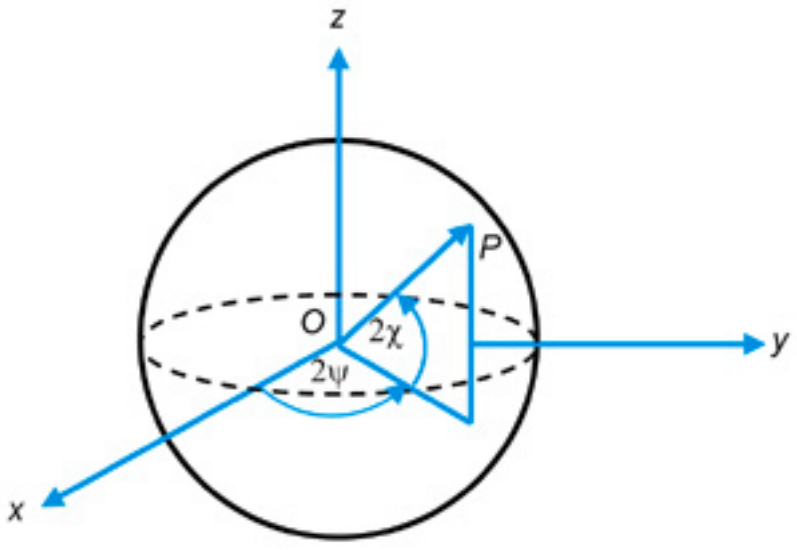

Figure 2.9: Poincaré sphere[44]

The sphere illustrated in figure 2.9 is known as a Poincaré sphere. The different state of polarizations are represented as points on the Poincaré sphere. For light that is right-handed elliptical polarized the points representing this state of polarization lie on the northern hemisphere. For left-handed elliptical polarized light the points representing the state of polarization lie on the southern hemisphere. The points for linearly and circular polarized light lie on the equator and poles of the sphere respectively[25].

2.5. Optical link Components Instability Contribution

Direct modulation is widely used in optical links because of its simplicity and cost effectiveness though the system gets limited by the nonlinear distortion and bandwidth of the laser and at high frequencies the undesired frequency modulation (chirping). The maximum bandwidth exhibited by commercial lasers is 10GHz. The single frequency optical carrier is modulated by RF signal creating upper and lower sidebands. Transmission of the signal through optical fibre results in phase shift due to the effect of chromatic dispersion. At the receiver the photodiode converts the optical to electrical signal detecting destructive interference, attempting to recover the RF signal, which is attenuated, distorted and noise due to the optical link.

2.5.1 Laser

Semiconductor lasers are characterized by the electrical and optical properties. Optical fibre and the semiconductor lasers have changed the communication system becoming more reliable and efficient (with respects to the injected electrons) to meet the demand of high data communications and telecommunication networks, this taking advantage of the: bright output regardless of the small dimension, low power consumption as they have low threshold current and high mass production due to low cost of fabrication. A laser is electrically pumped based on a gain medium within an optical cavity composed by two cleaved facets of semiconductor[45]. Light is generated due to the two emissions taking place from the four basic electronic transitions (spontaneous emission, stimulated

generation, stimulated emission, trap-assisted and Auger recombination) occurring between the valance and conduction bands of a solid semiconductor material as shown in figure 2.10.

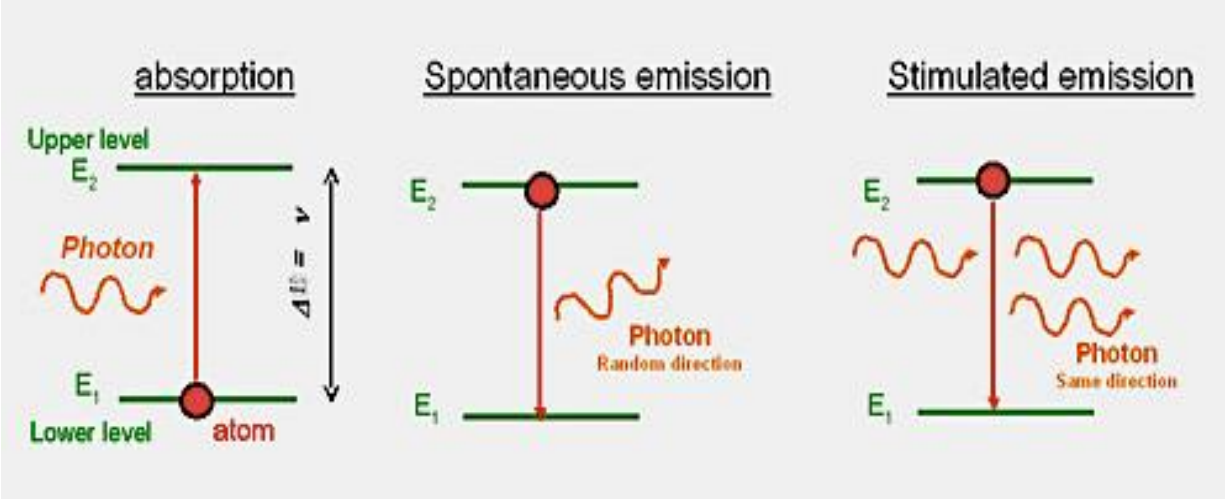

Figure 2.10: Electronic transitions[46]

The optical transitions are vertical in the k space and occur when an electron in the conduction band and a hole in the valence band recombine emitting a photon. The recombination time of direct bandgap semiconductors is very short. When the decay of the excited electron from the higher-energy level to the lower-energy level occurs without external influence a photon is emitted through spontaneous emission process. Spontaneous Emission is a random emission of photons so the phase is associated with the emitted photon. Electrons in an induced decay produce a photon identical to the incoming photon amplifying the intensity of light[47]. A laser emits electromagnetic radiation based on the stimulated emission of photons through a process of optical amplification. Stimulated emission is the process by which excited electrons decay to lower-energy levels upon interacting with an incoming photon of specific frequency, it is the main signal power emitted by a laser. A material with more than one electron in the excited state results in radiation that is monochromatic[48], [49]. This allows the laser to output a narrow beam of light thus being essential elements in optical communication systems. The range of emission wavelengths of semiconductor lasers covers the optical spectrum from near ultraviolet to far infrared depending on the materials used in the lasing region. The emission wavelength depends on the semiconductor bandgap. Long

wavelength lasers in the range of 1.1 to 1.6 μm are desirable in optical fiber communication since the optical fiber attenuation in this window is very low.

In this work two types of lasers will be studied: vertical cavity surface emitting lasers, VCSEL and distributed feedback (DFB) lasers. The cavity and growth of VSCEL is in the vertical direction, and feedback is achieved by using a multilayer reflective stack grown below and above the active region. DFB lasers are usually within the in-plane cavity with active region and is assumed to be uniform over the volume. For standard double heterojunction semiconductors, a set of rate equations that govern the recombination effects of carriers inside the active region can be used describe the operating characteristics of semiconductor lasers. The unique characteristics of semiconductor lasers make them interesting sources for optical clock signal generation in distribution systems; these include the speed and ease for direct modulation. This is a way to convey information on the optical laser output by changing the strength of the laser excitation, adding a small time varying signal to the average pumping current, amplitude modulation. The optical output is proportional to the injected current. The current dependence of the refractive index within the laser active region allows for frequency modulation of light to occur. The current to modulation of light conversion is linear and the optical power of the laser is determined by the operating point which is mid-point of this linear range. Even at fixed DC bias current the semiconductor laser emits optical signal with intensity and phase fluctuations due to the random nature of photons generated during electron-hole recombination and spontaneous emission. The use of a large time varying signal may lead to distortion and noise; the laser has both amplitude and phase noise. The distortions limit the bit rate in the distribution systems. The amplitude noise of a laser quantifies the fluctuations of the laser output power.

The relative intensity noise RIN is a number that sums up all the noise contributions of a laser. This includes the quantum effects and environmental condition variations. RIN is the ratio of intensity fluctuations about the average to the square of the instantaneous optical intensity[50]. Intensity noise of the laser can be characterized by the relative intensity noise at a given angular frequency. At a given frequency, the RIN decreases

with increasing laser power. It is the fluctuation of the power emitted by a laser around its steady-state value measured by detecting the laser output using a wide bandwidth photodiode and an electrical spectrum analyzer[51], [52]. The spectrum of these fluctuations is associated with the total power. The phase fluctuation is brought about by the phase change associated with variations in the carrier density and spontaneous emission. The phase change is linked to changes in the refractive index related to the optical gain with changes with the carrier density[53]. The refractive index and frequency of the optical signal is affected by the carrier concentration variation in the active region due to direct intensity modulation. Semiconductor lasers in direct modulation operation are subjected to carrier density variation in the active region. Modulation occurs for the output optical power main signal and unwanted optical phase leading to frequency chirping. The frequency chirp as a function of optical output power P(t) can be expressed as:

$$\Delta\nu(t) = \frac{1}{2\pi}\frac{d\phi(t)}{dt} = \frac{\alpha}{4\pi}\left[\frac{d}{dt}\ln P(t) + \kappa P(t)\right] \qquad (2.29)$$

here α is the linewidth enhancement factor, $\Delta\nu(t)$ is the instantaneous frequency deviation and κ is the structure dependent constant, adiabatic chirp coefficient. The instantaneous frequency deviation is directly proportional to α. The linewidth enhancement factor gives the proportionality between gain and refractive index. This constant can be used to determine the linewidth of a laser and instantaneous change in the emission wavelength[54]. The linewidth of the laser is the full-width at half-maximum of the light spectrum. The linewidth is dependent on α^2 and inversely proportional to the optical power. The first term of the equation represents the transient chirp which is proportional to the logarithmical power deviation. This kind of chirp is sensitive to the shape of the pulse slopes. In the presence of transient chirp the rising edges of the light pulse propagate faster than the flat parts distorting the output signal, in digital systems this leads to the wavelength of 1 being lower than that of a 0. The second term of the equation represents the adiabatic chirp. This kind of chirp is due to temperature variation, it is proportional to output power[55][56]. In the optical transmission links adiabatic

chirp and optical fibre dispersion interaction leads to increased group velocity resulting in faster output pulse rising edges compared to input.

The total chirp is the sum of contributions from carrier density variation and temperature effects. Phase is the integral of a laser instantaneous frequency deviation.

$$\phi(t) = 2\pi \int_0^t \Delta\nu(t)\, dt \qquad (2.30)$$

The phase noise of a laser is related to the fluctuations of the optical phase output associated with the quantum effect during the lasing process, the carrier recombination phenomena in the laser cavity[57]. The frequency chirp associated with laser intensity modulation can be demonstrated as a real-time analogue signal using the direct method of electrical spectrum analyzer. The technique is also used to extract phase noise and frequency instability through coherent up-conversion of optical clock tone heterodyne mixing with the local oscillator at the receiver. A photodiode is used to convert the optical signal to electrical signal. Photodiode thereforecontributes to the overall system noise.

2.5.2 Photodiode

The photodiode converts optical signal to electrical signal called the photocurrent. This can be measured as photo voltage depending on the load resistor of choice. For a P-N junction with no bias the incident photons are absorbed, exciting electrons from the valence to the conduction bands resulting in optical generation of electron-hole pairs[58]. Under the influence of bias voltage the electron-hole pairs are separated and collected by an external circuit. The charge carrier is directly proportional to the incident power falling on the detector.

$$I_{ph} = r_{PD}\ \mathrm{P(t)} \qquad (2.31)$$

The incident power and the generated photocurrent are related by the proportionality constant r_{PD}, the responsitivity of detector given by A/W[59]. At very low optical power (around noise floor) and near saturation limit this relationship does not hold. Saturation is

defined as the point when the optical power increases until the bias and output voltages are relatively close. Noise floor and saturation are affected by reverse bias voltage, responsitivity and the bandwidth of the detector. Applying the reverse bias voltage to the photodiode creates a photoconductive mode. This operation has low capacitance, high speed and improved photodiode linearity, with the dark current being directly dependent of the reverse voltage[60], [61]. Dark current is due to the random generation of electrons and holes within the depletion region of the device that are then swept by the electric field applied to the diode, it is the constant response exhibited by a detector during periods when it is not actively being exposed to light. The noise contribution of the photodiode arises from the physical effects of the photodiode and the surrounding environment.

Noise equivalent power (NEP) is the minimum detectable power, it is reported in units of $W/\sqrt{Hz}$. It can be used to address the intrinsic noise of the photodiode. Light sources emit photons at random and the amount emitted is not constant. Photodiode convert these incoming photons into electric current within the semiconductor media. To characterize the excess noise due to the photodiode on starts with the known sources: shot noise, thermal noise and amplitude to phase noise conversion[62]–[64].

Shot noise of the dark current is not dependent on the quality of the detector nor is it avoidable. It is related to the randomness of the incident photon stream, the statistical fluctuation of photocurrent. The RMS shot noise current variation can be expressed as:

$$I_{dark} = \sqrt{2ei_{avg}B} \qquad (2.32)$$

where e is the elementary charge 1.6×10^{-19} C , i_{avg} is the average photocurrent created by the incident optical power measured at the output of the PD and B is the detection bandwidth. Shot noise is dominating when the photodiode is operated in biased mode and becomes a real issue at low optical intensity[65]–[67]y. The shot noise power as a function of shot noise current is given by:

$$P_{shot} = ei_{avg}R \qquad (2.33)$$

The SSB phase noise due to the phase fluctuations is the shot noise power ratio over the power from the signal generator:

$$\mathcal{L}_{\mathrm{dBc}}(\mathrm{f_m}) = 10\log\frac{P_{shot}}{4P_{rf}} \approx -177 + 10\log\left[\frac{I_{dark}}{P_{rf}}\right]\left[\frac{\mathrm{dBc}}{\mathrm{Hz}}\right] \quad (2.34)$$

where the power P_{rf} is in mW units and current I_{dark} in mA units. Thermal noise of shunt resistance is associated with the random fluctuation of the current across the resistive elements of the photodetection circuit[68]. It is generated by the thermal motion of the electrons inside an electrical conductor at equilibrium, which happens regardless of any applied voltage. This type of electric noise is dominant in photovoltaic mode of operation.

The RMS thermal noise as a function of absolute temperature of the photodiode can be expressed as:

$$I_{Rsh} = \sqrt{\frac{4kTB}{R_{sh}}} \qquad (2.34)$$

where k is the Boltzmann's constant and R_{sh} is the shunt resistance of the photodiode. The shunt associated with reversed biased P-N junctions is large and for this reason the thermal noise is usually neglected[22], [25] .The voltage variance of the power in the 1 Hz bandwidth is given by:

$$\overline{V^2} = 4kTR \quad (2.35)$$

This results in a noise power reduction by a factor of four since both the source and the load have 50 Ω impendance. Noise power contributes equally to the phase and amplitude of the signal, resulting in further reduction by an additional factor of two. The thermal noise induced SSB phase noise is expressed as[68], [71]:

$$\mathcal{L}_{dBc}(f_m) = 10\log\frac{kT}{2P_{rf}} \approx -\frac{177dBm}{Hz} - P_{rf}\left[\frac{\mathrm{dBc}}{\mathrm{Hz}}\right] \quad (2.36)$$

where Prf is the power in dBm units, as measured with an electrical spectrum analyzer at the output of the photodiode at the desired offset frequency.

In this work effects of gain, shot noise and thermal noise will be studied for the performance comparison of the conventional PIN photodiode with the voltage hungry Avalanche photodiode. APD photodetectors have shown supremacy in long haul communication due to the internal variable avalanche gain M. The APD is the preferred photodiode for loss limited systems. The PIN photodiode produces a photocurrent that fluctuates randomly about the mean value. The produced photocurrent is an aggregate of two current contributions: Drift current associated with the carriers generated inside the intrinsic region and the diffusion current caused by generation of carriers on the edges of the intrinsic region[71]. The intrinsic layer is inserted between the n-type and p-type layers. Most of the incident power is absorbed inside the intrinsic layer, making the drift component the main contribution over the diffusion component. The 1310 nm window uses InGaAsP and Ge materials. The 1550 nm window is absorbed strongly by the InGaAs material with 0.77 eV bandgap, eliminating the diffusion current contribution. The responsitivity of the PIN photodiode is very small[58], [65]. It is more cost efficient, less sensitive to temperature and requires lower reverse bias voltage compared to the APD.

The intrinsic gain provides APD with useful high sensitivity, this is a result of an additional p-type layer inserted between the intrinsic and n-type layer. The additional layer allows for the generation of secondary electron-hole pairs through impact ionization, avalanche multiplication. The process of electron-hole pair multiplication is random and increases the noise of the optical generated carriers[69], [70], [72]. The statistical nature of the avalanche processes result in the APD generating excess noise NF as a function of the carrier ionization ratio k. The ratio of hole-to-electron ionization probability is greater than 1. The shot noise of the photodiode can be assumed to be[61], [67]:

$$\mathrm{I^2_{dark}} = 2\mathrm{ei_{dark}BM^2NF} \qquad (2.36)$$

The total noise for both photodiodes is a summation of the shot noise and thermal noise.

$$I_{total} = \sqrt{I^2{}_{dark} + I^2{}_{Rsh}} \qquad (2.37)$$

and the NEP of the photodiode can be calculated as:

$$NEP = \frac{I_{total}}{r_{PD}} \qquad (2.38)$$

In a typical high-speed detection system with a 50 Ω termination at room temperature the thermal level is approximated by:

$$N = kTB = -174dBm/Hz$$

This represents the thermal noise power generated in every Hz of bandwidth B. The amplitude and phase fluctuations contribute equally to the total noise. For two-port devices, which add noise figure (NF) dB[70], and known power input the phase noise floor is:

$$N_{phase} = 10\log\frac{kTNF}{2} = -177dBm/Hz + NF$$

$$\mathcal{L}_{\mathrm{dBc}}(\mathrm{f_m}) = 10\log\frac{kTNF}{2P_{in}}\left[\frac{\mathrm{dBc}}{\mathrm{Hz}}\right]$$

Power-to-phase noise is defined as the root-mean-square phase variation due to fractional optical power fluctuation. It is related to the laser amplitude noise conversion to electronic phase noise and arises due to the saturation and other nonlinearities in strongly driven photodiodes. The electrical pulse of the photodiode is distorted and broadened experiencing phase fluctuation due to the fluctuation of incident optical power[59]. The transmission of the photocarriers generated by the incident light across the photodiode is delayed.

2.5.3 Amplifier

The electronic regenerator did the inline amplification of signals when the optical fibre became the medium of choice for data transmission. These optical-electrical-optical (O-E-O) repeaters regenerate the optical signal by converting to the electrical, processing it and retransmitting it as an optical signal. In optical communication systems the repeaters are used to extend the reach by overcoming loss induced by optical fibre attenuation and

the optical signal distortion. The regenerator required synchronization to data amongst other problems such as distance limitation due to intermodal dispersion, chromatic dispersion at high bit rates and the system is expensive[73], [74]. In long haul systems the O-E-O repeaters were replaced by optical amplifiers. The noise characteristics of amplifiers was problematic and thus reduced the usefulness of the amplifiers. In 1987 the development of erbium-doped fiber amplifier (EDFA) at the University of Southampton was a major milestone for optical fibre transmission systems[75]. The atoms in the Erbium doped fibre are pushed from the ground to excited state using a pump source as seen in figure 2.10.

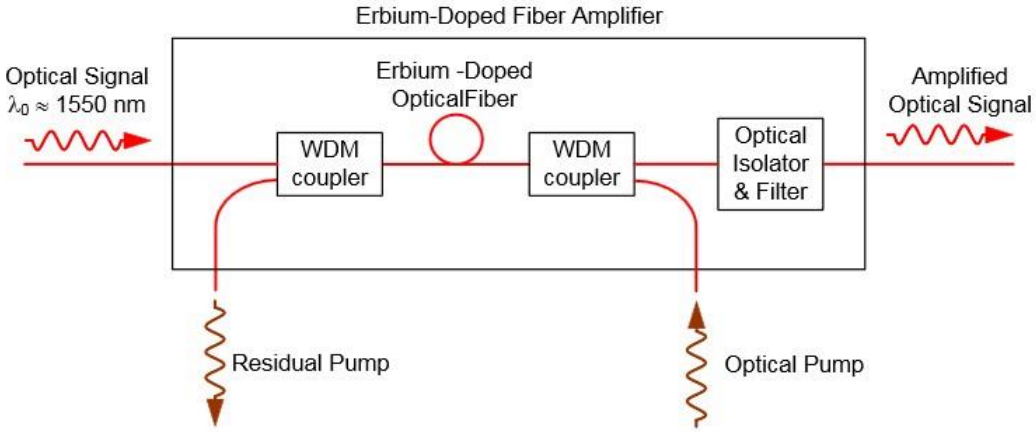

Figure 2.10: Schematic diagram of Erbium-doped fiber amplifier (EDFA)[76]

A transition of the atom from excited to ground state is triggered by the incoming signal photons. The atoms absorb the laser light and use it for spontaneous emission which amplifies the signal and adds noise as seen in figure 2.11.

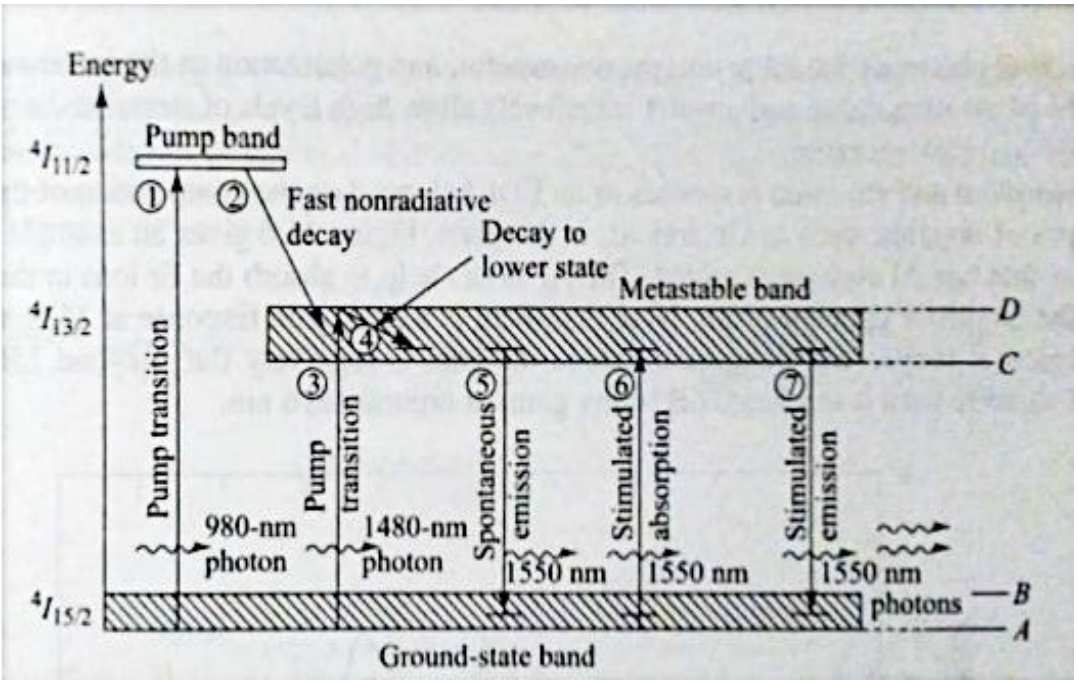

Figure 2.11: Erbium-doped fiber amplifier (EDFA) amplification mechanism

The EDFA improved availability and bandwidth with mass migration to 1550 nm. Long distance transmission without regeneration every 40 to 80 km using expensive electronics makes the EDFA cost efficient. The optical amplifier can amplify signals with different wavelengths simultaneously; this is used in WDM systems and can increase capacity of networks. The spontaneous emission of the EDFA which amplifies the signal adds noise and limits the performance of the amplifier in the distribution system[77]. For clock tone distribution done for a large number of antennas or at long distances, the received signal is weak and results in strong degradation in the stability. In such cases an optical amplifier is an essential component for retrieving a highly degraded signal time and frequency signal on the photodiode. An amplifier involved in the optical fibre link add its own noise, which makes a significant contribution to the link phase noise both close and far away from the carrier frequency. It affects the quality of the signal by adding amplified spontaneous emission noise ASE.

The ASE noise power can be due to signal and ASE noise interaction, and the noise power of the ASE noise. Amplifiers are characterized by gain, output power and noise figure[78]. These can be used to choose an amplifier and the operation conditions that

will help reduce the noise contribution. Operation conditions can affect the stability performance of the optical link. These are classified as: linear (the small signal gain) and saturated (gain decreases with increasing optical power) regime[79], [80]. The EDFA improved the noise characteristics and the noise performance can be characterized using noise figure. The noise figure of the amplifier can be expressed as:

$$NF = \frac{2P_{ASE}}{Ghv B} \quad (2.39)$$

where P_{ASE} is the average power of the spontaneous emission integrated on the spectral analyzer resolution B and G is the gain. In a link with an erbium-doped fiber amplifier (EDFA), additive noise is affected by the gain. High noise contribution by amplifiers occurs at the maximum gain. The phase fluctuation spectral density with amplifier noise contribution to the clock signal is expressed as:

$$S_{\phi} = \frac{2hvI^2{}_{PD}NF}{P_{in}} \quad (2.40)$$

relating the phase noise to the noise figure, photodiode current I_{PD} and the amplifier available optical power input P_{in}. Regardless of the optical power input the noise of the amplifier is present. The phase instability of the link can be reduced by operating the EDFA at higher optical input power level[63], [81], [82]. In order to achieve this requirement, the amplifier could be placed closer to the transmitter. This means boosting the signal before transmitting via optical fibre as opposed to amplifying before receiving.

In this chapter optical fibre waveguide theory was addressed. Two models were used to approach the propagation of light through a waveguide. Optical fibre design and the fibre types were studied with focus on the conventional transmission window and the parameters that affect the signal distribution such as attenuation, chromatic dispersion and polarization mode dispersion. In the sections to follow the use of light sources to generate an optical clock signal for stable reference frequency distribution over optical

fibre in telescope networks, and the effect the waveguide birefirence has on the clock phase stability, will be investigated.

Chapter 3

Phase Stability in the Optical Fibre Links for Telescope Networks

This chapter serves as a general introduction to the Square Kilometre Array telescope network. The development and architecture of the radio telescope is discussed for all its different phases. Timing and synchronization is an essential part of the project and thus the stability requirements for successful operation of the telescope will be addressed. There are different of sources of noise classified as short and long –term instability. In this work these will be measured and analyzed for the RF frequency reference clock characterized in the time and frequency domain as Allan Deviation and Phase noise, respectively.

3.1 Introduction To Square Kilometre Array Architecture

Square Kilometre Array (SKA) is an international science project in the radio astronomy field aimed at building the world's largest radio telescope with a square kilometre collective area. The system will be a configuration of thousands of radio telescopes deployed in an array achieving 50 times sensitivity and 1000 times fast survey speed than any existing telescope[83]. This will enable astronomers to monitor the sky exploring the origin of the universe, expanding our understanding on star and galaxy formation, galaxy evolution, and dark matter and dark energy. The SKA telescope will be co-located in two continents with telescopes in Australia and South Africa. The project will be built in two phases, with the first phase construction set to commence in 2017 for completion in 2023. SKA phase 1 consists of three individual elements: SKA1-low, SKA1 –mid and SKA1-survey.

SKA1-low and survey are located in Western Australia with the headquarters (responsible for operation and maintenance) and science data processing centre (collects digitized data sent from antennas to the centralized signal processing facilities on site) in Perth. The SKA1-low operation frequency ranges from 50 MHz to 350 MHz. The system

is a collection of ~ 250 000 antennas spread out between 911 low-frequency aperture array stations[84]. Most of the antennas are arrayed in a compact 1 km diameter core. The rest is arranged in 35 km diameter stations, consisting of 500 antennas configured into three equally spaced spiral arms. The SKA1-low telescope has a $\sim 0.4\, km^2$ collective area with 65 km maximum baseline between stations[85]. The system has 25% resolution, 8 times sensitivity and 135 times survey speed more than the LOFAR Low-Frequency Array, an instrument for performing radio astronomy in the Netherlands. The system conducts low radio frequency of pulsars, magnetized plasmas (in galaxy and intergalactic space), recombination lines and potentially extrasolar planets. It addresses observations of highly redshifted 21 cm hyperfine line of neutral hydrogen from the Epoch of reionization.

SKA1- survey will build up on to the existing Australian Square Kilometre Array Pathfinder (ASKAP). ASKAP consists of 36 antennas each 12 m in diameter with 6 km maximum baseline between any two antennas and a 700 MHz to 1.8 GHz operation frequency range. Sixty SKA1 antennas with 15 m diameter will be added making up the 96 antennas of SKA1-survey. The antennas are arranged within a 2 km diameter core with three spiral arms equally spaced expanding up to 25 km from the center. The system is capable to operate for frequencies up to 20 GHz. The telescope can survey large fractions of the sky mapping for spectral lines and continuums.

The SKA1-mid will be located in central South Africa, in the Karoo. Developing from the seven mid-frequency antennas making up Karoo Array telescope (KAT7) located in the core of the site operating since 2010. The KAT7 has been used to study Circinus X-1 an X-ray binary star system that includes neutron star containing x-ray jets normally found in black hole systems. The Karoo Array telescope has observed radio signals associated with hydrogen emission from a nearby galaxy (NGC3109) and Blazer (PKS 1510-089). It has peered into a small region (Hubble ultra deep field) of space in the constellation Fornax consisting of ~ 10 000 galaxies, the Hubble space telescope's deepest optical observation. The telescope is currently being developed to MeerKAT, "more of KAT", which will consist of 64 antennas with 13.5 m diameter concentrated in

a 1 km diameter and 8 km maximum baseline as shown in figure 3.1. The MeerKAT antennas are equipped with x-band (8- 14.5 GHz) receivers.

Figure 3.1: development of the MeerKAT telescope array and KAPB construction[86]

Each MeerKAT antenna houses four receivers and digitizers that capture the electromagnetic radiation and convert it to voltage signal, which is then converted to digital signal. The antennas are linked by optical fibre to the Karoo Array Processing Building situated at Losberg site complex, KAPB contains the central computing engine responsible for beamformation and astronomical data correlation. One hundred ninety SKA1 15 m diameter antennas operating up to 20 GHz will be added to make up the 254 antennas SKA1-mid telescope. The rest of the antennas will be randomly placed in a 3 km diameter connected to KAPB by optical with distance up to 100 km[1]. The major increase in the electrical equipment will bring about challenges such as radio frequency

interference producing devices which requires suppression or shielding. The KAPB houses an RFI shielded rack room. The KAPB can shield 70 MHz to 10 GHz range up to 100 dB.

Once the signals are digitized in each antenna the data is transferred to the correlator inside KAPB to form an image of deep space astronomical phenomena that the SKA is set out to explore. The high sensitivity of the telescope explores the continuum emitting objects, observing the radio pulsars and 21 cm hyper fine line of neutral hydrogen from the universe to moderate redshift. For high resolution images the antennas must be phase coherent with low levels of RFI so as not to reduce the detection sensitivity of the electromagnetic waves from cosmic radio sources[84][87]. The existence of coherent signals at every antenna could generate correlated radio frequency interference (RFI). Electrically small antennas with small collection area and very large field of view can be used as elements of phase array with beamformers performing the function of geometrical signal delay compensation to form a single output as shown in figure 3.2. For the SKA1-mid telescope array network coherence is maintained by distributing a synchronization and timing signal from the central processing point to each antenna via optical fibre. The highly stable RF time and frequency reference clock tone drives the digitizer, time-stamps the data and is used for monitoring and control functions.

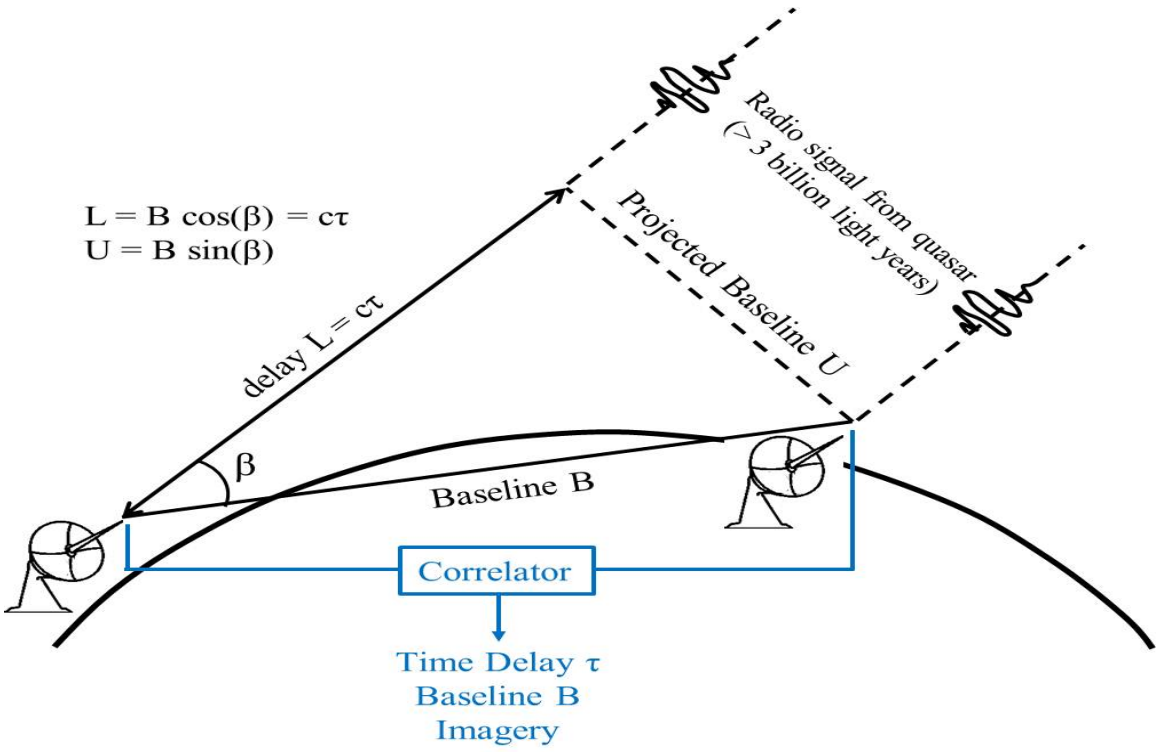

Figure 3.2: Geometrical signal delay compensation[88]

3.2 Synchronization And Timing For Telescope Array Network

There are two types of signals transported by the telescope array network: astronomical data signals that are sent from the remote antennas to the correlator and the timing signal distributed from the central processing point to each antenna. The astronomical data can be disseminated as either digital data as in SKA medium frequency array, or radio over fibre as proposed for SKA low frequency aperture array. The synchronization and timing signal in the SKA telescope network is required to meet a number of different but related requirements to ensure phase coherence for the array, provide high precision long-term timing, provide absolute time for antenna pointing, beam formation and data time stamping. It provides a reference sine wave from the clock. The synchronization and timing can come from an ensemble of clocks of a single centralized reference clock system linked to timing standards, distributing time, phase and frequency reference signal to the required level of accuracy[89], [90]. This and the stability requirements determine which clock system is to be used. The clock exhibits noise, a signal instability that consists of random noise processes and linear frequency drift.

The stochastic noise process is a short-term instability measured as phase noise (signal phase fluctuation in the frequency domain), it is integrated over the offset frequency of interest and is given in terms of timing (phase) jitter. The deterministic aging characterizes the long-term instability of the clock, it is expressed as Allan deviation computed from observing instantaneous frequency of the signal recorded over long periods of time. The typical clock references used are hydrogen maser, cesium and rubidium. The rubidium clock offers good short-term stability with 8×10^{-14} Allan deviation for averaging time of hour for a day frequency observation[91]. High performance cesium clock is less sensitive to environmental variations and is free from linear frequency drift with 3×10^{-14} Allan deviation for hour averaging time. Hydrogen maser has good stochastic noise properties with 1×10^{-15} Allan deviation for averaging time of hour[92]–[94]. The highly stable reference is used to determine the geographical delays of signals as offsets from the synchronization system to each antenna.

A centralized hydrogen maser reference clock system will be required for both South African and Australian sites. The centralized clock is an ensemble of up to three hydrogen masers to correct for drift and for redundancy. The clock tone is distributed

from the central point and transferred to each antenna via optical fibre to ensure phase coherence of the telescope array network. The clock performance test is based on how the signal travels down the optical fibre and still maintains a useful level of stability even with changes such as the environmental condition variations induced noise. Any difference in the delay measurements indicates phase error, instability in the RF distribution system.

Only 2% maximum sensitivity degradation is allowed with a 11° (~ 0.2 rad) RMS phase error[95]. For observation time interval from 1 s to a few min a phase coherence in the picoseconds range is expected, this corresponds to ~ 1 ps for the maximum observation frequency. The aim is to distribute the RF time and frequency reference clock signal to the remote sites from the central point over optical fibre with an RMS jitter close to 1 fs. The MeerKAT and SKA1 telescope both rely on the highly stable and precise clock tone to be distributed from the KAPB central processing point via optical fibre to each antenna. The instability is determined by the sources of phase and frequency fluctuations subject to the clock signal along the transmission link and the receiver installed on the focus or within pedestal of antenna exposing it to harsher environmental conditions than the temperature regulated KAPB. The optical fibre is buried beneath the earth surface to shield it from temperature fluctuations and reduce environmental variation induced instability. The clock signal phase stability is nonetheless still susceptible to optical fibre birefringence and polarization fluctuation. Optical fibre birefringence introduces instability on the clock phase as the polarization of the lightwave fluctuates. For successful operation of the MeerKAT the instability should remain within several hundred femtoseconds RMS jitter with the requirement being more stringent for the overall SKA telescope, a few fs jitter.

3.3 SKA Stability Requirements

The SKA RF clock distributing system should be capable of transmitting a highly accurate time, phase and frequency reference signal over long optical fibre path length up to 100 km, whilst maintaining a certain level of stability. Optical fibre network in clock reference signal distribution for timing and synchronization is a suited option due to the

low attenuation, high bandwidth and immunity to electromagnetic interference of the medium, however optical fibre introduces excess phase instability. Similar transfer methods are being used in projects such as MERLIN and ALMA. The Multi Element Radio Linked Interferometer Network (MERLIN) is an array of radio telescopes spread across the United Kingdom (central and Northern England) with a maximum baseline of 217 km. To achieve coherence a 1486.3 MHz oscillator locked to a 5 MHz frequency standard is transmitted over fibre to the 7 stations that make up the telescope network. For 1550 nm intensity modulated laser transmitted over 110 km shielded fibre the distribution stabilities of 1ps over 1s, 2 ps over a minute and 4 ps over 10 minutes have been obtained as demonstrated in [3]. Atacama Large Millimeter Array (ALMA) situated in Northern Chile desert is a 64 antennae array with a maximum baseline of 20 km. The distribution system phase coherence requirement is 0.1 ps in 1 s stability for a reference signal distributed over 15 km buried fibre[96]. The methods both rely on a common frequency standard and phase locked loop to perform round-trip phase corrections for the temperature induce instability, variable delay between antennas and the central processing point[97].

The RF time and frequency reference distribution system stability depends linearly on the observing frequency and the different distribution lengths. There are three frequency clock operations for the SKA telescope with varying baselines: MeerKAT L-band at 1.712 GHz with 12 km maximum baseline, 100 km maximum baseline SKA1-mid operating at 14.5 GHz and the SKA phase 2 1000 km spiral arms at 20 GHz clock. The clock stability budget for the SKA telescope MeerKAT L-band and MeerKAT X-band (SKA1-mid) is 18.6 ps and 2.2 ps timing jitter respectively. The timing jitter budget for the maximum observing frequency is 1.6 ps with a long-term frequency stability requirement of 3.2×10^{-15} for 1000s averaging time[84], [87]. The clock stability 0.2 rad phase error requirement for each observing frequency increases with optical fibre path length as seen in table 3.1.

Table 3.1: clock stability budget for MeerKAT and SKA telescope [29]

	Clock (GHz)	Clock Stability Budget (ps)	PMD penalty for L=12 km [MeerKAT] (ps)	PMD penalty for L=100 km [SKA Phase1] (ps)	PMD penalty for L=1000 km [SKA Phase2 spiral arms] (ps)
MeerKAT L-Band	1.712	18.6	0.20 (1.1% of budget)	0.58 (3.1% of budget)	1.84 (9.9% of budget)
MeerKAT X-Band/ SKA Phase1 mid	14.5	2.2	0.20 (9.2% of budget)	0.58 (26.5% of budget)	1.84 (83.8% of budget)
SKA Phase2	20	1.6	0.20 (12.7% of budget)	0.58 (36.6% of budget)	1.84 (115.6% of budget)

The phase instability introduced by the optical fibre depends more strongly on the environmental conditions in which it is installed than it does the link length. A lower level of vibration induced phase instability is expected on a long fibre installed in the Karoo than a short optical fibre in a metropolitan environment.

Round-trip corrections might not be necessary for short links where the temperature variation may be reduced significantly by using a thermally controlled laser and burying the fibre beneath the ground[97]. There is an active delay compensation required for links as short as 1 km buried at shallow depths. The environmental condition variation of the optical fibre path length affects the phase stability of the reference signal. The temperature induce instability is a limiting factor in the Karoo which experience harsh conditions. The physical length of the optical fibre changes with fluctuating temperature levels by a factor 5 ppm/℃ which affects the propagation delay. Exposed optical fibre sections are subjected to temperature changes up to 10℃ from direct sunlight in less than 30 min. These can be diurnal or seasonal temperature changes[98]. A 12 km optical fibre link in such condition would experience a 600 mm path length change. The temperature fluctuation can be reduced by a factor of 1000 by burying the optical fibre 1 m below the earth's surface. This is active compensation for the phase fluctuation and frequency drift introduced by temperature variation related delay due to optical fibre length change.

3.4 Phase instability in Optical Fibre Links for Telescope Networks

The performance of the RF time and frequency reference clock tone is characterized by accuracy and instability. A periodic voltage signal is generated by the clock whose ideal frequency is defined by a number of oscillations per second. The clock tone contains noise, a combination of generated signals and nondeterministic noise. These random and systematic effects result in a signal with offsets compared to the nominal frequency. Accuracy is used to specify how the systematic offset frequency in the RF clock signal can be quantified. It is an uncertainty, a measure (proper summation) of the estimates of various systematic offset frequency and random noise. Every RF source exhibits frequency instability, which includes random noise (thermal and shot noise), modulation (both intended and incidental), and other undetermined origins that affect the output[99]. The random noise relates the signal to noise ratio of the clock, the power at nominal frequency to the offset frequency power. Systematic noise is the slow deterministic changes in the frequency observed over time.

Instability is a measure of how much the frequency fluctuates, the degree by which the same frequency value is produced over a specified period of time[100]. This decreases the stability of the frequency of the signal expressed as a perfect sine function. The frequency instability of the RF clock can be classified into two basic types: short-term instability and long-term instability. Short-term instability refers to the random fluctuations where frequency is observed over several seconds to few minutes sampling time. Long-term instability is the systematic effect, the deterministic frequency drift due to changing environmental conditions surrounding clock and the frequency aging due to changes in the components that make up the clock. The generated noise signals can be described in the time and frequency domain.

In the frequency domain it is characterized as phase noise obtained from the power spectral density of the signal measured by a spectrum analyzer. Power spectral density is the graphical representation of the signal fluctuations in the frequency domain. Phase noise is the ratio of the signal power at the nominal frequency to the offset power in a 1 Hz bandwidth. In the time domain the frequency fluctuation is characterized as an Allan variance, a two-sample frequency variance[101], [102]. This is based on the instantaneous frequency deviation from the nominal frequency with time. The frequency

deviation is normalized to the nominal frequency (fractional frequency) and reported as a function of the averaged observation time. The phase noise can be converted to phase jitter, integrated phase noise over a range of offset frequency and presented in the time domain. The graphical presentation of the signal frequency is used to characterize the types of noise present in the RF clock tone and source of instability.

3.5 Signal Fluctuation

3.5.1 Time Domain

A signal generator produces a signal that changes with time as the amplitude changes with the phase. Figure 3.3 shows the ideal instantaneous output voltage from signal generator which is undisturbed and can be described by a perfect sine wave expressed as:

$$V(t) = V_o \sin[2\pi v_o t] \qquad (3.1)$$

where V_o is the nominal amplitude and v_o the frequency produced by the clock at time t. The nominal phase of the signal at a given time is given by:

$$\theta(t) = 2\pi v_o t \qquad (3.2)$$

The nominal angular frequency of the clock is obtained from the time derivative of the phase; this comes with the natural relation between the phase and frequency:

$$\omega_o = \frac{1}{2\pi}\frac{d\theta(t)}{dt} \qquad (3.3)$$

This equation expresses the relationship between phase and frequency stability. Frequency stability is the degree to which an oscillating signal produces the same value of frequency for any interval over a specified period of time[103]. This is mainly used for comparison between signal generators.

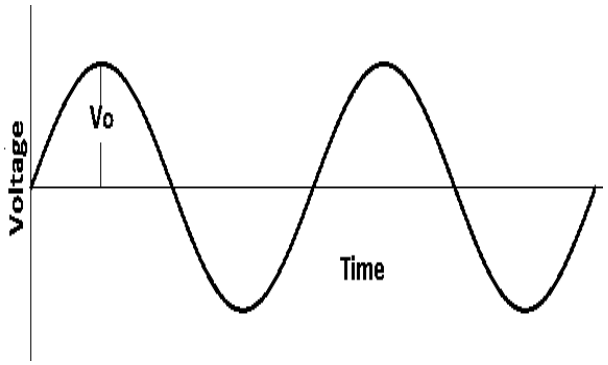

Figure 3.3: ideal output voltage of an unperturbed RF clock signal[104]

The signal is undisturbed, there is no fluctuation in the frequency and the phase is not shifted. There is no source of noise, signal is highly accurate and stable.

In real situations the output signal is perturbed. The RF clock tone frequency has deviated from the nominal as seen in figure 3.4. There are many sources of noise in the signal generator including contribution from the components that make up the oscillator and the surrounding environmental conditions. The fluctuation of peak value of voltage results in amplitude instability. Phase instability is due to zero crossing fluctuations[105]. The frequency instability results from the period of signal fluctuating. Frequency instability is the spontaneous and/or environmentally caused frequency change within a given time interval. If a carrier is considered a dc, the frequencies measured relative to it are the offset noise or Fourier frequencies. The output voltage of the signal generator can be expressed as:

$$V(t) = [V_o + \epsilon(t)] \sin[2\pi v_o t + \phi(t)] \qquad (3.4)$$

Where $\epsilon(t)$ amplitude fluctuation and $\phi(t)$ phase fluctuation of the signal, deviation from the nominal. The amplitude deviation is assumed to be substantially smaller than the nominal value. These instabilities are directly related since period thus the frequency, amplitude and phase of a signal are related

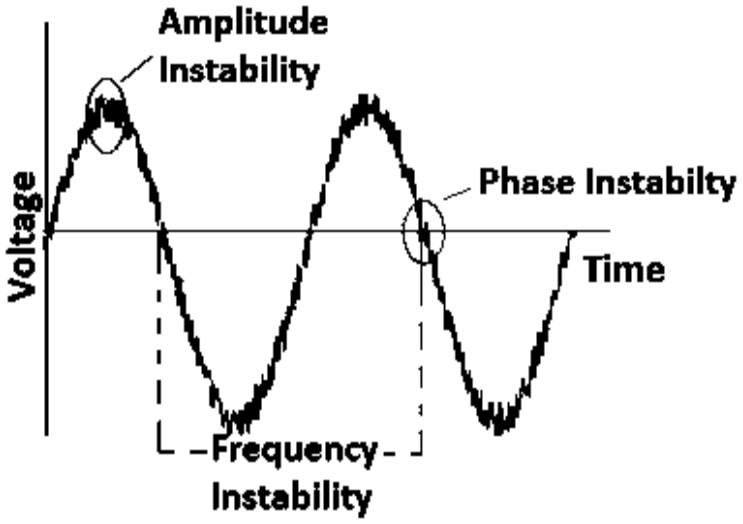

Figure 3.4: The output voltage of noise infested RF clock signal[104]

The amplitude fluctuation can be neglected since RF time and frequency reference signal distribution systems are more interested in zero crossing levels. The instantaneous frequency of the signal is defined as:

$$\upsilon(t) = \upsilon_o[1 + \frac{1}{2\pi\upsilon_o}\frac{d\phi(t)}{dt}] \qquad (3.5)$$

The second term is the fractional frequency fluctuation of the RF clock signal with time. It relates the frequency deviation from nominal to the phase fluctuations and can be expressed as:

$$y(t) = \frac{1}{2\pi\upsilon_o}\frac{d\phi(t)}{dt} = \frac{v(t)-\upsilon_o}{\upsilon_o} \qquad (3.6)$$

Frequency fluctuation is the instantaneous frequency deviation from the nominal frequency, it corresponds to the fluctuation in the period of the signal generator oscillations ($v = \frac{1}{T}$). A signal counter is used to measured the frequency fluctuations of the RF clock, it uses a reference oscillator (considered to have a zero phase instability term) sensing the zero crossing of the output voltage analyzing the phase and period fluctuations and reporting back the instantaneous frequency over a desired time period at defined intervals[106].

The phase instability can be expressed in terms of time fluctuation defined in units of time as:

$$x(t) = \frac{\phi(t)}{2\pi v_o} \qquad (3.7)$$

Since x is a random quantity it is described by statistical parameters. This parameter can represent any parameter disturbed by noise. The random phase fluctuation in the time domain can be described by a distribution function as seen in figure 3.5.

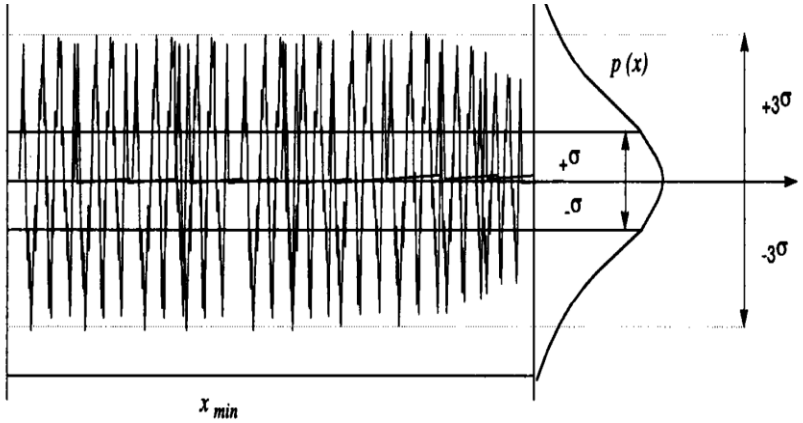

Figure 3.5: RF clock signal random phase fluctuation in the time domain[107]

3.5.2 Frequency Domain

The frequency domain is the commonly used measure for characterizing clock tone instability. It is analyzed by looking at the power distribution of a given signal. The technique takes a Fourier transform of the signal, converting the universal time domain representation of the signal to a more localized signal. A power spectral density S_x can be used to represent the total noise of the signal resulting from the amplitude and phase deviation from nominal, it does not indicate the contribution of each fluctuation[108], [109]. In the frequency domain a RF clock signal instability is characterized by the power spectral density of phase fluctuation.

The undisturbed signal in the frequency domain is a single spectral line located at the frequency of the generator as seen in figure 3.6. It corresponds to the perfect sinusoidal wave (equation 3.1) and includes all the energy of the signal. In the frequency domain the signal is represented by a delta function:

$$S_x(f_m) = \frac{{V_o}^2}{\delta(f_m - f_o)} \qquad (3.8)$$

The equation is defined for Fourier frequency f_m from zero to infinity. It is the total power of the signal.

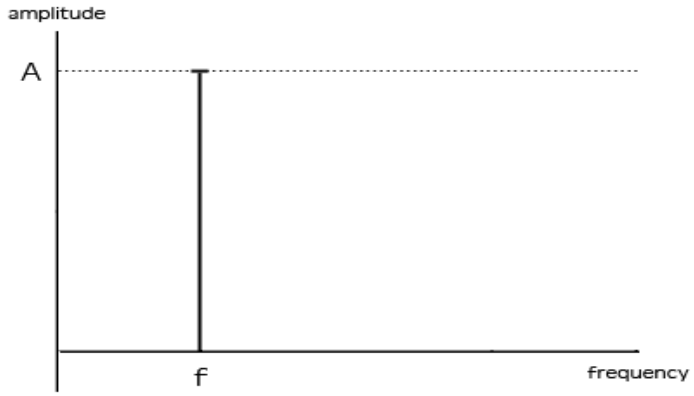

Figure 3.6: ideal RF clock signal in the frequency domain[110]

In real situations the output signal is perturbed in amplitude, frequency and phase as depicted in figure 3.7. The perturbed signal produces other frequencies f_m at every given instant, Fourier frequencies measured as offset from the carrier frequency. It has several spectral lines spread out on either sides of the carrier frequency as seen in figure 3.7. The time taken to produce f_m relative to f_o is the probability density[111]. The total noise power is obtained by integrating the noise power in a defined bandwidth B over the frequency.

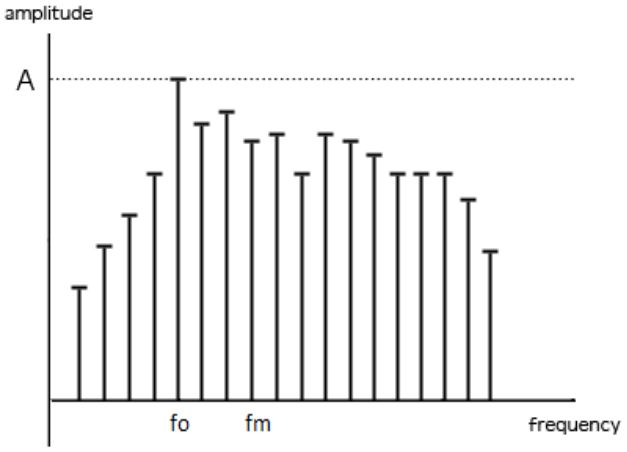

Figure 3.7: disturbed RF clock signal in the frequency domain[110]

The power spectrum displays upper sideband and lower sideband power at offset frequencies above and below the carrier frequency respectively. The power sidebands result from signal amplitude and phase deviating from the nominal values. The noise components in the signal cause broadening of the power spectrum around the carrier frequency.

The power spectral density of amplitude, phase and frequency fluctuation is a noise power distribution as a function of the Fourier frequency an offset away from the carrier given as:

$$\text{Amplitude noise } S_{\epsilon}(f_m) in \left[\frac{Volts^2}{Herts}\right]$$

$$\text{Frequency noise } S_{\nu}(f_m) \quad \text{in } \left[\frac{Herts^2}{Herts}\right]$$

$$\text{Phase noise } S_{\phi}(f_m) \quad \text{in } \left[\frac{Radians^2}{Herts}\right]$$

Spectral density is a plot of the signal RMS power at a specified bandwidth as a function of Fourier frequency.

The power spectral density of phase fluctuation provide immediate estimation of the spectral purity, signal frequency instability. The noise power integral over the defined offset frequency range for the specified total noise power[112]. The phase fluctuation that occurs on a signal is analyses as a low frequency continues spectrum defined for positive offset frequencies in a 1 Hz bandwidth, the single sideband phase noise spectrum as shown in figure 3.8.

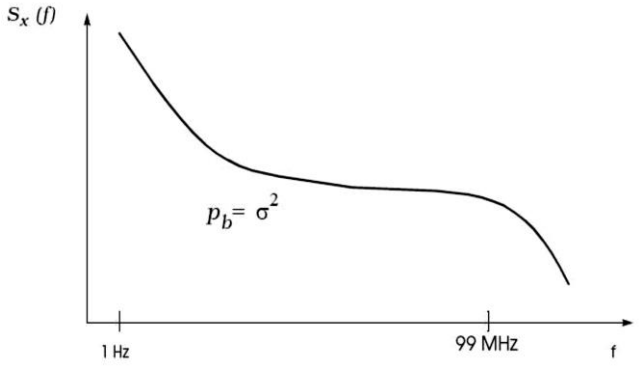

Figure 3.8: single sideband total noise spectrum[107]

3.6 Instability Characterization

Signal instability is the fluctuation of the frequency of the RF clock. It is how close the frequency of the signal remains to the nominal value over various time periods. The frequency fluctuation of the signal is affected by the random and deterministic noise. The amount of random fluctuations and drift occurring on a RF clock tone is based on the stability of a highly accurate and precise reference oscillator. The frequency/phase instability is categorized into two forms: short–term and long-term instability, these reflect the signal's sensitivity to temperature, vibrations, power supply, variation, humidity and atmospheric pressure. Short-term instability is the measurement of the random fluctuation of the unwanted modulation over a short sampling time. It reflects the uncertainty of the RF clock at a given instant in time. Long-term instability is an analyses of the progressive change in the frequency of a signal, the frequency drift. The drifting process is predicted based on the past events. The smaller the frequency drift, the better the performance of the system.

3.6.1 Short-Term Stability

Short-term stability is referred to as the random fluctuations that are related to the signal-to-noise ratio of the system. It represents the phase modulation of the clock output signal[113].It describes all the fast fluctuations about the nominal frequency, these changes occur in duration less than a few seconds as shown in figure 3.9. These are small random processes that change very rapidly and result in the clock signal spectrum spreading[114]. The short-term stability measurements are dependent on the measurement interval with a large peak-to-peak jitter obtained for longer observation time. In this period the oscillator stability is sufficient for the phase to stay in the $(-\pi, \pi)$ interval[115]. It is measured at offset frequencies greater than 1 Hz.

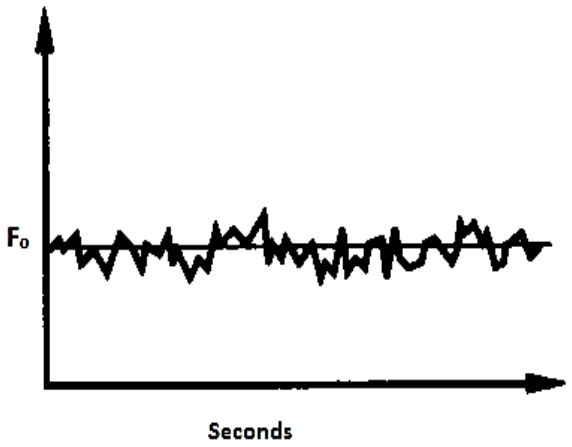

Figure 3.9: Clock signal short-term frequency fluctuation[116]

In the frequency domain it is expressed as Phase noise measured using a narrowband fast Fourier transform (FFT) spectrum analyzer, which characterizes the shape of the clock signal power spectrum[117].

3.6.2 Long-Term Stability

Long-term stability is referred to as the deterministic change in the signal that includes random-walk frequency noise. It describes the slow changes of the clock signal from nominal value over time[114]. It can be treated as systematic instability as it is derived from slow processes such as frequency drift, clock aging and effects of the environmental conditions like temperature variation. Aging is the change of the RF signal frequency that occurs due to aging of the elements or the materials of the electronic components of the oscillator. Drift is the frequency change due to aging and temperature variations is characterized as the long term instability[118]. The RF signal frequency can drift more than a half-cycle of the carrier frequency leading to indefinite phase. It can be used to describe the phase noise close to the carrier.

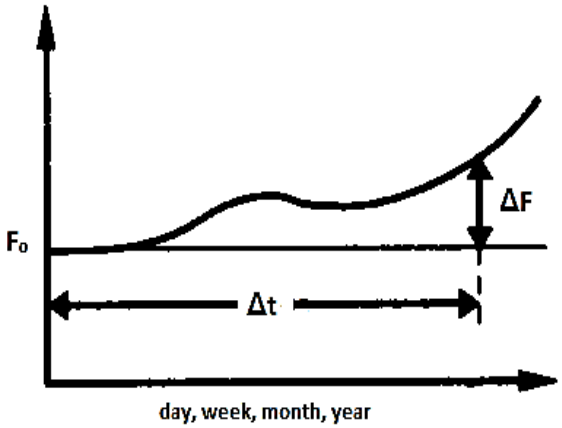

Figure 3.10: Clock signal long-term frequency drift[116]

Long-term stability is expressed in parts per million per specified time span (hour, day, week, month or year) describing the percentage by which the frequency may drift (frequency fluctuation normalized to the nominal frequency)[119].

A hydrogen-maser clock has higher frequency stability compared to a Cesium clock from second to second, while Cesium has a better long-term stability. Quartz-oscillators are highly stable in the short-term, but drift in frequency. They do not the have excellent long-term frequency stability of atomic clocks.

3.7 Phase Noise and Allan Deviation

3.7.1 Single Sideband Phase Noise

The signal frequency instability can be characterized by measuring the phase fluctuation. The method is useful for determining short-term instability of the RF reference signal used in the telescope network for synchronization of the remote antennas. The phase fluctuation is measured with respect to a lower phase noise frequency reference oscillator. Phase fluctuation creates noise sidebands on either side of the carrier frequency, this attenuates the power in the carrier as it is spread to the sidebands as noise power. The phase noise is expressed as a power spectrum density of phase fluctuation, the mean square of the phase fluctuation at Fourier frequency offset from the carrier for a defined bandwidth. The spectral density is the total noise distribution in the frequency domain. The distribution includes both the amplitude and phase fluctuations. It is the power obtained from the voltage measurement of a signal[120]. An electrical spectrum

analyzer is used to measure clock output amplitude signal as a function of frequency, resonance curve. The frequency of the RF clock must be in the range of the measuring instrument. The signal under test is mixed down to direct current by a reference signal from the electrical spectrum analyzer local oscillator using a double balance mixer. The mixer multiplies the two signals which are 90° out of phase[121]. The mixer products are the sum and difference of the frequencies. The quadrature suppress the amplitude modulated signals and the phase modulated remains[122]. If the sum of frequencies signal is filtered out, the output voltage signal from the mixer is proportional to the phase fluctuation:

$$\Delta V(f_m) = K_d \Delta\phi(f_m) \qquad (3.9)$$

where K_d is the mixer phase sensitivity. It depends on the input powers and frequencies. One of the requirements is that the voltage measurement be squared[2]. The power on both sidebands of the carrier is measured. The plot is double sided as the Fourier frequency ranges from negative to positive infinity offset from the carrier. The random phase fluctuation is referred to as the phase noise. The deterministic phase fluctuation is known as spurious noise. Discrete- frequency noise is a dominant observable probability due to power line frequency, vibrational frequency or frequency chirping. It appears as a distinct spectral line and could have its own spectral density as seen in figure 3.11. Phase noise quantifies the noise power at given offset f_m from the carrier normalized to a 1 Hz bandwidth. Phase noise is one of the most significant measurements of the RF clock, there are phase noise requirements that have to be taken into account during the design and construction of the telescope network.

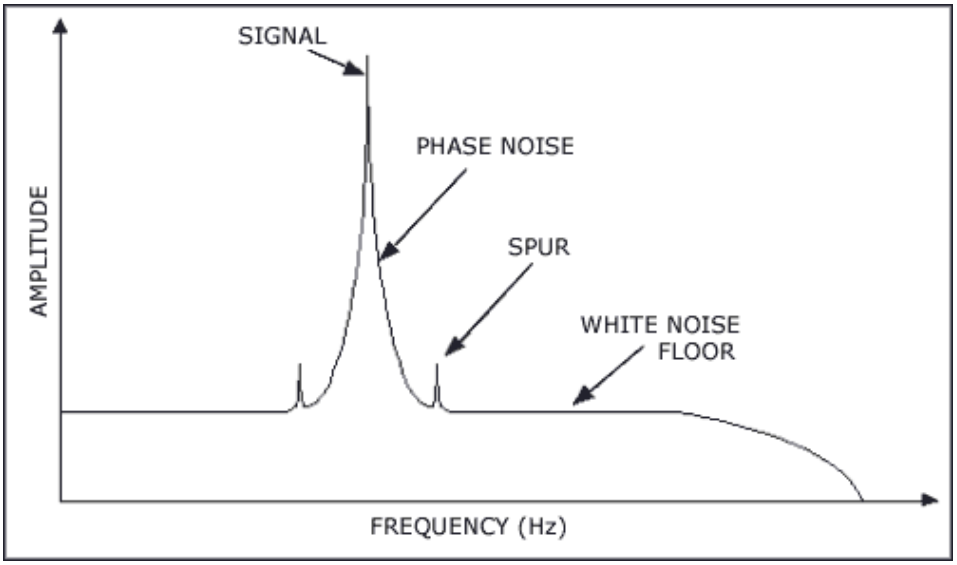

Figure 3.11: power spectrum density of a real RF clock tone over a range of Fourier frequency[124]

At offset frequencies very close to the nominal frequency it is difficult to separate the noise from the power. At offset frequencies very far away from the carrier, the power of the signal is low in the specified bandwidth.

The amplitude fluctuation effect on the output signal is reduced, this is achieved by operating the mixer in saturation mode. Neglecting the amplitude contribution, the phase fluctuation spectral density can be expressed as:

$$S_{\phi}(f_m) = \frac{\Delta\phi_{rms}{}^2(f_m)}{B}\left[\frac{\text{Radians}^2}{\text{Herts}}\right] \qquad (3.10)$$

The spectral density of the phase fluctuation is a normalized frequency measure of the phase variation sidebands.

The single sideband is commonly used to characterize the instability of the signal, it is measured for the positive offset frequencies (above the nominal frequency). It is used to quantify the phase fluctuation on the signal with small deviation $\Delta\phi$ <<0.1 rad[122]. The single sideband phase noise is expressed as:

$$\mathcal{L}_{\phi}(f_m) = \frac{1}{2}S_{\phi}(f_m) = \frac{1}{2}\frac{\Delta\phi_{rms}{}^2(f_m)}{B}\left[\frac{Radians^2}{Herts}\right] \qquad (3.11)$$

with

$$\frac{P_b}{P_s} = \frac{1}{2}\frac{\Delta\phi_{rms}{}^2(f_m)}{B} \qquad (3.12)$$

This is based on the assumption that single sideband phase noise is half that of the double sideband phase noise (the upper and lower power side bands are equal at given absolute

Fourier frequencies away from the carrier) because of the symmetry of the density close to the nominal frequency. The bandwidth should be narrow to produce a trace that is flat within the bounds of the bandwidth, whilst avoiding the presence of spurious noise within the bandwidth and wide enough to provide smoothing (enough integration)[109], [123]. The integrated phase noise from far offset frequencies to the f_m is very small. Single sideband (SSB) is the ratio of the power density at an offset frequency from the carrier normalized to 1 Hz bandwidth, to the total power of the carrier signal.

$$\mathcal{L}_{\mathrm{dBc}}(\mathrm{f_m}) = \frac{\mathrm{P_b}}{\mathrm{P_s}}\left[\frac{\mathrm{dBc}}{\mathrm{Hz}}\right]$$

The phase noise is given in units $\frac{dBc}{Hz}$ at an offset frequency f_m with c index implying the power is related to the carrier.

In logarithmic scale

$$\mathcal{L}_{\mathrm{dBc}}(\mathrm{f_m}) = 10\log\mathcal{L}_{\phi}(\mathrm{f_m})\left[\frac{\mathrm{dBc}}{\mathrm{Hz}}\right] \qquad (3.13)$$

The direct measurement of single sideband phase noise from a spectrum analyzer not resolved to 1 Hz (without noise cancellation) is obtained by subtracting the power at the power of the carrier from the desired offset frequency and an additional subtraction of converting from present bandwith to 1 Hz.

The single sideband phase noise is plotted as a function of the Fourier frequency. The phase noise curve is approximated by a number of line segments. The one sided spectral density plot contains random walk of frequency, flicker of frequency, white of frequency, flicker of phase and white of phase as seen in figure 3.12, which can be used to identify the source of instability on the signal.

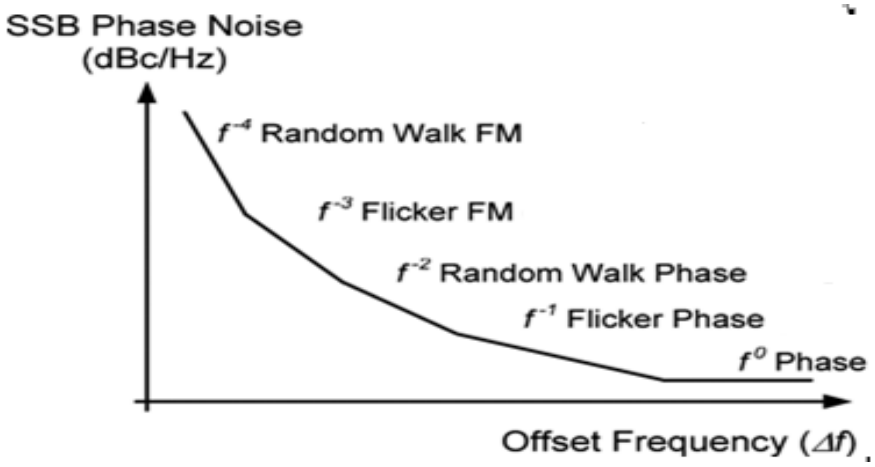

Figure 3.12: single sideband phase noise of a signal[124]

For RF time and reference signal distributed to remote antenna the signal instability is commonly expressed as phase jitter. Jitter species the magnitude of disturbance on a signal[8], [16]. SSB phase noise can be converted to phase jitter used to calculate the signal to noise ratio degradation. Jitter analyses the phase deviation from nominal value due to timing uncertainty. Integrating the phase noise power over a frequency range of interest offset frequency) results in phase jitter. The area under the phase noise curve:

$$\phi_{jitter} = \sqrt{\int_0^{\infty} S_{\phi}(f_m) df_m}[\text{Radians}] \qquad (3.14)$$

This is the phase difference of the disturbed signal and the ideal signal. It relates the phase noise to the clock performance. Single sideband phase noise curve is approximated by a number of individual line segments with different slopes[12]. The area under each individual line segment yields different power ratio, whose sum is the integrated phase noise power (A) given in dBc units. Once the phase noise power is known it can be converted to phase jitter:

$$\phi_{jitter} = \sqrt{2 \times 10^{\frac{A}{10}}}\,[\text{Radians}] \qquad (3.15)$$

Timing jitter in seconds is obtained by dividing the phase jitter by $2\pi v_o$ the nominal angular frequency. The jitter is a result phase fluctuation of the clock tone associated with thermal noise and drift. For successful operation of the MeerKAT the clock signal should remain within several hundred femtosecond jitter, the requirement is more stringent for the SKA telescope with a stability of few femtoseconds.

3.7.2 Non-Overlapping Allan Deviation

The characterization of the RF frequency reference signal instability in the time domain measures the frequency over a given interval. The signal instability is analyzed as fractional frequency fluctuation and characterized by Allan variance a two-sample frequency variance. It is a prediction of the expected frequency over an observation period. It can be used to measure the instability at offset frequencies lower than 1 Hz away from carrier for long-term instability[126]. It conveys details of the sources of instability on the RF clock and the factors that affect the signal. The Allan variance characterizes both the random and deterministic variations. The environmental effect on the clock signal is estimated by the random fluctuations. Characteristics and specifications of the RF reference clock are important for telescope network design to ensure the stringent requirements are met. For successful operation of the MeerKAT and SKA telescope an Allan deviation of 1.3×10^{-14} at 100 seconds averaging time is required[87].

The single sideband power spectral density of fractional frequency can be used to measure the clock stability. The power spectral density of phase and that of fraction frequency fluctuation are related by:

$$S_y(f_m) = \left(\frac{1}{2\pi f_o}\right)^2 (2\pi f_m)^2 S_\phi(f_m) = \left(\frac{f_m}{f_o}\right)^2 S_\phi(f_m) \left[\frac{Herts^2}{Herts}\right] \quad (3.16)$$

Fractional frequency is related to the power spectrum of the normalized frequency deviation ($S_y(f_m) \sim {f_m}^{\alpha}$) where α is the spectral density coefficient[127]. Allan variance can be calculated from the power spectral density of the fractional frequency fluctuations, thus allowing for the long-term signal instability to be characterized in the time domain.

A number of instantaneous frequency values are measured over a specified time period at fixed sampling time intervals τ_o seconds. A frequency/signal counter built into the electrical spectrum analyzer samples the frequency of the clock tone under test and the instantaneous frequency measurement data is logged into a computer. Fractional

frequency is obtained from the sample data using equation 3.6. The fractional frequency can be averaged over different time intervals $\tau = n\tau_o$ where n > 0[101], [105]:

$$\bar{y}_i = \frac{1}{\tau}\int_{t_i}^{t_{i+\tau}} y(t)dt \qquad (3.17)$$

Fractional frequency fluctuation is a dimensionless deviation from the nominal value and its integral gives time deviation of a signal as a function of phase deviation as show in figure 3.13.

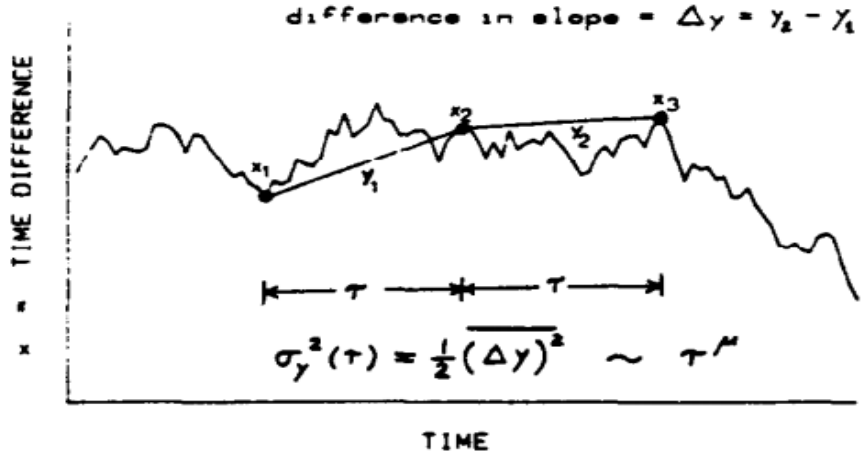

Figure 3.13: time deviation and fractional frequency fluctuation as a function of observation time[128]

It is used to approximate the Allan variance:

$$\sigma_y{}^2(\tau) = \frac{1}{2(M-1)}\sum_{i=1}^{M-1}(\bar{y}_{i+1} - \bar{y}_i)^2 \qquad (3.18)$$

The statistical sample assumes there is no dead time between samples and takes a difference of two adjacent measurements $\bar{y}_{i+1}$ and $\bar{y}_i$ for large observation time for M number of data points. Dead time results in loss of coherence between data point, and depending on its length white phase noise may be detected as white frequency noise. Longer observation time improves the accuracy of the prediction and quality of the analysis. By choosing different averaging time, a new data set from the total number of sample points in a data set divided by the number of points within the new averaging time (M/n) can be formed and different Allan variance values can be obtained from the same data set M[129]. The number of points plotted depends on the length of the data set M

and averaging time τ. The averaging time must be bigger than the sampling time interval, resolution. Low resolution can hide significant effects of instability on the signal.

Allan variance can be modeled by a sum of four different power laws:

$$\sigma_y{}^2(\tau) = \sum_{\mu=-2}^{1} p_\mu \, \tau^\mu \qquad (3.19)$$

The square root of Allan variance is Allan deviation $\sigma_y(\tau)$. According to the power law spectral can be approximated as $\sigma_y(\tau) \sim \tau^{\frac{\mu}{2}}$[130]. The Allan deviation curve is made up of individual line segments. It is used to predict how far the clock frequency is likely to drift one interval based on the averaging interval observed. The signal stability may increase, decrease or remain the same as the averaging time is shortened or lengthened causing the curve to go in an upwards, downwards or flat pattern.

The log-log plot of Allan deviation as a function of averaging time exhibits the five common types of noise estimating the value of μ as shown in figure 3.14. For $\mu = -2$ one cannot differentiate between the white phase noise and flicker phase noise (in the frequency domain α is 2 and 1 respectively) as they are on the slope [18],[21]. The different types of noise and the corresponding estimated exponentials in both the frequency and time domain are illustrated in table 3.2.

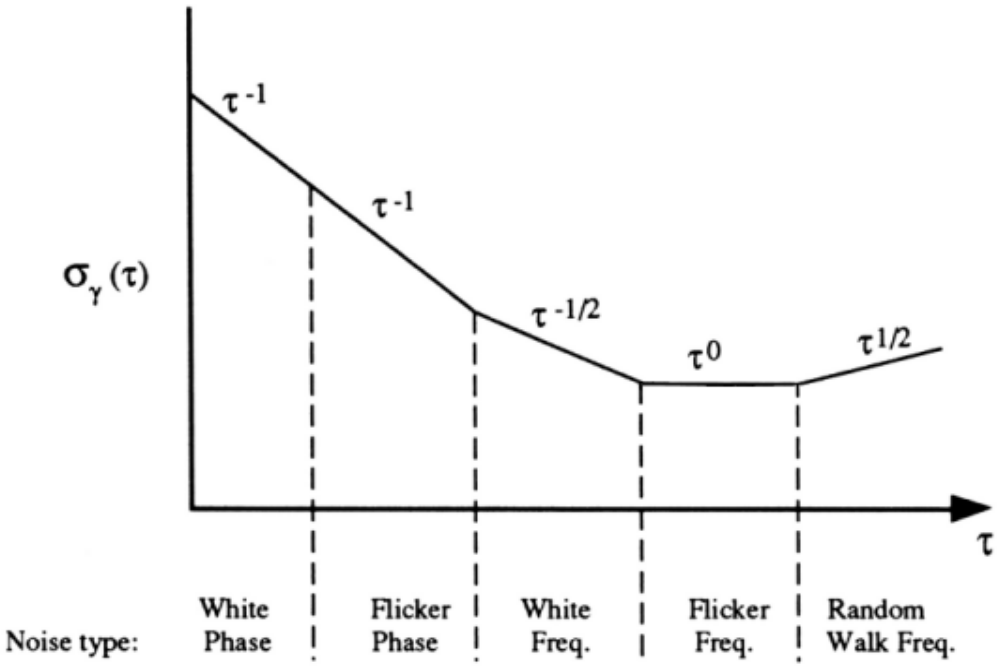

Figure 3.14: log-log plot of non-overlapping Allan deviation as a function of averaging time

The five noise processes that make up the phase noise with characteristics based on the dependence to frequency (time) for phase noise, spectral density of fractional frequency fluctuations and Allan deviation are given as[131],[132]:

Table 3.2: power noise processes as a function of averaging time and the offset frequency[21]

	L(f)	$S_y(f)$	$\sigma(\tau)$
Random walk frequency	f^{-4}	f^{-2}	$\tau^{0.5}$
Flicker frequency	f^{-3}	f^{-1}	τ^{0}
White frequency	f^{-2}	f^{0}	$\tau^{-0.5}$
Flicker phase	f^{-1}	f^{1}	τ^{-1}
White phase	f^{0}	f^{2}	τ^{-1}

Each process identified in the phase noise plot should also be identifiable in the Allan deviation log-log plot.

The noise processes can be described in the following manner[101], [106], [123], [133]:

1) Random walk of frequency

The $\frac{1}{f^4}$ slope noise is difficult to measure as it is very close to the carrier. It is related to the signal generator's physical environment. If random walk of frequency is the dominant feature of the spectral density of phase or fractional frequency fluctuation plot then mechanical shock, vibration, temperature, or other environmental effects may be causing "random" shifts in the carrier frequency

2) Flicker of frequency

The$\frac{1}{f^3}$ sloped noise is common in high-quality signal generators, but may be disguised by white of frequency $\frac{1}{f2}$ or flicker of phase $\frac{1}{f}$ in lower-quality signal generators. It is related to the power supply, parts used for the electronic and environmental properties. All semiconductors exhibit flicker noise. The frequency stability in the time domain is constant over an extended observation time period.

3) White of frequency

This type of noise is common amongst passive resonant generators, it gets better with time until converting to flicker of frequency.

4) Flicker of phase

The$\frac{1}{f^1}$ sloped noise is introduced by noisy electronics such as amplifiers which brings the amplitude of a signal up to a usable level and can be reduced by careful design and critical component selection (link performance optimization).

5) White of phase

Broadband phase noise is dominant in passive components. White of phase is flat and can be reduced by narrow-band filtering at the output. It is commonly known as thermal noise.

In this chapter the architecture for MeerKAT and overall SKA telescope network was introduced. The RF signal crucial for timing and synchronization was addressed with the focus on the requirements for successful distribution system operation. The short and long-term RF signal instability was discussed. The characterization time domain and frequency domain instability in terms of phase noise and Allan deviation was studied. In the sections to follow these will further be used to analyze the magnitude and type of noise induced by different components making up the transmission link of a distribution system over optical fibre similar to the MeerKAT telescope network.

Chapter 4

Techniques for Measuring Instability

In this chapter three different techniques for measuring signal instability are described. The measurement setup for each technique and the necessary calibration required are addressed. The signal instability can be characterized in the time and frequency domain. In this work extraction of phase noise and Allan deviation information from the different techniques is discussed.

4.1 Phase Lock Loop Measurement Technique

The phase noise associated with the RF distribution telescope network can be the limiting factor of the system. Hewlett-Packard pioneered the frequency instability measurements[133] and its importance is explained for a number of applications. The difference between short-term (random) instability and long-term (drifting) instability of the signal is discussed in reference [134]. The short-term and long-term stability of a signal generator and the two-port components (added noise) that make part of the system is quantified by measuring the Phase noise in the frequency domain and the Allan deviation in the time domain.

4.1.1 Signal Source Analyzer

Phase lock loop (PLL), also referred to as the direct homodyne is formed by the feedback control system. The linear function of PLL is used to describe the response to small signal modulation, phase noise, and spurious (discrete) noise[135][136]. The signal under test is multiplied by the reference signal 90° off phase to separate the amplitude noise from the perpendicular phase noise. The method measures the voltage fluctuation produced by combining two input sources, this is proportional to the phase fluctuation. The control system maintains the phase of the output signal in-step with the phase of the

reference signal, tuning it using the output voltage. It has low noise floor making it a sensitive method with high noise detection capability.

4.1.2 Experimental Set-Up

The phase-lock loop is a feedback system that drives a voltage-controlled oscillator to maintain a constant phase angle coherent with the clock signal frequency.

The method uses two sources, the device under test and the reference signal are input into the RF and LO ports of the mixer at phase quadrature. The system behaves as phase detector for the input signals adjusted into the mixer to be 90 ° out of phase as seen in figure 4.1, achieved by offsetting the frequency of one source. Good quadrature guarantees maximum sensitivity of phase noise and neglects amplitude noise[137]. For sources with the same frequency the output signals at the IF port of the mixer are the sum and the difference of the frequencies. The low pass filter removes the higher frequency component of the mixer output signal allowing the difference corresponding to 0 V DC average voltage[138][139].

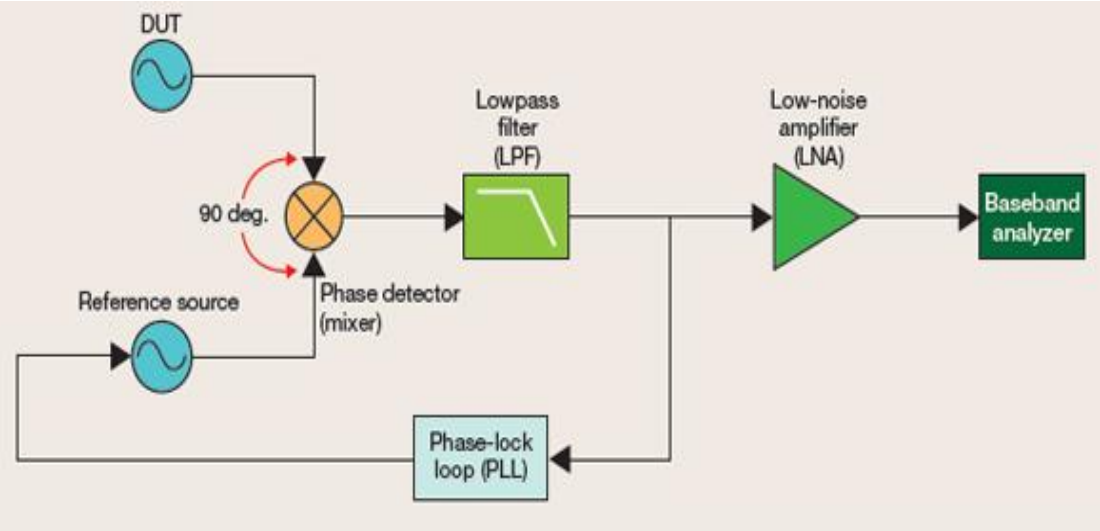

Figure 4.1: basic phase lock loop measurement technique[140]

The DC voltage signal contains AC fluctuations proportional to the phase difference between the two input signals[141]. The AC fluctuations rising on the DC voltage are proportional to the combined noise of the two sources. The output voltage fluctuation is given as:

$$\Delta V = \mathrm{K}_{\phi} \cos(\Delta\phi - \overline{\Delta\phi}) \qquad (4.1)$$

where K_{ϕ} is the phase detector constant in $\frac{V}{rad}$ dependent on the phase deviation. At $\overline{\Delta\phi} = 90\,^{\circ}$ the mixer functions as a phase demodulator suppressing the amplitude modulated signal. Phase fluctuation $\Delta\phi$<< 1rad thus cos$\Delta\phi$ ~ $\Delta\phi$ resulting in the output fluctuation voltage being:

$$\Delta V = \mathrm{K}_{\phi}\Delta\phi \qquad (4.2)$$

The phase constant is equal to the peak voltage of the sinusoidal control signal for a linear mixer. For phase noise above 0.1 rad the mixer response is non-linear and degrades the accuracy of the measurement system[137][135]. The voltage-control oscillator replicates the input frequency so that upon mixing the output voltage is zero volts. To ensure that the sources maintain the phase quadrature a phase lock loop is used in a feedback path to the reference source.

This measuring technique is implemented in the round trip path length compensation of the ALMA and e-MERLIN telescope array. It uses a multiplexed pulsed system on a single fibre to correct for the large temperature swings and delay variations. The compensation is based on the return signal sent back from the antenna to the central processing site having twice the delay as that of the one-way trip delay[87]. The delay difference measurement is used to correct for the phase changes of the input signal propagating the optical fibre path length through a PLL circuit connected to the VCO reference clock. For e-MERLIN the compensation for path changes in 1 s time scale are done after correlation. In timescale the back to back clock distribution, 1310 nm laser transmission over 28.6 km optical fibre and 1550 nm thermal controlled laser transmission over 110 km optical fibre were analyzed, a stability of 1 ps RMS was recorded for all three distributions[98]. The system has been further developed to improve the accuracy and precision of the high stability time and frequency reference clock distribution over optical fibre. The National Physical Laboratory group improvement of the PLL technique uses a mode-locked laser to generate femtosecond

pulses transmitted over 86 km dark fibre. The path delay is compensated using the combination of slow thermal and fast piezoelectric effects induced on fibre-stretchers controlled by measuring the phase difference of the return signal. The distribution system achieved a fractional frequency stability of 4.00×10^{-17} for 1600 s averaging time, corresponding to 64 fs RMS[94].

4.1.3 Extracting Phase Noise From Phase Lock Loop

The average voltage signal is amplified with low noise amplifier (LNA) and is input to a spectrum analyzer. The spectrum analyzer measures variations of the output voltage for phase difference between the signals thus the direct measure of phase noise. On the spectrum analyzer the measured output voltage is expressed as function of the offset frequency as:

$$\Delta V_{rms}(f_m) = \mathrm{K}_{\phi}\Delta\phi(f_m)\,[V] \qquad (4.3)$$

The phase fluctuation can be defined in terms of the power spectral density of the voltage fluctuation out of the phase detector:

$$\Delta\phi(f_m)^2 = \frac{S_{Vrms}}{\mathrm{K}_{\phi}{}^2} \qquad (4.4)$$

The power spectral density of phase fluctuation becomes:

$$S_{\emptyset}(f_m) = \frac{\Delta\phi(f_m)^2}{B} = \frac{S_{Vrms}}{\mathrm{K}_{\phi}{}^2}\left[\frac{rad^2}{Hz}\right] \qquad (4.5)$$

The single sideband phase noise:

$$\mathcal{L}(f_m) = \frac{1}{2}S_{\emptyset}(f_m) \qquad (4.6)$$

The performance of the reference source must be well characterized and perform better than the signal under test. The phase noise contribution of an ideal reference oscillator is significantly lower than that of the RF oscillator[142] resulting in the total phase noise being equivalent to the signal under test phase fluctuation. The noise contribution of the reference source and signal under test can be separated using correction factors ranging from 0-3 dB, with the highest being when the oscillators equal noise level. The phase noise of the reference cannot deviate from measured total noise by more than 3 dB.

4.1.4 Pros and Cons of Signal Source Analyzer Measurement Technique

The narrow bandwidth PLL tracks the sources within the bandwidth and neglects phase fluctuations outside the PLL bandwidth. The system is insensitive to the amplitude noise, suppressed due to quadrature set up. The reference source is a crucial component of the phase lock loop method. A highly stable low-noise reference source is required which is electronically tunable. The noise of the reference source must be known and must be lower than that of the signal under test (20 dB margin) [141]to be neglected. The system uses two oscillators; the noise measured by the spectrum analyzer is the sum of the two source's noise contribution, it is 3 dB higher. The voltage error output by the mixer is applied to a source with capability of electronic tuning with a wide frequency range for clock signals that have high frequency drift rate; this is the complexity of the phase locked loop method. If the signal under test has a large drift it may drive the reference source tuning range to its limit. A mixer detains the overall performance of the system (in the linear region it outputs a sinusoidal signal), thus its selection is very important[137]. The noise floor sensitivity is a function of the mixer input level, better performance is expected from high power level mixers with precautions taken not to mismatch the mixer drive to available source power.

4.2 Delay Line Measurement Technique

4.2.1 Frequency Discriminator

The frequency discriminator method translates the short-term frequency fluctuation to low voltage fluctuation that can be measured by the spectrum analyzer. The frequency fluctuation is converted to a power spectral density used to calculate phase noise from the phase and frequency instability relationship.

4.2.2 Experimental Set-Up

The signal from the device under test is split into two channels using a 3 dB splitter. One channel is sent through a discriminator (delay line) relative to the other and another channel and is input to the RF port of the double balance mixer as seen in figure 4.2. The reference channel passes through a variable phase shifter, the local oscillator channel contains the signal that drives the mixer at the prescribed load[143]. The delay line converts the frequency deviation to phase fluctuation relative to the LO channel. Voltage fluctuation of the mixer output signal is proportional to the frequency variation of the signal under test.

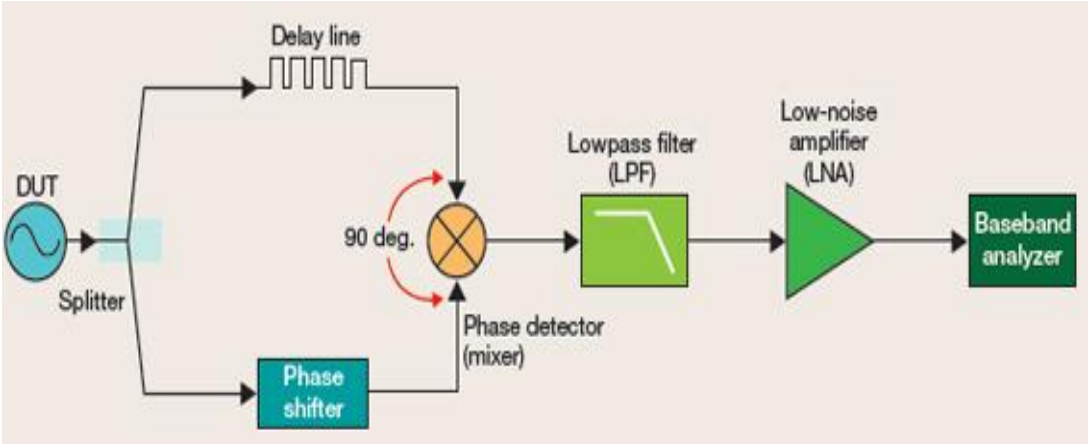

Figure 1.2: basic frequency discriminator technique[8]

The RF and LO are input into the double balance mixer acting as a phase detector. The phase quadrature is adjusted with a phase shifter. The phase shifter eliminates the need for a reference source. The delay line converts the frequency variation of the signal into phase variation. The phase difference between the RF and LO channel signal is converted to the DC average voltage signal by the phase detector. The output voltage is proportional to the delay $\tau_d$in seconds, it exhibits null in frequency $f_{null} = \frac{1}{\tau_d}$. The output signal goes through a low pass filter and is amplified by LNA before being measured by a spectrum analyzer.

The Instrumentation Technology group in Slovenia have implemented the technique to test the short and long-term stability of a 2998 MHz reference clock distribution system[96]. The RF signal is split into two branches using a thermally stabilized power splitter to achieve the 90° phase shift (maintained by the phase shifter). The distribution system uses a 300 m optical fibre spool to transfer the reference signal between the transmitter and receiver; this fibre serves as a delay line. The fibre spool is surrounded by foam to reduce temperature variation induced instability thus simulating the installation site conditions. A long-term stability of 20 fs peak-to-peak over 180 hrs was observed using this phase detection system, this corresponds to 8 fs RMS jitter[144].

4.2.3 Extracting Phase Noise From Delay Line

The output voltage from the mixer is proportional to the phase shift (dependent on the instantaneous frequency of the signal)[145]. The output signal is amplified to a dynamic range of the spectrum analyzer using a low noise amplifier. Voltage fluctuation is measured as frequency noise and converted it to phase noise. The output voltage as a function of the offset frequency can be expressed by:

$$\Delta V_{rms}(f_m) = \left[\mathrm{K}_\phi 2\pi\tau_d\right]\Delta f(f_m) \qquad (4.7)$$

This small frequency fluctuation is as a function of offset frequencies $\Delta f(f_m)$ in$\left[\frac{Hz^2}{Hz}\right]$, relating the phase detector constant $\mathrm{K}_\phi$and the delay time of the delay line τ_d in

seconds[146]. If the discriminator constant $K_d = \mathrm{K}_\phi 2\pi\tau_d \left[\frac{V}{Hz}\right]$ is known, the peak frequency fluctuation as a function of offset can be measured[146]. The output voltage is measured as a double sideband voltage spectral density, which can be converted to a frequency fluctuation spectral density $S_{\Delta f}$ in a 1 Hz bandwidth[147]:

$$S_{\Delta f} f = \frac{{\Delta V_{rms}}^2(f_m)}{{K_d}^2} \qquad (4.8)$$

The presence of frequency fluctuation on the signal gives rise to the phase fluctuation difference at the output mixed differential signal associated with delayed and local oscillator channel. This frequency noise can be converted to phase noise[138].

$$S_\phi(f_m) = \frac{S_{\Delta f}(f_m)}{{f^2}_m} \qquad (4.9)$$

4.2.4 Pros And Cons Of Delay Line Measurement Technique

The method does not need a second source; it is useful for free running sources, for noisy signals with high spurious sidebands close to the carrier that pose problems for PLL technique. It measures the frequency fluctuation of the device under test directly, even those with strong drift, and it suppresses amplitude noise. The sensitivity of the method is sacrificed at offsets close to the carrier decreasing as a quadratic function[148]. Though a longer delay line can improve sensitivity, it reduces the signal to noise ratio due to insertion loss [138]. The loss of the delay line restricts the system performance; it should be within the mixer power requirement, limiting the maximum offset frequency that can be measured away from carrier. The sensitivity is decreased at high offset frequencies with $f_m = \frac{1}{\tau_d}$ being the limit.

4.3 Direct Method Measurement Technique

This is the simplest and easiest way to measure instability. The output signal of the source under test in the frequency range of the spectrum analyzer is connected directly to the spectrum analyzer. The spectrum analyzer displays the total power at the respective offset frequencies about the carrier[131]. Upon rejecting amplitude noise from the total

noise, the power spectrum is converted to a phase noise plot rejecting amplitude fluctuation. The frequency instability in the time domain is commonly measured by Allan deviation, estimated by signal counter[149]. Real signal is not constant and stable, its instantaneous frequency can be defined as a time derivate of the signal phase. Using a signal counter the actual frequency can be tracked and represented over time[105][150].

4.3.1 Spectrum Analyzer

The spectrum analyzer measures the total power spectral density respective at the offset frequencies. The power spectral density of the signal under test is measured. The power spectral density includes both phase and amplitude fluctuations. The amplitude fluctuation results from the power output variation[131]. For the transfer of power spectral density to phase noise plot to occur the amplitude noise must be neglected. If the amplitude fluctuation is not rejected it must be significant lower than the phase fluctuation, as the component would add to the phase noise and cannot be separated by the direct method[142].

The signal instability can be characterized in the time domain, it is specified as frequency instability in terms of frequency deviation from the nominal value. Frequency noise can be derived directly from phase noise, defined in terms of instantaneous frequency as a function of instantaneous phase of the signal[137][151]. Random phase variation causes short-term frequency instability. The frequency fluctuation of the clock is characterized using the frequency drift of the signal and is estimated using statistical analysis.

4.3.2 Experimental Set-Up

The signal under test is mixed with an internal local oscillator of the spectrum analyzer. The LO acting as a reference source, mixes down the signal under test to produce a DC average voltage signal output. The LO adds noise to the input signal as shown in figure 4.3.

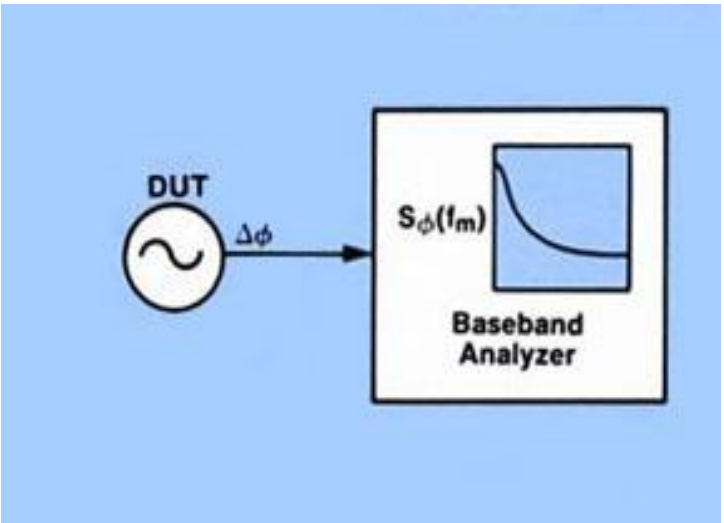

Figure 4.3:basic direct spectrum analyzer measurement technique[152]

The spectrum analyzer displays the SSB phase noise due to the phase fluctuation of the signal as a function of the offset frequency from the carrier to the total signal power. The phase noise is normalized 1 Hz bandwidth at each offset frequency, a bandwidth of an ideal rectangular filter[107]. A signal counter tracks the phase of the signal by detecting the zero crossing occurring over time involved in the integer number of counted signal cycles. The signal cycles occurring at regular time intervals are continuously counted[150]. The signal counter measures the change of phase at the beginning and end of a measurement period. This is used to determine the frequency from the time derivative of signal phase. In this work the method uses a frequency counter built into the spectrum analyzer to measure the instantaneous frequency in Hz. The counter repeatedly measures the frequency at fixed time intervals relative to the resolution, using a GPIB or LAN connected computer to remotely control the measurements using Labview to log the data over a specified time interval. The variation between successive frequency measurements is used to characterize the frequency stability of the source.

The direct method has been implemented in the University of Applied Sciences (UAS) (German tertiary education institution) by the Faculty of Electronics to measure and analyze the short and long-term of a RF- Field control system composed of a master oscillator and very complex reference clock distribution[106]. The performance of the

master oscillator was characterized by phase noise measurement conducted using a FSEM30 spectrum analyzer from ROHDE and SCHWARZ. Three observing frequencies were tested: 9 MHz, at 1.3 GHz and 2.856 GHz. The phase instability was measured for an offset frequency range 1 Hz- to 1 MHz integrated to give the timing jitter. The stability of 611 fs RMS was observed for the master oscillator at 9 MHz. at 1.3 GHz and 2.856 GHz the stability is 281 fs and 114 fs respectively[107].

4.3.3 Extracting Phase Noise From Spectrum Analyzer

The spectrum analyzer is calibrated to display sinusoidal signals. Phase noise is normalized for 1 Hz bandwidth of ideal rectangular filter, the true filter has Gaussian characteristics. This results in the measured power being 2.5 dB lower in level, systematic error[141][123].

Example:

The power spectral density of phase fluctuation per unit bandwidth can be measured by the spectrum analyzer. A center frequency 1 GHz with 10 dBm power is displayed on the electric spectrum analyzer over a 500 MHz span. At 15 kHz offset frequency away from the carrier the power is -60 dBm and the resolution is 3 kHz as measured in the NMMU optical fibre lab. In the frequency domain the spectral density is characterized by the phase noise on either side of the carrier:

$$\mathcal{L}_{\phi}(f_m) = \frac{P_b}{P_s}[\mathrm{dB}] \qquad (4.10)$$

At a given offset frequency away from the carrier, the single sideband phase noise is defined in decibels relative to the carrier:

$$\mathcal{L}_{\mathrm{dBc}}(f_m) = 10\log\mathcal{L}_{\phi}(f_m)\left[\frac{\mathrm{dBc}}{\mathrm{Hz}}\right] \qquad (4.11)$$

The phase noise with all the power correction will be:

$$\mathcal{L}_{\mathrm{dBc}}(15\ kHz) = -60 + 2.5 - 35.6 - 10 = -103.1\left[\frac{\mathrm{dBc}}{\mathrm{Hz}}\right]$$

$10 * \log 1.2 * 3$ kHz =35.6 dB is the filter characteristics correction achieved by[153]:

$$B_{noise} = 1.2\ B_{3dB} \qquad (4.12)$$

1.2 is the correction factor for the error between the ideal rectangular filter and the real Gaussian filter and B_{3dB} is the 3 dB corner frequency of the resolution bandwidth filter [14].

4.3.4 Extracting Allan Variance From Spectrum Analyzer

The data is logged for the desired time period and used to obtain fractional frequency, thus Allan variance. The time series will have a length of T (duration) consisting of M sample points in τ desired time intervals, minimum τ depends on the signal counter resolution[105][151]. The difference of two successive fractional frequencies from the nominal value is obtained using two-sample variance. It is expressed as a mean square of all the signal counter samples calculated in Matlab as Allan variance, thus Allan deviation. This was an implementation made at NMMU optical fibre lab for the computation of the non-overlapping Allan deviation from the instantaneous frequency of an RF clock signal for characterization of the long-term instability.

Instantaneous frequency:

$$f(t) = \frac{1}{2\pi}\frac{d\phi(t)}{dt} \qquad (4.13)$$

Fractional frequency:

$$y(\tau) = \frac{f(t) - f_o}{f_o} \qquad (4.14)$$

Allan deviation:

$$\sigma_y(\tau) = \sqrt{\left(\frac{1}{2(M-1)}\right)\sum_{i=1}^{M-1}\left(\bar{y}_{i+\tau} - \bar{y}_i\right)^2} \qquad (4.15)$$

This is a direct method for measuring the frequency fluctuations. It is a standard technique for obtaining Allan deviation. It is used to characterize the long-term stability of the frequency source in the time domain.

4.3.5 Pros and Cons of Direct Method Measurement Technique

The sensitivity of the method is limited by the dynamic range, resolution bandwidth, and local oscillator phase noise of the spectrum analyzer[142]. The instrument adds noise to the signal. The smallest offset frequency depends on the minimum resolution bandwidth available on the spectrum analyzer. The direct method is not suitable for heavily drifting signals and measuring phase noise at small offset frequencies. The maximum allowable drift depends on the measurement sweep time in a given frequency range[107]. If the signal drifts out of the resolution bandwidth, the small offset frequency measurement takes longer and results in errors as they dependent on the purity of the internal LO[137].

The SSB phase noise of the spectrum analyzer is required to be lower than that of the signal under test. The technique does not require additional components, making it easy and quick to configure. For high noise oscillators it provides convenient and quick qualitative evaluation, providing preliminary view of the phase noise plot and the sources[148]. The cost and availability of spectrum analyzers make the method cost efficient. It is easy to calibrate and operate. It offers a high offset frequency range, making it possible to measure phase noise at high offset frequencies (far away from the carrier). The spectrum analyzer has built in amplitude noise rejection and spurious noise suppression[151]. The spectrum analyzer built in signal counter functionality compares the signal under test to the reference oscillator, with major uncertainties rising from

reference oscillator. The signal counter is required to be fast and have high resolution. It should be able to take continuous measurements and time stamp the signal zero crossing every τ seconds for the Mτ measurement duration time, where M is the number of samples.

4.4 Overall Comparison of Techniques

The three techniques each have different advantages and disadvantages as discussed in the previous sections. The measurement setups come with different complexities and unique limitations. For phase locked loops and delay line method, calibration and component matching is essential, especially the mixer. The different techniques offer unique sensitivity to noise and thus may be used based on the signal stability requirements of the system being analyzed. In the Centre for Broadband Communications the signal stability characterization is conducted for RF time and frequency reference clock distribution, similar to that of the MeerKAT. Short and long-term signal stability measurements will be used and analyzed as phase noise and Allan variance for observation time of a day. This will be the first time these techniques are used to analyze a system and the lab is being developed to support such tests. The MeerKAT telescope requires the RF clock to maintain a stability of several hundred femtoseconds jitter for successful operation. Since this is obtainable using the direct method, which is more cost effective and easy to calibrate, this will be the technique of choice for characterization.

This chapter covered the different techniques commonly used for signal instability in both the time domain and frequency instability, with focus on the complexity of setting up and calibration for each technique. The advantages and disadvantages of the techniques was discussed. In the chapters to follow the direct method is going to be the technique of choice for all measurements and analyses of the RF distribution system stability characterized in the frequency and time domain, in terms of phase noise and Allan deviation respectively.

Chapter 5

Experimental Apparatus

This chapter covers all the different instruments used to build up the distribution system and the different purpose each instrument served. Collectively several instruments were used mainly for the formulation and implementation of a suite of measurement tools suitable for complete characterization of clock tone distribution similar to the telescope network. Secondly, the equipment was used for the generation of a stable optical clock signal for distribution over optical fibre. In this chapter the operating principle of apparatus such as electrical spectrum analyzer, signal generator, distributed feedback laser, temperature controller and positive intrinsic negative photodiode, are described.

5.1 Electrical Spectrum Analyzer

The electrical spectrum analyzer used in this study was the Rohde & Schwarz FWS signal and spectrum analyzer operational in a broad frequency spectrum ranging from 2 Hz to 26.5 GHz as shown in figure 5.1. The electrical signal transmitted by the RF clock and passing through different devices through the system is characterized by the ESA. The precision and performance of system is characterized as phase noise, achieved by measuring the power at the desired offset relative to the carrier frequency.

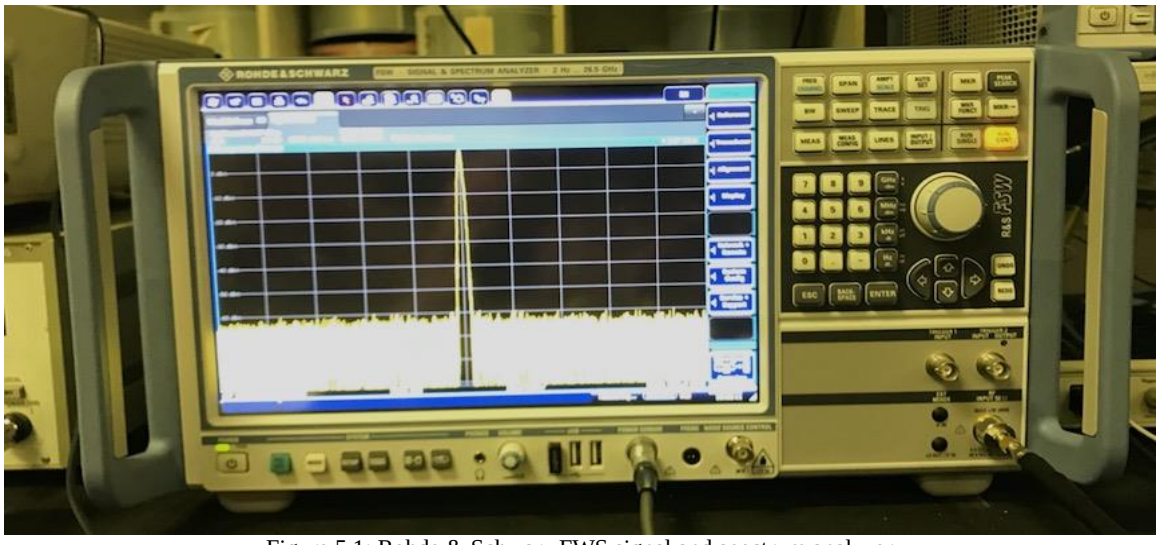

Figure 5.1: Rohde & Schwarz FWS signal and spectrum analyzer

The electrical spectrum analyzer is used primarily to display and analyze the frequency spectrum of the RF signal with the ability to make power measurements. It analyzes different aspects of the RF signal, taking frequency and amplitude measurements. It reveals elements of the signal and is used to characterize the performance of circuits producing it. It shows the levels of the signal on different frequencies within the range of the particular span.

To observe how the signal varies in amplitude as time progresses, it is done by looking at waveform in the time domain. In the frequency domain the signal is viewed as a function of its frequency. Mathematical Fourier transformation accommodates the phase of the signal, which is a complex measurement for many test equipment[50]. The main issue in this context is the resolution bandwidth, R&S®FSW can achieve RWB of 1 Hz away from carrier frequency. Unwanted signals (noise) are kept below acceptable level. Harmonics and spurious content of the signal can be analyzed[154]. The large variety of measurement that the spectrum analyzer can perform makes it a helpful tool for the RF signal design development and system characterization. In this work the electrical spectrum analyzer was operating over a 500 MHz frequency span at a resolution bandwidth RWB of 3 MHz and sweet time 1.5 ms to measure and analyze a 10 GHz RF signal. The reference level was set to 10 dBm with the RF attenuation at 10 dB to keep the unwanted signals below acceptable level.

5.2 Signal Generator

Figure 5.2 shows the Rohde & Schwarz SMB100A RF and Microwave signal generator with frequency range from 100 kHz to 20 GHz. It is an electronic device that generates electronic signals and waveforms with variable output by setting the amplitude and the frequency. It is based on the sine wave oscillator with distinction in design of RF and Audio frequency signal.

Figure 5.2: Rohde & Schwarz SMB100A RF and Microwave signal generator

The signal generator covers a range of frequencies that need to be generatored for different applications. The time and frequency reference in telescope network uses 1.712 GHz in MeerKAT L-Band, 14.5 GHz for MeerKAT X-Band/ SKA Phase 1 mid, and 20 GHz for SKA phase 2 with phase error not exceeding 0.2 radians. The signal generator output range is controlled to a high degree of accuracy. A constant level is maintained and passed through a variable attenuator to change the range. The high level of 30 dBm reached is governed by an amplifier built into the RF signal generator[155]. It offers a virtual electronic for the telescope network clock tone used for RF signal distribution, to test and develop the system. In this work, the signal generator was operated at 10 GHz RF clock tone at 795.5 mV RMS level for the intensity modulation of DFB laser and at 61.87 mV RMS for VCSEL intensity modulation corresponding to the peak-to-peak current of each laser.

5.3 Rubidium Frequency Standard

For phase noise and Allan deviation measurement of the RF clock tone to be accurate and precise, a more stable reference signal is needed. The signal under test stability is measured based on how its phase, frequency and amplitude drifts and fluctuates about the highly stable and spectral pure reference signal. In this study a Stanford Research Systems (SRS) Model FS725 rubidium frequency standard was used as seen in figure 5.3. The Rb clock maintains a fractional frequency stability of $< \pm 1 \times 10^{-10}$ in an

environment with temperature variation ranging between 10 ℃ to 40 ℃. Rear panel connection to a 10 MHz sine wave was used as an external reference oscillator for the electrical spectrum analyzer. The sine output is 0.5 V RMS level[156].

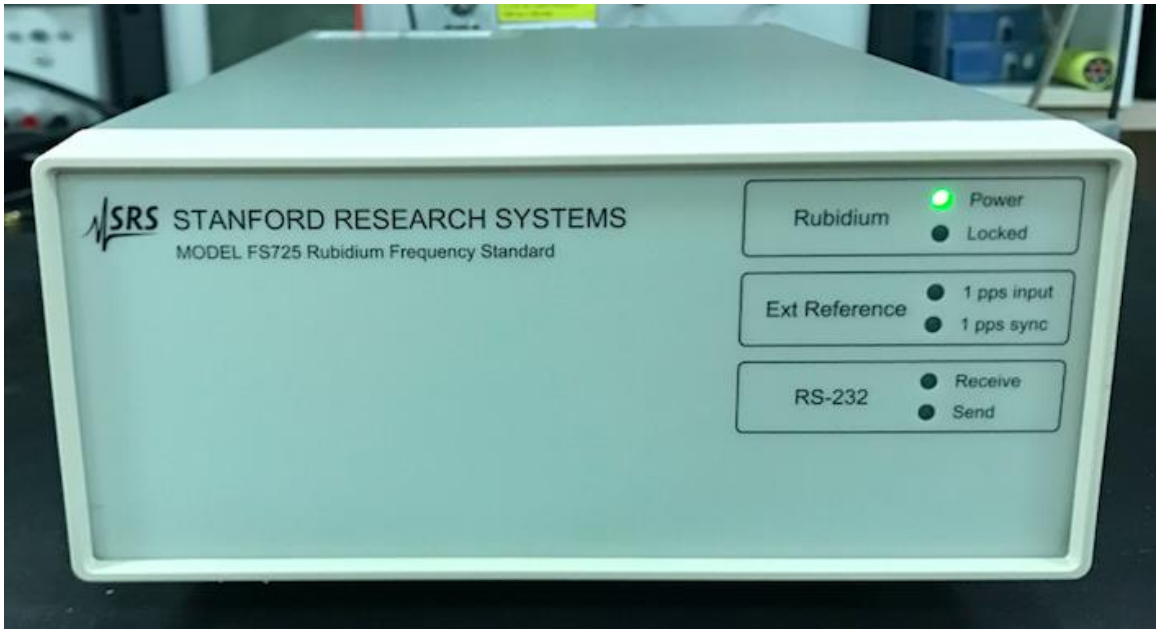

Figure 5.3: SRS FS725 Rubidium frequency standard

The noise contribution of the reference oscillator must be well known and lower than the signal under test. At 10 kHz offset frequency the phase noise of the reference oscillator is $< -155\ dBc/Hz$. In the time domain the frequency instability in terms of Allan deviation is $< 2 \times 10^{-12}$ for 100 s averaging time.

5.4 Laser Diode Controller

The Thorlabs LDC 201C laser diode controller as seen in figure 5.4, was used with a current range from 0 to 100 mA. The current limit can be adjusted and can not be exceeded. A 5-digit LED displays the laser current, photodiode monitor, or current limit. The laser diode or photodiode are connected in the rear of the unit via 9-pin connector. The LCD has two modes by which the laser diode can be driven: constant current (CC) is used when lowest noise and highest response speed is required, and constant power (CP) actively stabilizes the laser diode output power using the internal photodiode adjusted by

the feedback circuit[157]. Laser diode is driven with respect to the ground, an operation that offers low noise, current transient suppression and stability. At the rear of the laser diode control unit there is a modulation input for laser current or power used to pulse the laser diode output. In this work it was used to tune the bias current of both the DFB laser and VCSEL as discussed in the following sections.

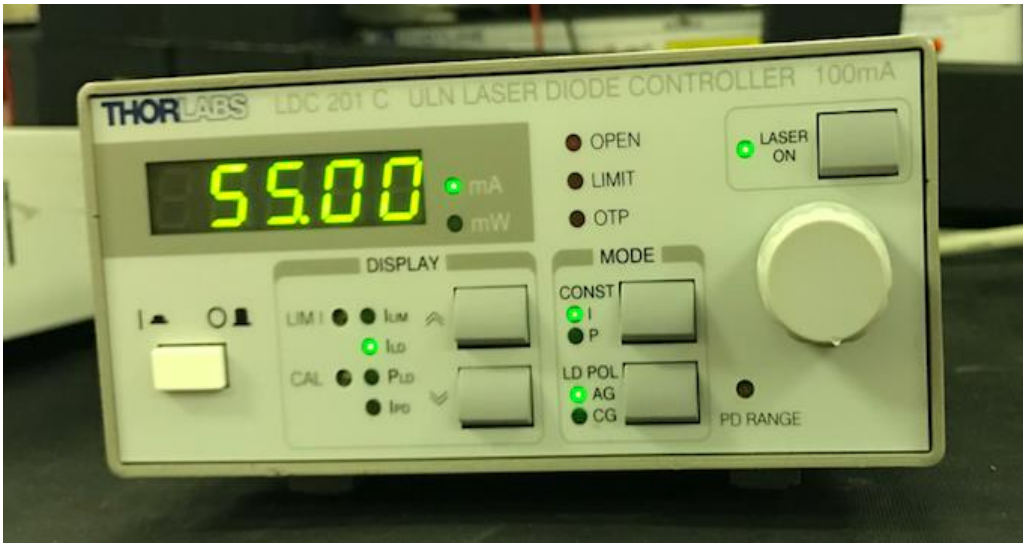

Figure 5.4: Thorlabs LDC 201C laser diode controller

5.5 Laser Diode Temperature Controller

Figure shows a Thorlabs TED 200C precision temperature controller designed to drive the thermoelectric cooler element with current ranging from 0 to 2 A. The temperature reading of the heating current is shown on the 5-digit LED display. The temperature measure is directly proportional to the produced voltage output using a sensor that can adapt to different thermal loads. The compact design of the TED unit makes it easy for system integration[158]. For applications such as time and frequency reference RF clock tone distribution where temperature compensation and cooling are crucial, the laser diode temperature control can be used to maintain temperature stability < 0.002 ℃ for noise reduction and system stability. In this work the TED was operated by setting the sensor thermistor in the 20 kΩ range as seen in figure 5.5.

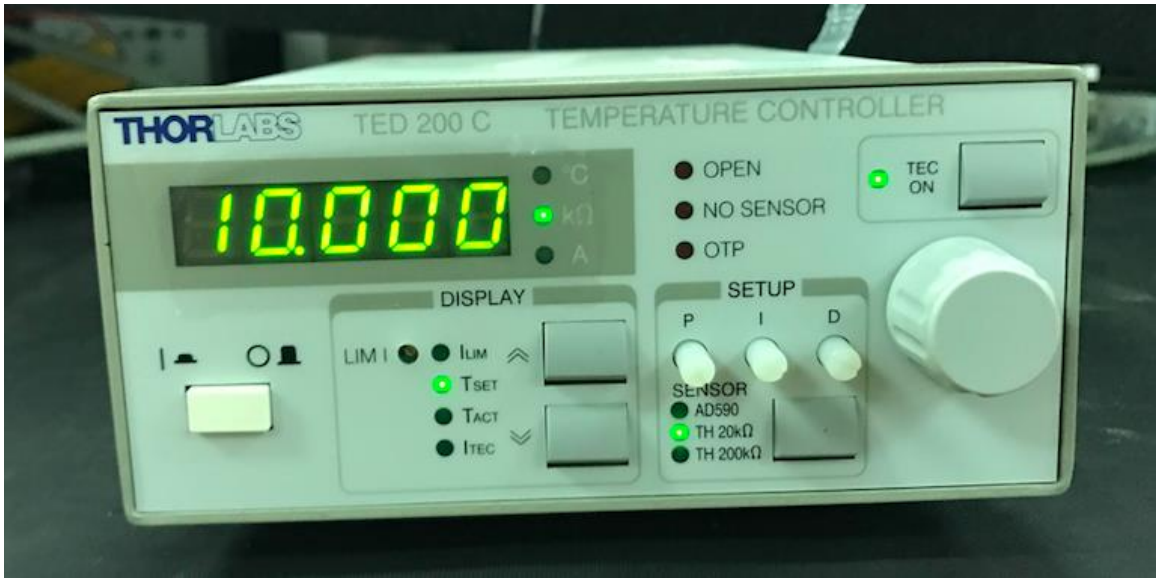

Figure 5.5: Thorlabs TED 200C temperature control

The temperature control value is given in Ohms as the resistance of the thermistor is the control parameter for adjusting. The resistance to temperature stability conversion is nonlinear and depends on the thermistor. The 10 kΩ resistance translate to 20 ℃ with 0.5 Ω (1 mK) stability[159].

5.6 Laser

5.6.1 Vertical Cavity Surface Emitting Laser (VCSEL)

Figure 5.6 shows the RayCan 1550 nm vertical cavity surface emitting laser (VCSEL). VSCEL is a semiconductor laser diode that emits highly efficient optical beam in the vertical cavity. The light is emitted perpendicular to the surface layer of the laser. Fabrication costs are kept at a low by using traditional semiconductor manufacturing (while in wafer form) equipment[55]. The laser shown in figure was optimized to operate at current ranging from 2 mA (the threshold current) to 9 mA, with wavelength adjustable between 1548 nm to 1554 nm, and 0.5 mW typical optical power output. Short resonator makes it easy to achieve single-frequency operation. The wavelength is adjusted by varying the bias current from the laser diode controller, resulting in a more controlled and

predictable yield. The relatively low power is favorable for short distance distribution and use in access network applications.

Figure 5.6: RayCan 1550 nm single mode vertical cavity surface emitting laser

The electro-optical properties and the ability to be directly modulated at high frequencies makes it ideal for high-speed optical fibre communication. It can be used as a miniature optical clock in a virtual telescope network system. Wafer integration of VSCEL makes it compatible with commercial detectors. In this work the VCSEL with use of a laser diode controller at bias current 5.5 mA achieved an optical power output of – 6.23 dBm at 1552.8 nm wavelength. The VCSEL was directly modulated by a 10 GHz RF clock tone at 61.87 mV RMS level corresponding to 3.5 mA peak-to-peak current to allow for a complete modulation swing[160].

5.6.2 Distributed Feedback (DFB) Laser

The distributed feedback laser has a diffractive grating in its active region. The diffractive grating is a periodic structure made with phase shift in its middle; it functions as a Bragg reflector to provide the optical feedback. It reflects a narrow band of wavelengths to produce a single lasing mode (single-frequency operation), optical guiding improving efficiency. The divide electrode structure on one of the surfaces of the DFB laser allows injected current distribution to be modified so as to enable control of the laser output power and wavelength[54]. The spectral range of the NEL DFB laser is from 1530 nm to 1565 nm, with 0.4 spectral width, and a typical optical power of 4 mW. Highly stable wavelength can be produced by temperature stabilization of the laser.

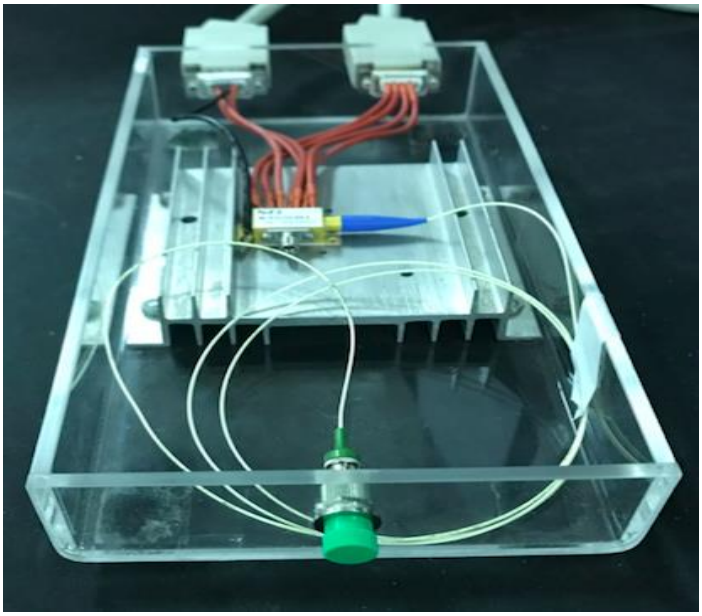

Figure 5.7: NEL distributed feedback laser

In this work the DFB laser with use of a laser diode controller at bias current 55 mA achieved an optical power output of 4.08 dBm at 1551.48 nm wavelength. The DFB laser was directly modulated by a 10 GHz RF clock tone at 795.5 mV RMS level corresponding to 45 mA peak-to-peak current to allow for a complete modulation swing[161].

5.7 Photodetector

5.7.1 Positive Intrinsic Negative (PIN)

The positive intrinsic negative photodiode was invented in the late 1950's. It is a diode with a wide undoped intrinsic semiconductor region between the p and n-type heavily doped semiconductor regions used for ohmic contact. The width of the intrinsic region is larger than the space carrier width of normal p-n junction. The photodiode converts the optical signal to electrical. It operates with an applied reverse bias voltage, with space charge region completely covered by intrinsic region[58]. The photoconductive mode is ideal for applications in which rapid signal response is required, with the dark current exponential growth with the temperature being the downfall. It generates charge carriers (electron hole pairs) in the space charge region by absorbing photons of sufficient energy,

thus creating photocurrent. For diodes not operating in the state of saturation, the photocurrent remains linear to the absorbed light.

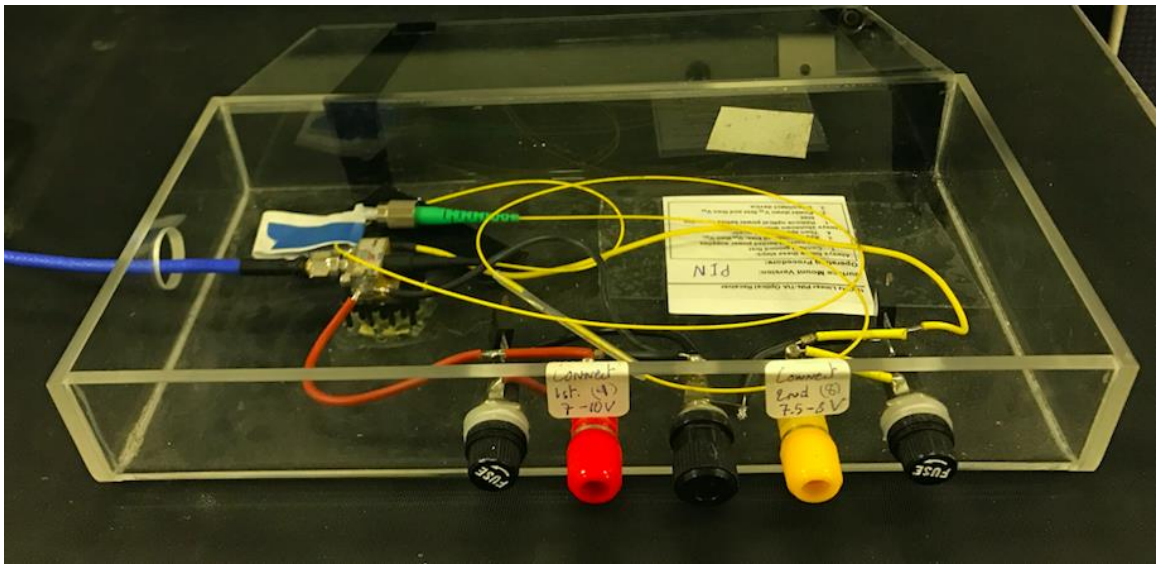

Figure 5.8: 10 GHz linear PIN-TIA optical receiver

In this work a Discovery Semiconductor, Inc® 10 GHz linear PIN optical receiver was used as shown in figure 5.8. The photodiode is operated by applying a 10 V bias voltage, then a bias voltage amplifier of 8 V from a current limited power supply. For operation at 1550 nm the photodiode has a responsivity of 0.8 A/W and sensitivity is – 19 dBm at 10 Gb/s with optical input power damage threshold of 8 dBm peak[162].

5.7.2 Avalanche Photodiode (APD)

The avalanche photodiode is similar to the PIN, with an internal gain mechanism. It uses a large reverse bias voltage to cause impact ionization. The first electron hole is generated by photon absorption in the depletion region. The electron-hole pairs are accelerated by applying an external voltage, further generating more pairs through on impact ionization. In high frequency modulation where the optical signal is very low, the APD is employed[69]. The additive noise level associated with this detector is lower than the combined contribution of the conventional photodiode and amplifier. In this work a Discovery Semiconductor, Inc® 10 Gb/s APD with low-noise 500 Ω transimpendance amplifier (TIA) optical receiver with optical data recovery (CDR) was used, as shown in

figure 5.9. This InGaAs APD has a variable gain of M=2 to M=7 and a sensitivity of -25 dBm.

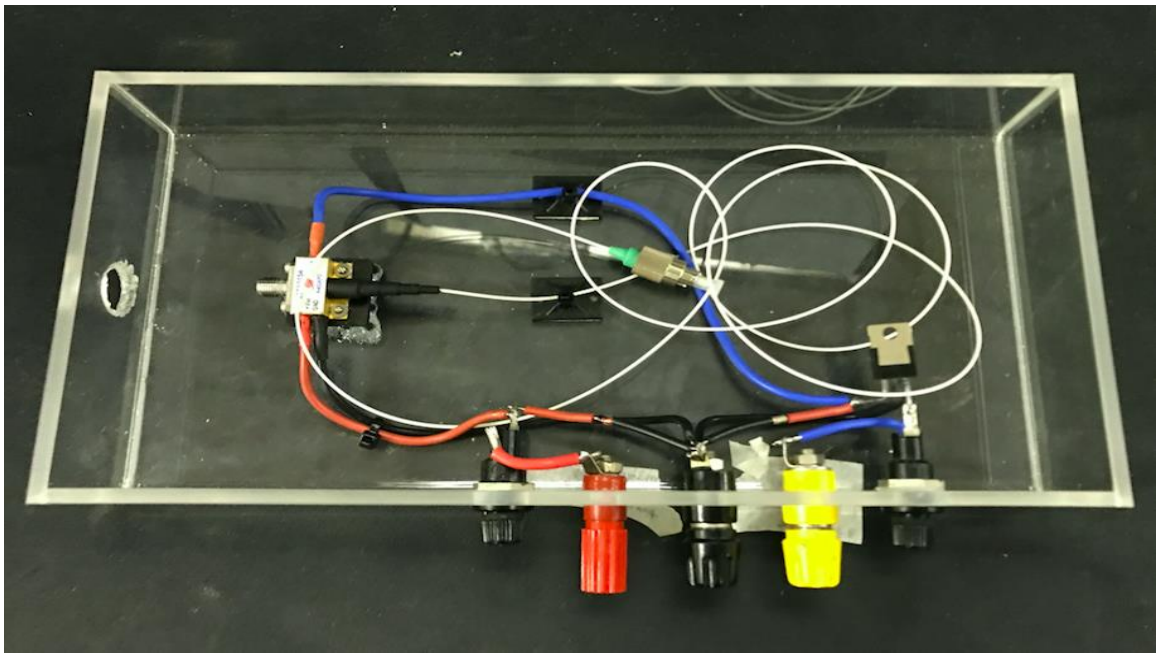

Figure 5.9: InGaAs 10 Gb/s APD+TIA optical receiver with CDR

The APD was operated by applying 10 V stabilized bias voltage V_{bd} from a current limited power supply. The amplifier bias V_{dd} was then turned to 8 V; the desired multiplication gain M was achieved by adjusting the bias voltage between 24 V to 35.6 V. For operation at 1550 nm at room temperature the sensitivity is 0.7 A/W. The APD was paired with a 3 dB attenuator for the DFB laser optical to electrical signal conversion as it has an optical input power damage threshold of 3 dBm[162].

Chapter 6

Phase Noise Measurements with Direct Method

In this chapter the direct method is used to measure the phase noise of a signal generator and the additive noise introduced by single mode fibre of different types and different lengths. The experimental configuration associated with the direct measurement technique is discussed in chapter 4.3. This measurement will be used as a reference for the noise contributed components in the distribution system transmission link. It will serve as a guide to check that the stability requirements of the telescope network are met and to complete a clock stability budget.

6.1 Experimental Setup for Back-To-Back Measurement

The signal generator generates a sine wave signal with high spectral purity. The RF signal is used for phase noise measurement and direct modulation of the optical source. In the frequency domain an ideal sine wave appears as a single spectral line, a real signal appears with sidebands about the carrier. The following results show the single back-to-back power spectrum in the frequency domain as measured by the electrical spectrum analyzer as shown in figure 6.1. A detailed description is provided to illustrate the single sideband phase noise extraction from first principle.

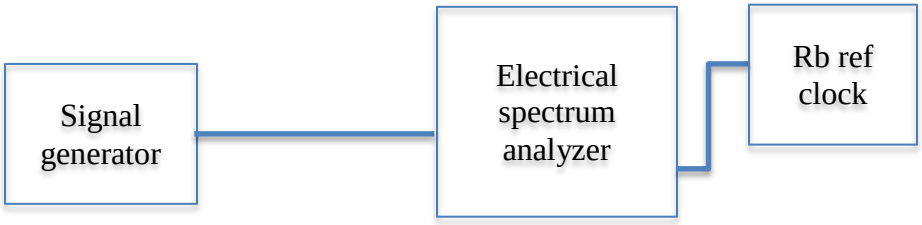

Figure 6.1: experimental setup measuring the frequency instability of the 10 GHz RF clock from the signal generator in the frequency domain

The spectrum analyzer was used to observe the signal generated by the RF source in the frequency domain. This includes spurious signals, harmonics and noise signals. The spectrum analyzer provides signal amplitude against frequency plot that has a graticule

with 10 major horizontal divisions linearly calibrated in frequency and 10 major divisions calibrated in amplitude in either linear or logarithmic scale. The amplitude scale is in dBm. Unlike a power metre that measures the total power within the bandwidth of the sensor head regardless of the frequency, the spectrum analyzer measures the power level at a specific frequency. The oscillator under test must have a low level drift compared to the spectrum analyzer sweep rate. The electrical spectrum analyzer was paired with a rubidium atomic clock as an external reference to ensure that the instrument has the lowest phase noise level to be able to measure the noise of the RF clock.

6.2 Extracting Phase Noise from Power Spectrum Density

A certain amount of phase noise exists on all real signals. These random perturbations manifest themselves by broadening the bandwidth of the signal and extending out on either side of the carrier. A 10 GHz signal generator at 795.495 mV V_{RMS} level signal is measured by the electrical spectrum analyzer sampled at 500 MHz span with a sweep time of 1.5 ms at 3 MHz bandwidth. The result is plotted on the screen and can be saved for analysis. The power spectral density was normalized to 10 dB. The input signal results in a power spectrum with Gaussian distributed noise symmetric about the carrier.

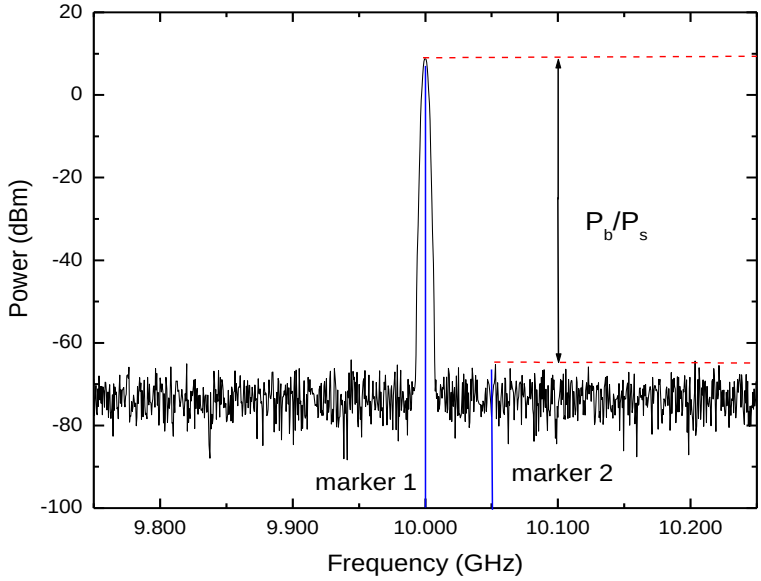

Figure 6.2: the power spectral density of the RF clock signal

In the spectrum analyzer the delta marker was used to extract the noise power at specific frequencies relative to the signal power directly from power spectral density. Using a marker the carrier power can be identified and given in dBm, with the noise power given as the integrated power normalized to a 1 Hz bandwidth. The phase noise is measured by placing the markers at the respective positions as seen in figure 6.2. The power difference between marker 1 and marker 2 corresponds to the relative single sideband phase noise ratio of noise power in the 1 Hz bandwidth offset from the carrier by a desired offset frequency relative to the wanted signal power. The power at the central frequency was recorded as 6.14 dBm by marker 1 and average noise power at 50 MHz offset frequency was -82.78 dBm as noted by marker 2. By substituting the values into equation 3.13 the phase noise was calculated as a function of frequency.

The single sideband phase noise can be calculated from the power spectrum of a signal at a desired offset frequency. Example: The power at 10 kHz away from a 10 GHz central frequency with 6.14 dBm is -33.71 dBm measured at 3 MHz bandwidth, to arrive at $\frac{\text{dBc}}{\text{Hz}}$: -33.71- (6.14) - 10log$\frac{3\ MHz}{1\ Hz}$= -104.64 $\frac{\text{dBc}}{\text{Hz}}$. The phase noise at 10 kHz offset from the carrier is -104.62 $\frac{\text{dBc}}{\text{Hz}}$ as marked on figure 6.3.

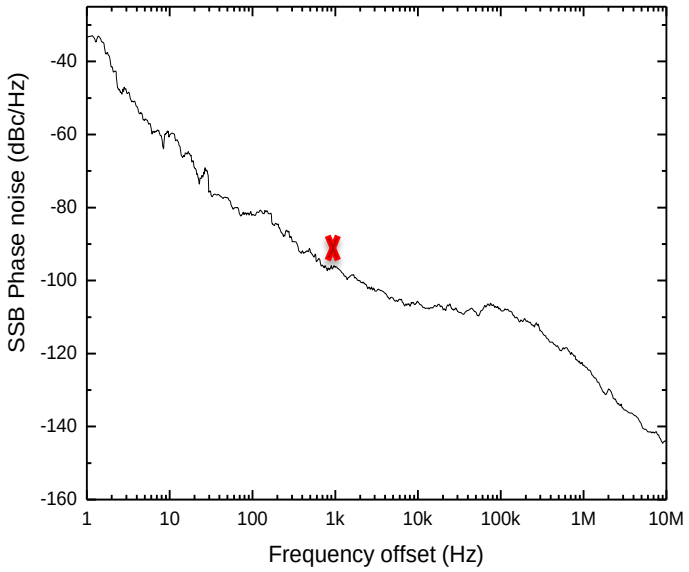

Figure 6.3: single sideband phase noise for RF clock signal as a function of offset frequency

Table 6.1: summary of the RF clock signal SSB phase noise at different offset frequencies

Frequency offset (Hz)	Phase noise (dBc/Hz)
1	-30.65
10	-54.76
100	-82.62
1000	-96.17
10000	-104.62
100000	-107.76
1000000	-123.38
10000000	-143.36

The RMS jitter expressed in seconds can be determined by integrating the SSB phase noise over the spectrum associated with the given frequency range. The signal generator has a 501.99 fs phase jitter in the 1 Hz – 10 MHz frequency range. The RF clock tone is within the stability requirements for MeerKAT telescope of several hundred femtoseconds jitter for successful operation. The RF signal may be used to directly modulate a laser to generate a stable optical clock signal for a distribution system over optical fibre similar to that of the MeerKAT and SKA telescope.

6.3 The Effect of Optical Fibre Link on The RF Clock Stability

Transmission in single mode fibre is characterized by: attenuation, polarization mode dispersion, chromatic dispersion, and non-linear effects. These affect the phase stability and the power level of the RF time and frequency optical clock reference signal. Attenuation leads to the decrease in optical power of the signal. It may be caused by scattering associated with the fibre material and structural imperfections, and absorption related to fibre material. Polarization mode dispersion is the pulse broadening that occurs because of a phase delay between two orthogonal polarization states. The light pulse orthogonal components (polarization modes) generate a phase difference changing in time as they propagate through the orthogonal axes (principle axis) of the optical fibre. Chromatic dispersion is a pulse broadening due to the different wavelengths of light propagating at slightly different velocities through the optical fibre path length. In this section the G.652.C optical fibre phase instability contribution as a function of different lengths (11 and 22 km), and its limitations on the optical fibre link for telescope networks is studied. The requirements discussed will be based on the MeerKAT and SKA phase-1 telescope standards.

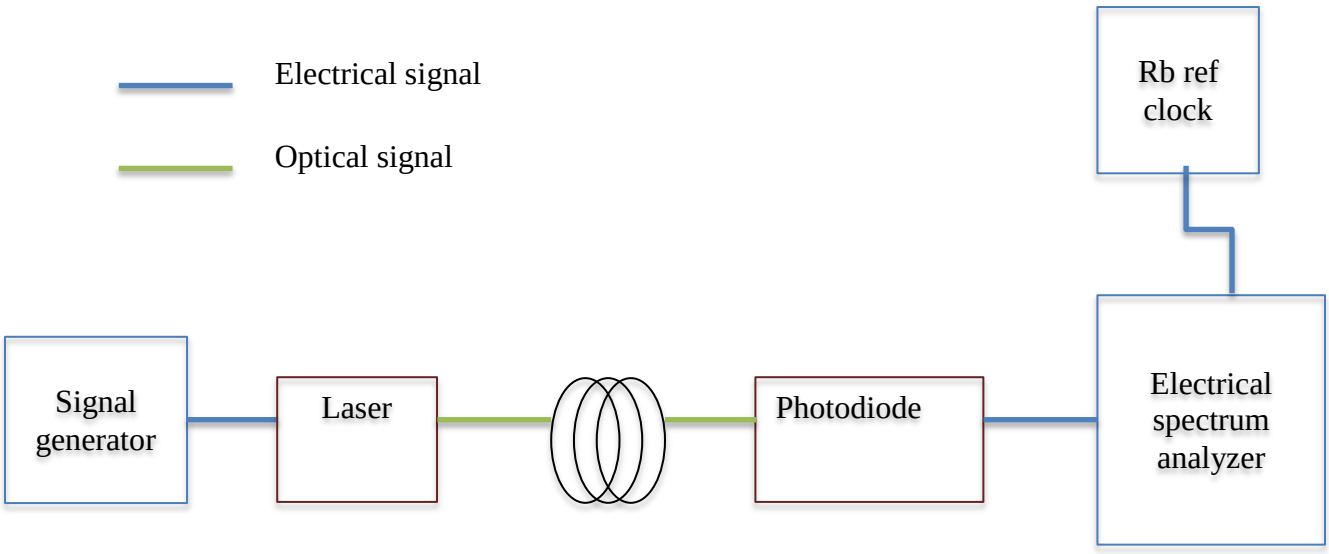

Figure 6.4: experimental setup measuring the frequency instability effect of optical fibre on the 10 GHz RF clock from the signal generator in the frequency domain

An optical fibre link is required to distribute the centralized RF time and frequency reference signal to the remote antennas. The 10 GHz RF clock signal directly modulated the NEL 1551.48 nm high speed DFB laser source, emitting a 5.33 dBm resultant optical clock signal for 55 mA bias current at room temperature. The optical clock signal was transported over a 11 km optical fibre. The optical signal was detected by the DCS-R402 10 GHz linear PIN photodiode, after which the electrical signal was passed on to a spectrum analyzer for analysis as shown in figure 6.4. The optical component noise contribution on the RF clock tone is studied as a real time analogue signal in the time domain to demonstrate the output wave distortion as seen in figure 6.5.

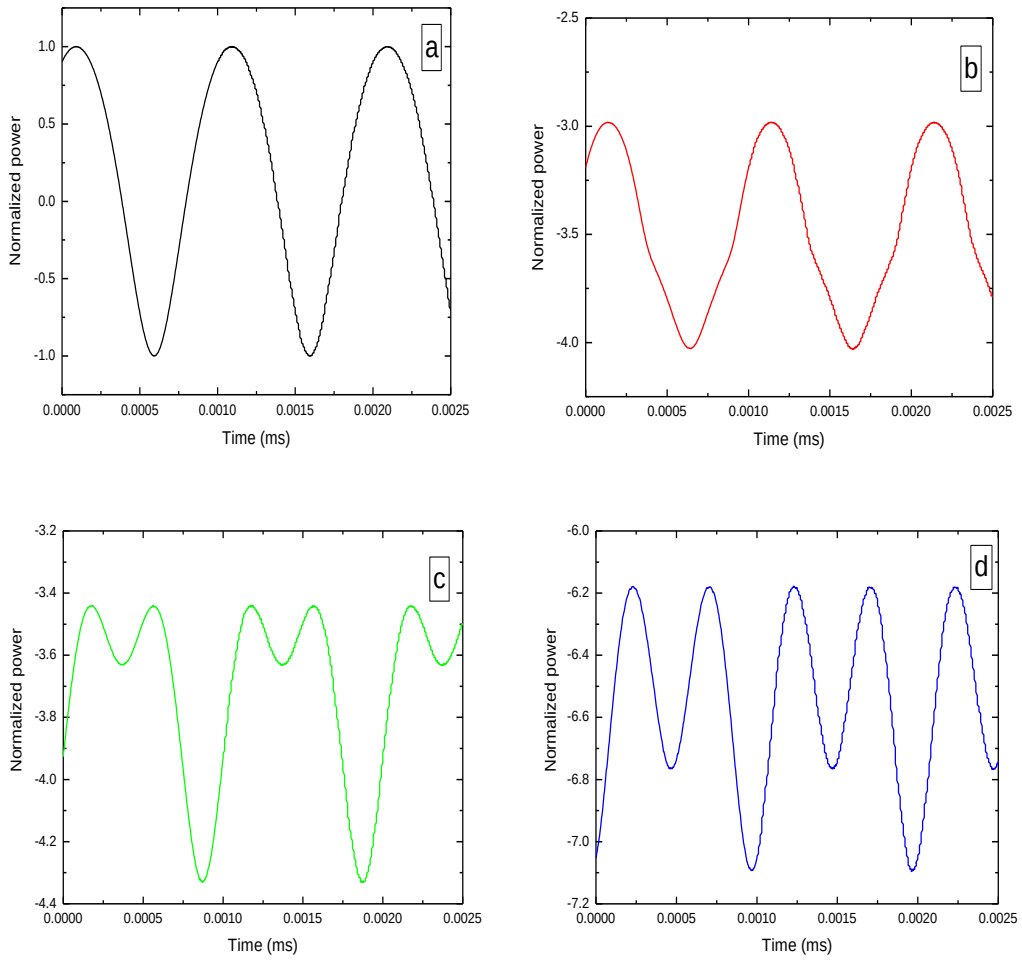

Figure 6.5: power spectrum in the time domain for a) back-to-back RF clock tone b) optical clock signal (laser and photodiode link) and after c) 11 km d)22.3 km optical fibre transmission

The spectral purity of the signal generator RF clock tone is shown in figure 6.5 a). The optical clock signal generated by intensity modulation is analyzed. Figure 6.5b) demonstrates the effects of the laser and photodiode on the signal stability. The rising and falling edges of the signals are distorted and the power level is lowered. This change affects the time taken to complete one cycle resulting in frequency fluctuation. The optical clock signal was transmitted over 11 km fibre which deteriorated signal shape and power level. The combined effect of laser frequency fluctuation and the chromatic dispersion of fibre results in additive noise contribution, dispersion noise. The presence of dispersion noise leads to difficulties in detection of the main power signal as the noise power appears as a discrete peak leading to spurious noise. Chromatic dispersion is a function of fibre length and wavelength, the longer optical fibre transmission signal degradation is severe as seen in figure 6.5 d). The pulse broaden and overlap due to the different wavelengths of light propagating at different wavelengths of light traveling at slightly different velocities through the optical fibre path length.

The optical fibre transmission link is a crucial part of the MeerKAT and Square Kilometre telescope Array which both rely on a highly stable clock tone to be distributed over optical fibre from a central processing point to the remote antennas. Futher more the optical fibre is required to transport the scientific data from individual antenna elements to the central computing engine for correlation. The MeerKAT telescope upon completion will consist of 64 antennas with a maximum baseline of 12 km. each antenna element linked to the central processing point by buried optical fibre to shield it from temperature and environmental perturbations. The optical clock signal clock stability of 18.6 and 2.2 ps is allocated for the 1.712 GHz MeerKAT L-band and 14.5 GHz MeerKAT X-band clock respectively with a 0.20 ps PMD penalty for 12 km optical fibre distribution.

The generated optical clock signal output from the laser is transported some distance over a G.652.C optical fibre. The optical fibre was protected within a cable shielding it from phase fluctuations due to thermal, environmental and mechanical variations of fibre. The G.652.C optical fibre has a maximum attenuation of 0.3 dB/km at 1550 nm. At a similar transmission window the maximum chromatic dispersion and polarization mode

dispersion is 18 ps/(nm.km) and 0.20 ps/$\sqrt{km}$ respectively. A RF optical clock signal was transmitted over 11 km and 22.3 km G.652.C fibre to demonstrate the effect of these parameters on the clock stability as a function of length.

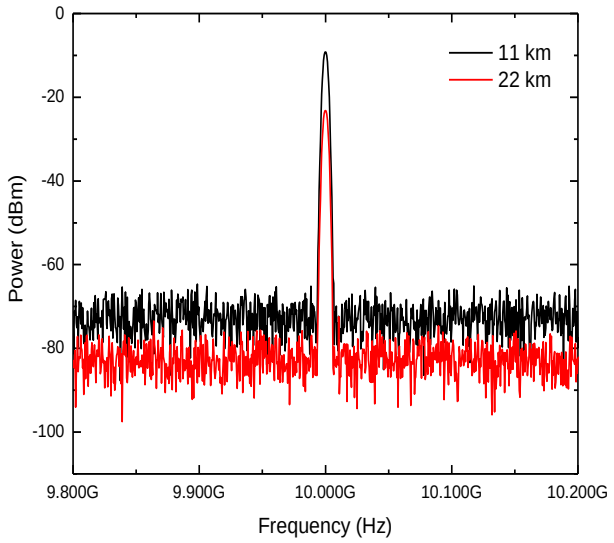

Figure 6.6: power spectral density of the RF optical clock signal transported over different optical fibre lengths

Figure 6.6 shows the power spectrum of the 10 GHz optical clock signal before and after transmission. For distribution over 11 km optical fibre the optical power is degraded to 2.30 dBm with a 2.2 dB loss, the central peak RF power of -6.57 dBm. For transmission over 22.3 km the loss is 4.46 dB bring the optical power to -1.15 dBm, the central peak RF power of -6.80 dBm. At offset close to the carrier and away the power difference and noise contribution of fibre increases with increasing length.

The power level in both optical and electrical domain is given in table 6.2 at different points of the transmission link as a power budget analysis of the distribution system.

Table 6.2: Power budget of the distribution system similar to telescope network

	RF clock	After laser	11 km	22.3 km
Optical power (dBm)		5.33	2.30	-1.15
RF central peak power (dBm)	6.14	-5.41	-6.57	-6.80
Loss (dB)			2.2	4.46

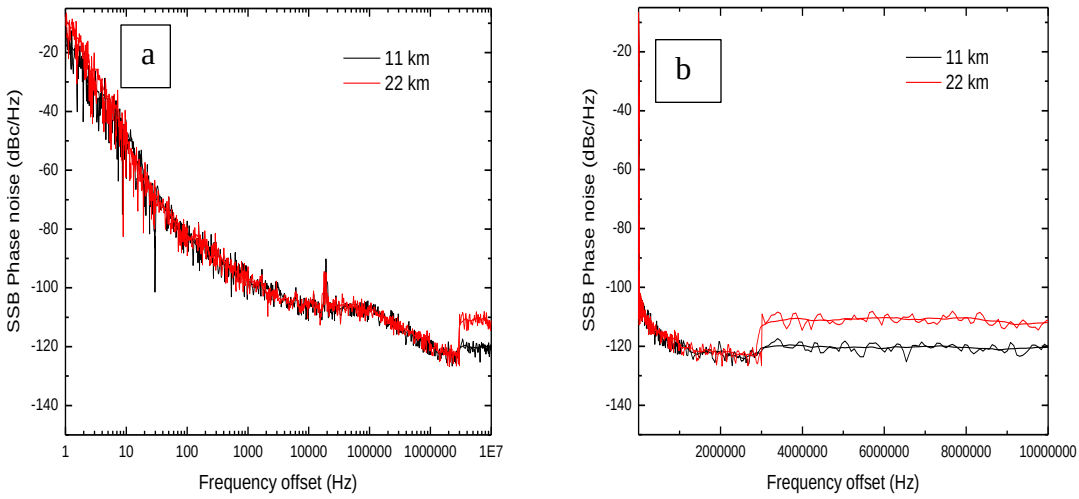

Figure 6.7: optical fibre additive single sideband phase noise on RF clock signal as a function of a) log offset frequency (close to carrier) b) offset frequency (far away from carrier)

The slight difference in noise power and RF power is translated to phase noise. At Fourier frequencies close to the nominal frequency the fibre length have similar noise trends, with a discrete noise peak above 10 kHz as seen in figure 6.7. The spurious noise appears as a result of severe light pulse distortion with noise peak appearing as a secondary peak, this effect is more pronounce over 22.3 km optical fibre distribution. At very high offset frequencies the 22 km fibre noise contribution is visibly higher. The phase noise of the signal at different offset frequencies presented in table 6.3

Table 6.3: experimental summary of the optical fibre effect on the frequency instability of RF clock signal in the frequency domain

G.652.C	Frequency offset (Hz)	Phase noise (dBc/Hz)
11 km	1	-18.56
	10	-47.72
	100	-81.83
	1000	-97.31
	10000	-105.98
	100000	-107.33
	1000000	-119.14
22 km	1	-08.26
	10	-45.99
	100	-82.49
	1000	-97.45

	10000	-105.35
	100000	-107.28
	1000000	-119.51

The characteristics of a single mode fibre transmission are a function of length and wavelength. These affect the power level and the phase stability of the optical clock signal propagating through the fibre. The short-term signal instability in the frequency domain is extracted from the sideband noise power associated with phase fluctuation, relative to the carrier power. The power budget is highly affected for longer optical fibre transmission links. Single sideband phase noise contribution of the 22.3 km is more than that of 11 km. Thermal, environment and mechanical perturbations mitigation by cabling may be used as passive noise compensation.

In this chapter the direct method using an electrical spectrum analyzer was used to measure the stability of an RF clock tone. The technique was used to obtain the power spectrum density for phase, frequency and amplitude instability analysis in the frequency domain. The central frequency peak was surrounded by sideband noise power on either side used to extract phase noise. The RF clock tone short-term signal measurement was used as a noise floor for studying the noise contribution of the optical fibre transmission link of the distribution system. The instability introduced by the optical fibre on the optical clock phase was studied as a function of optical fibre length for a distribution system similar to the telescope network such as MeerKAT. In the following chapter the direct method is used to analyze and characterize the long-term RF clock stability in the time domain as Allan deviation.

Chapter 7

Allan Deviation Measurements with Direct Method

Clock frequency otherwise known as clock rate is the reciprocal of the amount of time required for a signal to complete one cycle. The rising and falling edges of clock signal may vary, affecting the cycle time. This change in the clock rate is the signal instability. In this chapter the clock stability was measured and characterized in the time domain. The random fluctuation and frequency drift of the clock tone was analyzed as Allan deviation from the two-sample statistical variance obtained from the fractional frequency. The result of these measurements can be used to predict long-term signal stability of the radio frequency clock signal

7.1 Spectrum Analyzer for Allan Deviation Experimental Set Up

The real RF clock tone is unstable; the clock rate changes. This is ulike the ideal source that is constant in value, defined by a single spectral line in the frequency domain. The real RF clock tone contains sidebands on either side of the nominal frequency. Frequency fluctuation of the signal generator RF clock tone is measured by the spectrum analyzer which has a built in signal counter that monitors the instantaneous frequency, observing the drift at any given frequency over time. The instantaneous frequency is the derivative of the total phase.

$$\upsilon(t) = \upsilon_o[1 + \frac{1}{2\pi\upsilon_o}\frac{d\phi(t)}{dt}]$$

For RF clock time domain frequency instability analysis, we define the fractional frequency offset. Fractional frequency is the instantaneous frequency deviation from the nominal frequency normalized to the nominal frequency, it is denoted by y (t). Phase fluctuation and fractional frequency are directly related.

$$y(t) = \frac{1}{2\pi\upsilon_o}\frac{d\phi(t)}{dt} = \frac{v(t) - \upsilon_o}{\upsilon_o}$$

Time domain instability is a quantitative and standardized description of these values and their dependence to time and environmental conditions. The fractional frequency instability is characterized by the Allan variance, a two-sample frequency variance. The statistical measurement is accomplished with an array of frequency data points equally spaced in time.

$$\sigma_y{}^2(\tau) = \frac{1}{2(M-1)}\sum_{i=1}^{M-1}(\bar{y}_{i+1} - \bar{y}_i)^2$$

The sampling time, τ_o, is based on the resolution of the signal counter. For a RF clock whose frequency is taken every τ_o for M number of points, the Allan variance (dependent on the averaging time τ) can be computed for several $\tau = n\tau_o$ where the averaging factor is greater than zero. The data samples were recorded using LabView. The data file is transferred to a MatLab program were a code was written to compute the Allan deviation from the fractional frequency at different averaging times.

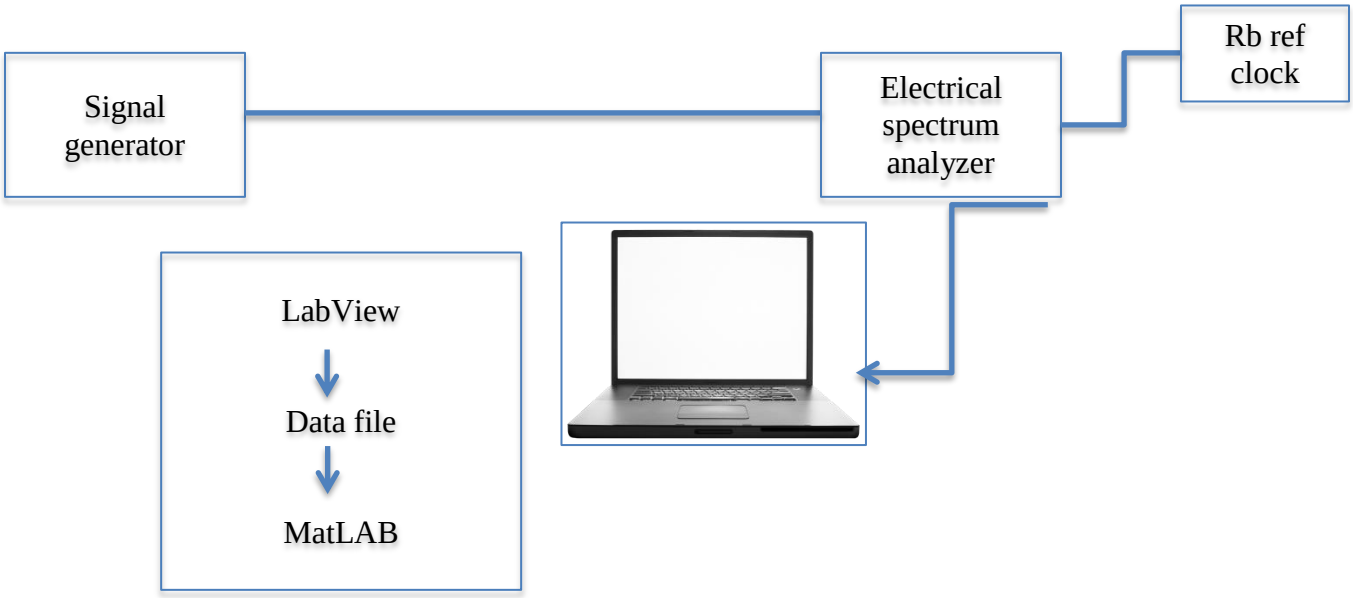

Figure 7.2: experimental setup measuring the frequency instability of the 10 GHz RF clock from the signal generator in the time domain

7.2 Extracting Allan Deviation from Frequency Measurements

A 10 GHz nominal frequency produced by the signal generator was measured, 20 data points were recorded at 1 s sampling time. The built in signal counter resolution of the spectrum analyzer is 100 ms. The phase of the signal under test was compared to the phase of the highly stable Rb clock connected to the electrical spectrum analyzer to serve as an external reference oscillator as seen in figure 7.1. The phase noise and Allan deviation of Rb is known. Over the sampling period of 20 s the instantaneous frequency of the 10 GHz RF clock tone was observed, ranging from 10000000143.90 and 10000000144.90 Hz. The equally spaced data sample was used to obtain the fractional frequency used Allan deviation computation at different averaging time, as seen in table 7.1. The averaging time can not be less than the sampling time. Allan deviation requires at least two frequency measurements separated by a fixed time interval to predict the clock drift one interval into the future based on the averaging interval in the past.

Table 7.1: experimental summary of frequency instability of RF clock signal in the time domain, characterized as Allan deviation obtained from instantaneous frequency

Observation time (s)	Instantaneous frequency v (t), (Hz)	Fractional frequency $y(t) = \frac{v(t)-v_o}{v_o}$	Allan deviation $\sigma(\tau) = \sqrt{\frac{1}{2(M-1)}\sum_{i=1}^{M-1}(\overline{y_{i+1}} - \overline{y_i})^2}$
1	10000000144.70	1.447e-008	3.825e-011
2	10000000143.90	1.439e-008	3.337e-011
3	10000000144.90	1.449e-008	2.871e-011
4	10000000144.40	1.444e-008	1.202e-011
5	10000000143.90	1.439e-008	9.129e-012
6	10000000144.00	1.440e-008	2.187e-011
7	10000000144.90	1.449e-008	1.313e-011
8	10000000144.90	1.449e-008	7.071e-012
9	10000000144.70	1.447e-008	7.857e-012
10	10000000144.40	1.444e-008	9.899e-012
11	10000000144.50	1.445e-008	
12	10000000144.90	1.449e-008	
13	10000000144.70	1.447e-008	
14	10000000143.90	1.439e-008	
15	10000000144.80	1.448e-008	
16	10000000144.50	1.445e-008	
17	10000000144.90	1.449e-008	
18	10000000144.70	1.447e-008	
19	10000000144.30	1.443e-008	
20	10000000144.90	1.449e-008	

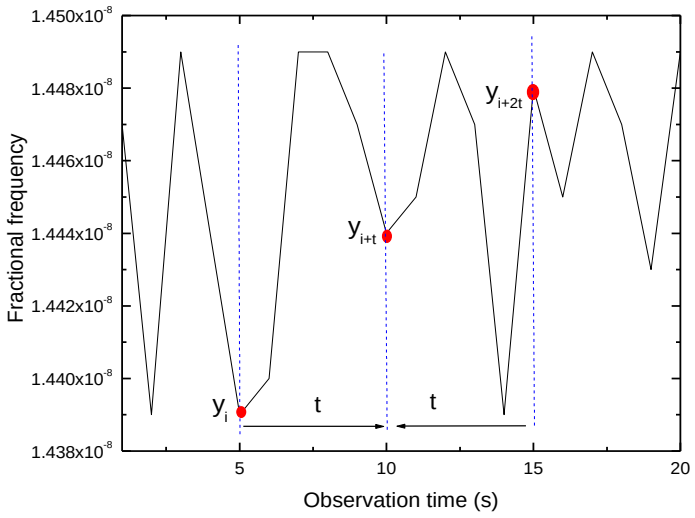

Figure 7.2: frequency deviation normalized to nominal frequency of a 10 GHz RF clock observed every second for 20 seconds

Figure 7.2 shows the fractional frequency averaged by a factor of 5, the 20 frequency measurements become M=4 frequency measurements. The mean frequency value $\overline{y_1} = \frac{1}{\tau}\int_{t_1}^{t_{1+\tau}} y(t)dt = \frac{y_1+y_2+y_3+y_4+y_5}{5}$ is computed for t_1 to t_5. Similarly, $\overline{y_2}$ is obtained for t_6 to t_{10}, $\overline{y_3}$ is obtained for t_{11} to t_{15} and $\overline{y_4}$ for t_{16} to t_{20}. The Allan deviation is computed from the root of the sum of the mean fractional frequency difference squared, divided by the number of frequency measurements less one. The number of pairs in this sequence is M-1=3.

Table 7.2: fractional frequency for RF clock signal for Allan deviation computation at 5 s averaging time

Mean fractional frequency $\overline{y_i}$	First difference $\overline{y_{i+1}} - \overline{y_i}$	First difference squared $(\overline{y_{i+1}} - \overline{y_i})^2$
1.444e-008		
1.446e-008	-2e-011	4e-022
1.446e-008	0	0
1.447e-008	1e-011	1e-022
$\sum_{i=1}^{M-1} (\overline{y_{i+1}} - \overline{y_i})^2$		5e-022

Therefore the Allan deviation $\sigma(5\ s) = \sqrt{\frac{5e-022}{2(3)}} = 9.129 \times 10^{-12}$

Detailed calculation of Allan deviation at 5 s averaging time

Average fractional frequency:

$$\overline{y_1} = \frac{1}{\tau}\int_{t_1}^{t_1+\tau} y(t)dt = \frac{y_1 + y_2 + y_3 + y_4 + y_5}{5}$$

$$= \frac{(1.447 + 1.439 + 1.449 + 1.444 + 1.439) \times 10^{-8}}{5}$$

$$= 1.444\text{e} - 008$$

$$\overline{y_2} = \frac{1}{\tau}\int_{t_6}^{t_6+\tau} y(t)dt = \frac{y_6 + y_7 + y_8 + y_9 + y_{10}}{5}$$

$$= \frac{(1.440 + 1.449 + 1.449 + 1.447 + 1.444) \times 10^{-8}}{5}$$

$$= 1.446\text{e} - 008$$

$$\overline{y_3} = \frac{1}{\tau}\int_{t_{11}}^{t_{11}+\tau} y(t)dt = \frac{y_{11} + y_{12} + y_{13} + y_{14} + y_{15}}{5}$$

$$= \frac{(1.445 + 1.449 + 1.447 + 1.439 + 1.448) \times 10^{-8}}{5}$$

$$= 1.446\text{e} - 008$$

$$\overline{y_3} = \frac{1}{\tau}\int_{16}^{t_{16}+\tau} y(t)dt = \frac{y_{16} + y_{17} + y_{18} + y_{19} + y_{20}}{5}$$

$$= \frac{(1.445 + 1.449 + 1.447 + 1.443 + 1.449) \times 10^{-8}}{5}$$

$$= 1.447\text{e} - 008$$

Non-overlapping Allan deviation:

$$\sigma(\tau) = \sqrt{\frac{1}{2(M-1)} \sum_{i=1}^{M-1} (\overline{y_{\iota+1}} - \overline{y_\iota})^2}$$

$$= \sqrt{\frac{1}{2(4-1)} [(\overline{y_4} - \overline{y_3})^2 + (\overline{y_3} - \overline{y_2})^2 + (\overline{y_2} - \overline{y_1})^2]}$$

$$= \sqrt{\frac{1}{2(6)} [(1.447 - 1.446)^2 + (1.446 - 1.446)^2 + (1.446 - 1.444)^2](10^{-8})^2}$$

$$\sigma(5\ s) = \sqrt{5 \times 10^{-22}}$$

$$= 9.129 \times 10^{-12}$$

Allan deviation was calculated using a MatLab program for averaging time $\tau = 1{:}\,10$ as seen in line 2 to 5 as seen in figure 7.3. The 20 fractional frequency data measurements are uploaded as nameArray on the program, which works out the mean fractional frequency for different averaging times as defined in line 10 to 12. The mean values $\overline{y_\iota}$ and $\overline{y_{\iota+1}}$ are defined by indexOne and indexTwo respectively, are stored as arrays used to calculate the first difference and first difference square as seen on the for loop in line 19. The sum of the first difference squared at a given averaging time is given by line 30 and the corresponding number of pairs M-1 given by 31, used to calculate the Allan deviation defined in line 34. The Allan deviation values are stored as an array with the corresponding averaging tau time values, used to plot the graph representing a relationship between the expected value and the deviation of the frequency fluctuation as a function of observation time for a finite number of data samples. The log-log plot of the Allan deviation against average time is used to identify the types of noise affecting the clock signal.

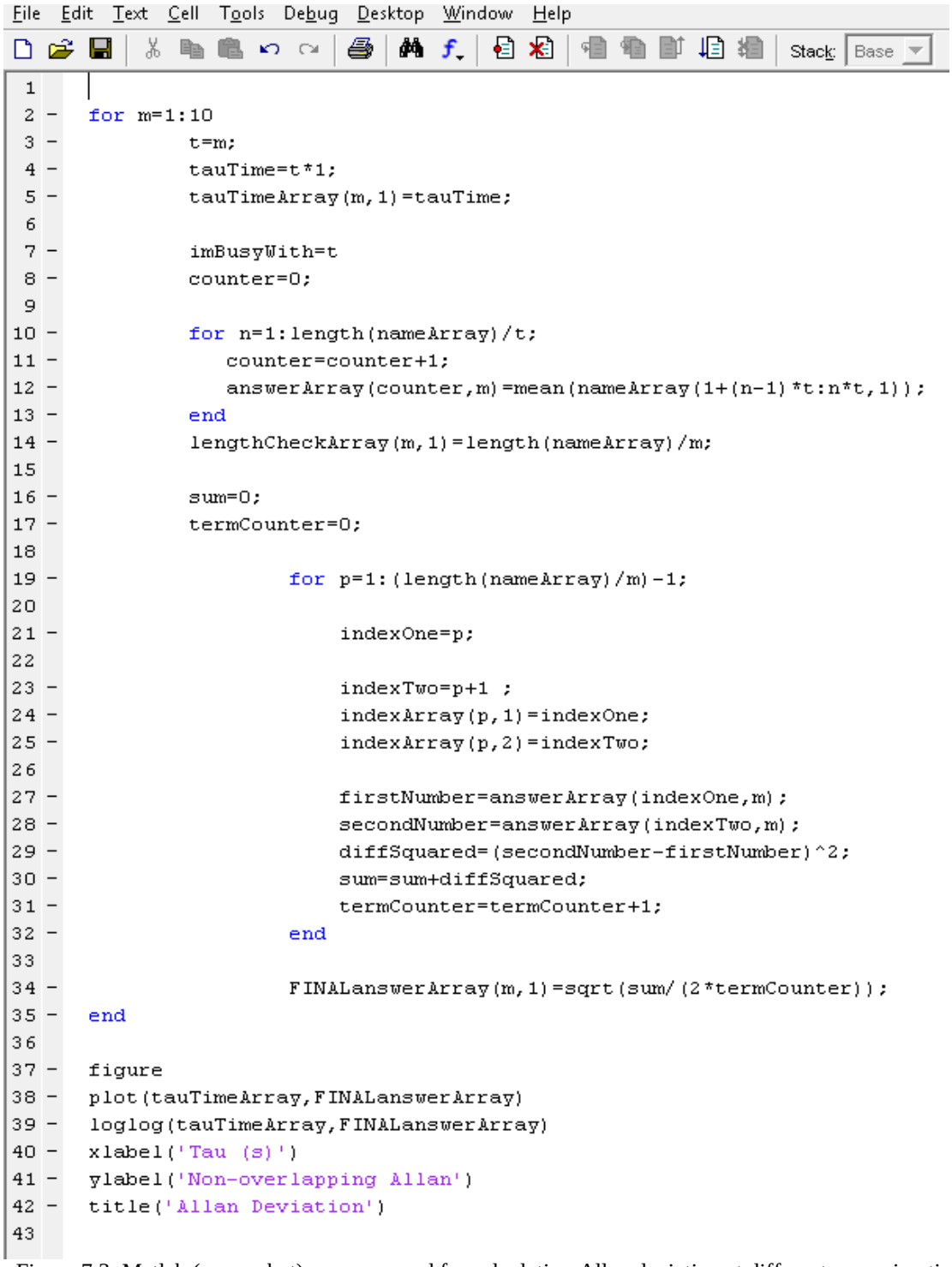

```
File  Edit  Text  Cell  Tools  Debug  Desktop  Window  Help
                                                  Stack: Base
 1
 2 -  for m=1:10
 3 -          t=m;
 4 -          tauTime=t*1;
 5 -          tauTimeArray(m,1)=tauTime;
 6
 7 -          imBusyWith=t
 8 -          counter=0;
 9
10 -          for n=1:length(nameArray)/t;
11 -             counter=counter+1;
12 -             answerArray(counter,m)=mean(nameArray(1+(n-1)*t:n*t,1));
13 -          end
14 -          lengthCheckArray(m,1)=length(nameArray)/m;
15
16 -          sum=0;
17 -          termCounter=0;
18
19 -                  for p=1:(length(nameArray)/m)-1;
20
21 -                      indexOne=p;
22
23 -                      indexTwo=p+1 ;
24 -                      indexArray(p,1)=indexOne;
25 -                      indexArray(p,2)=indexTwo;
26
27 -                      firstNumber=answerArray(indexOne,m);
28 -                      secondNumber=answerArray(indexTwo,m);
29 -                      diffSquared=(secondNumber-firstNumber)^2;
30 -                      sum=sum+diffSquared;
31 -                      termCounter=termCounter+1;
32 -                  end
33
34 -                  FINALanswerArray(m,1)=sqrt(sum/(2*termCounter));
35 -  end
36
37 -  figure
38 -  plot(tauTimeArray,FINALanswerArray)
39 -  loglog(tauTimeArray,FINALanswerArray)
40 -  xlabel('Tau (s)')
41 -  ylabel('Non-overlapping Allan')
42 -  title('Allan Deviation')
43
```

Figure 7.3: Matlab (screenshot) program used for calculating Allan deviation at different averaging times from fractional frequency observed at fixed intervals

An Allan deviation as a function of averaging time was plotted as shown in figure 7.4. This was used to determine how stable the RF clock tone from the signal generator is and how long will it remain synchronized for a distributed telescope network.

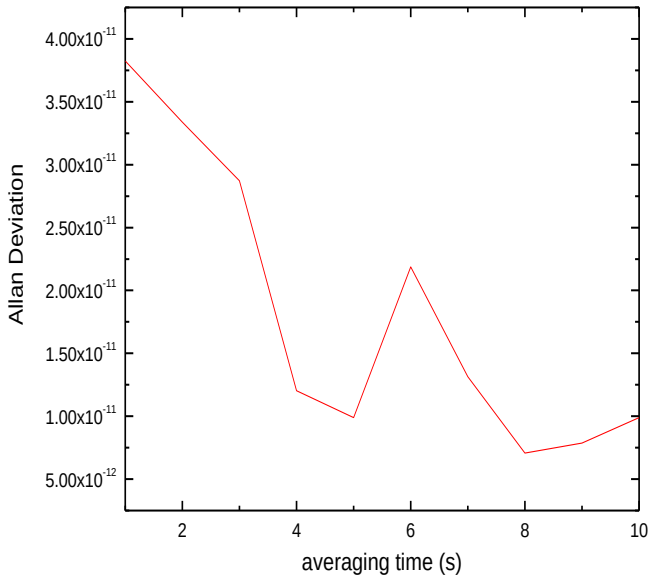

Figure 7.4: Frequency instability of RF clock signal in the time domain characterized as non-overlapping Allan deviation as a function of averaging time

The 10GHz clock instability can be predicted over long term based on the frequency deviation normalized to the nominal frequency over a 20 s observation time.

7.3 Allan Deviation of RF Clock Signal

The frequency instability of the RF clock signal was measured in the time domain using the experimental setup depicted in figure 7.1. The instantaneous frequency of the signal generator was observed over 24 hours, measuring the frequency changes every 0.2

seconds. The 10 GHz reference signal was observed drifting with time over a 10000000135.10 to 10000000146.70 Hz range. The frequency deviation was normalized to the nominal frequency for time domain signal instability computation. The result is shown in figure 7.5

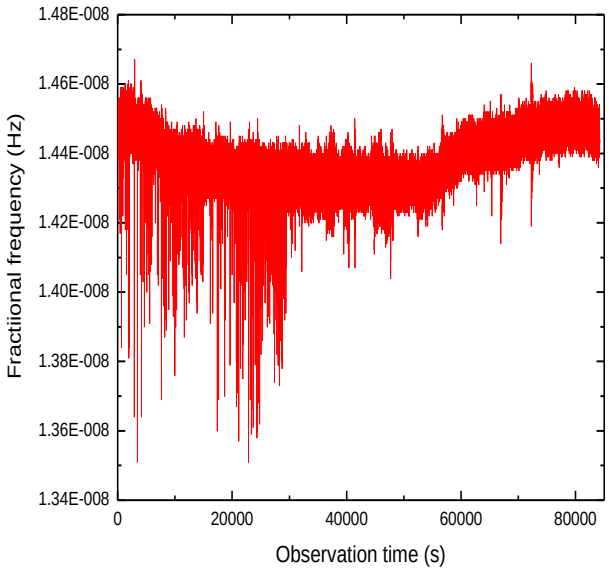

Figure 7.5: frequency deviation normalized to nominal frequency of a 10 GHz RF clock observed every 0.2 second for 24 hours

From figure 7.5 the random frequency fluctuation of the signal is apparent with significant changes occurring between 1 and 30 000 seconds. The signal frequency drifts with time. The fractional frequency data file as collected by Labview was loaded to the MatLab program and used to calculate the standard non-overlapping Allan deviation as a function of tau. The random frequency fluctuation is present and the linear frequency drift of the RF clock tone is demonstrated.

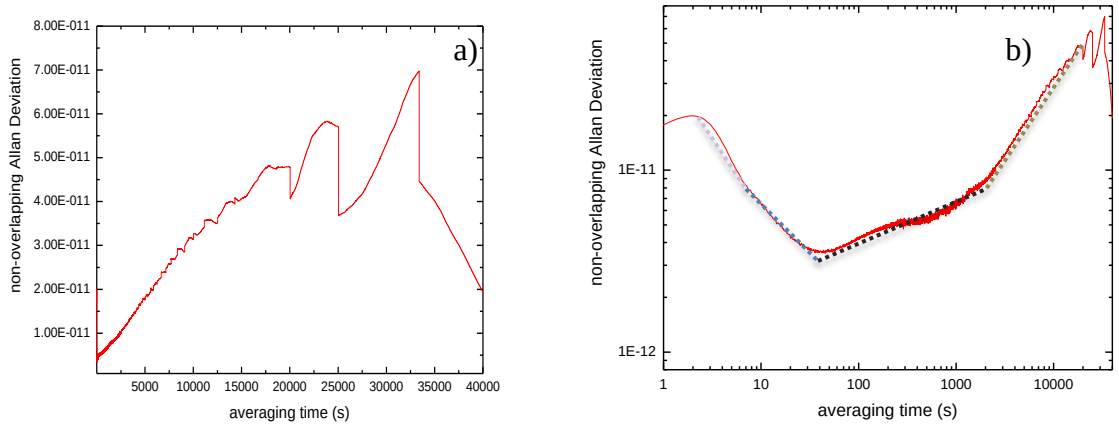

Figure 7.6: Frequency instability of RF clock signal in the time domain characterized as a) non-overlapping Allan deviation as a function of averaging time b)log-log plot of sigma tau as function of averaging time

The long-term instability of the RF clock signal is shown in figure 7.6. The frequency deviation is reported for tau 1s to 12 hours averaging time, as at least two data points are needed to compute the Allan deviation. In figure 7.6 a) the random and deterministic frequency fluctuations are demonstrated; with time the clock linearly frequency drifts from nominal value. At averaging time 100 s the non-overlapping Allan deviation was recorded as 4.03×10^{-12}.

Figure 7.6 b) is a log-log of the Allan deviation as a function of averaging time (sigma-tau) plot. The curve is made up of different slopes as illustrated by the different colour dash lines. The tangent lines can be used to estimate the magnitude contributed by the types of noise affecting the clock stability based on the type of oscillator the signal generator represents. The type of noise indicates the source of noise. The purple line contains white phase noise and flicker both in the τ^{-2} slope, this relates to physical resonance mechanism of an oscillator. The blue line represents the white frequency noise slope τ^{-1} common in passive resonator frequency standards. Flicker frequency noise slope τ^{0} is represented by the black line on figure 7.6 b). This type of noise is related to the physical resonance mechanism of active oscillator, parts used in the electronics and the power supply. The green slope represents the random walk frequency τ^{1} which relates to the oscillator's physical environment (temperature, vibration and mechanical effects).

In this chapter a suite of measurement tools suitable to characterize the long-term stability of a RF clock tone in the time domain was formulated and implemented in a frequency distribution system similar to the MeerKAT and SKA phase-1 telescope. The non-overlapping Allan deviation was used to analyze the random and deterministic frequency fluctuations of clock signal over time. The log-log sigma tau curve was used to demonstrate the types of noise sources contribution to the signal instability of signal generator frequency reference signal. The direct method of spectrum analyzer will further be used to characterize the noise contribution of different components of the transmission link, to optimize the stability of the distribution system by hand-selecting all components to reduce noise contribution.

Chapter 8

Optical Link Component Noise Contribution to RF Clock Tone Stability

In this chapter the noise contribution of the different components that make up the clock tone distribution system will be analyzed. The components will be tested under different conditions to optimize the performance of a distribution system similar to a telescope network. The transmission link additive noise will be characterized in the frequency and time domain using phase noise and Allan deviation as measured by the direct spectrum analyzer method using the clock stability budget of the MeerKAT telescope network as a guideline. The effect components have on the frequency stability of the RF reference clock signal is studied. Both the short and long term were investigated.

8.1 Effect of laser source temperature stabilization

In this section the performance of a semiconductor laser as a function of temperature stability is studied. The laser operates as high-frequency oscillator used to generate a RF optical signal in the gigahertz range. The laser diode has relatively better coherence and lower power consumption amongst other advantages compared to other commercial light sources. For successful operation of the telescope network distribution a highly stable and pure RF clock tone must be generated, this makes the stability of the laser wavelength crucial. Operating characteristics of a laser: emission wavelength and threshold current vary as a function of temperature. The threshold current of VCSEL is 2 mA and that of DFB laser is 11 mA as seen in figure 8.1

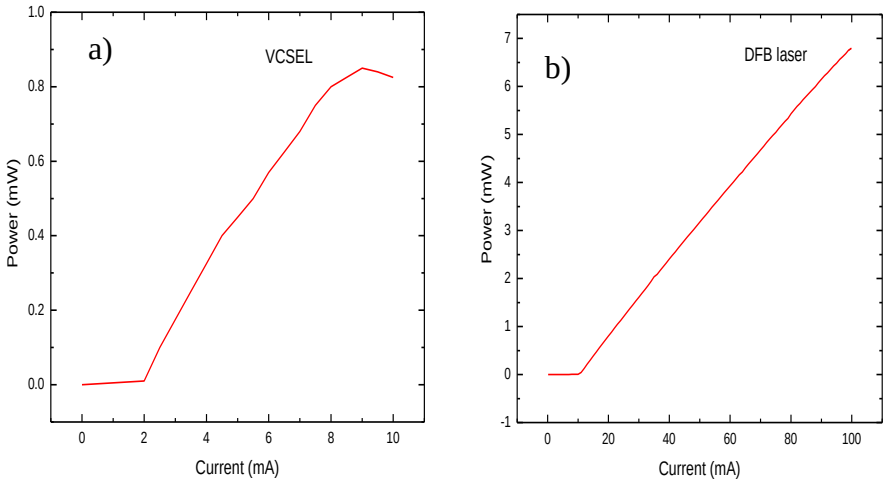

Figure 8.1: Operating characteristics of laser a) VCSEL b) DFB laser

The thermal expansion on the grating period of the laser changes with temperature, causing the peak wavelength to vary as the dimensions of the laser cavity change[163]. The wavelength shifts linearly with changing temperature, this affects the laser optical power output. The intensity of a laser power output decreases with increasing power, due to increased phonon radiation[164].The temperature controller system can heat or cool the laser to a constant temperature to achieve temperature stability. Temperature controller reduces frequency deviation by stabilizing the RF carrier to a specific frequency.

A DFB laser is directly modulated by a 10 GHz RF signal at 794.49 mV RMS from a signal generator. At a bias current of 55 mA, the optical power output of the laser is 4.08 dBm as measured by a power metre. The signal generator was operated at 795.49 mV RMS level to match the laser peak-to-peak current for a 50 Ω load, increasing the laser intensity to 5.33 dBm upon modulation. The performance of the DFB laser generated optical clock signal is compared to that of a VCSEL as a way to carefully design the transmission link and hand pick components to reduce the noise contribution affecting the clock stability. The optical power output of the VCSEL is -6.23 dBm at 5.5 mA bias current. The modulation with 10 GHz RF signal with 61.87 mV RMS level

corresponding to the peak to peak current of 3.5 mA for a 50 Ω load, results in -6.40 dBm optical power output.

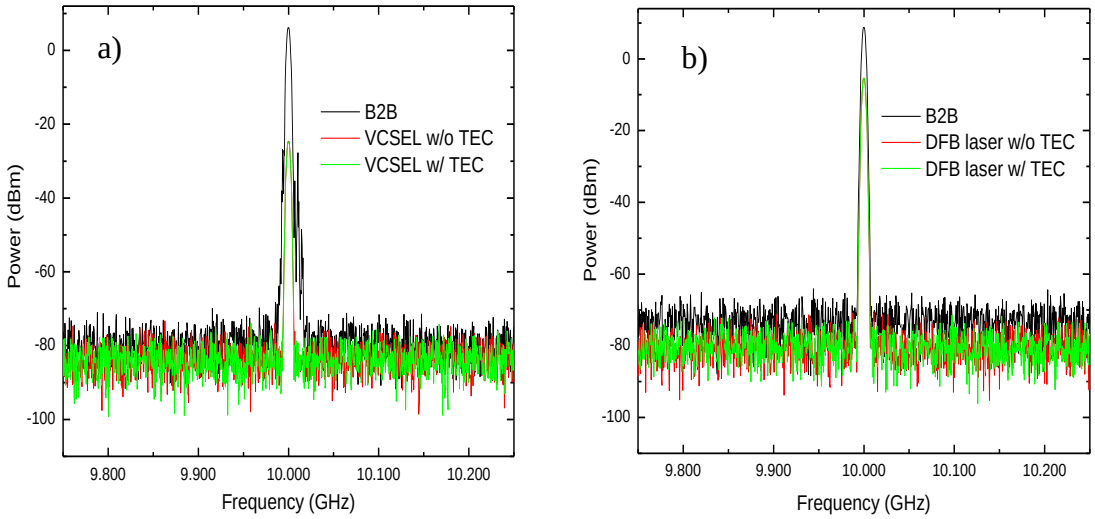

Figure 8.2: the power spectrum of signal generator against a) VCSEL with and without TEC b) DFB laser with and without TEC as observed on electrical spectrum analyzer

The optical signal from the carrier is sent to the PIN photodiode for electrical conversion before being plugged into the Spectrum analyzer. Figure 8.2 displays the signal as seen on the spectrum analyzer; from the power spectrum the effects of laser diode is visible. The central frequency RF power from the signal generator at 794.49 mV is 8.77 dBm as measured on the spectrum analyzer. Upon adding a DFB laser and PIN photodiode to the distribution link to generate optical clock signal, the central frequency power drops to -5.41 dBm. The RF power at the central frequency from signal generator at 61.87 mV RMS level is 6.14 dBm. Upon adding a VCSEL and PIN photodiode to the distribution link to generate optical clock signal, the central frequency power drops to -24.82 dBm both with and without TEC. The components affect the signal central power, which relates to the phase noise. The phase fluctuation brought by the spontaneous emissions phase change is associated with total power.

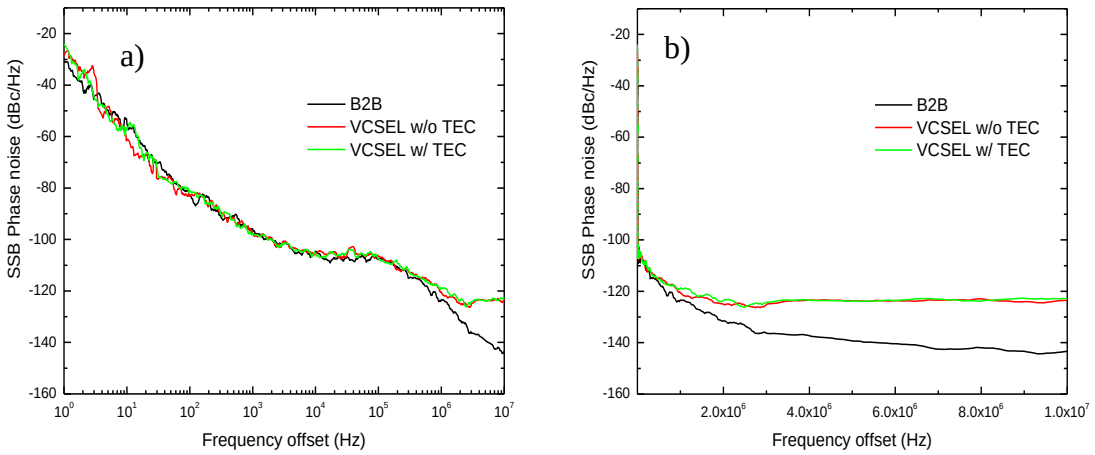

Figure 8.3: the SSB phase noise of VCSEL with and without TEC as a function of a) log offset frequency b) offset frequency away from carrier

Figure 8.3 a) shows the noise contribution of the VCSEL without TEC at offset frequency close to carrier is random and unstable, with a discrete peak between 1 and 10 Hz smoothened by addition of TEC. At 10 kHz offset frequency the phase noise is -97.61 dBc/Hz. The phase noise is represented in the time domain as RMS phase jitter. This is achieved by integrating the phase noise over the desired frequency offset, in this case the offset frequency ranges from 1 Hz to 10 MHz, for a laser with temperature control the RMS jitter is 798.43 fs compared to 847.42 fs when operated without TEC. Laser introduces additive noise to the clock signal. This is a drop in the clock stability from 501.99 fs corresponding to the phase noise of signal generator of -108.13 dBc/Hz at 10 kHz frequency offset.

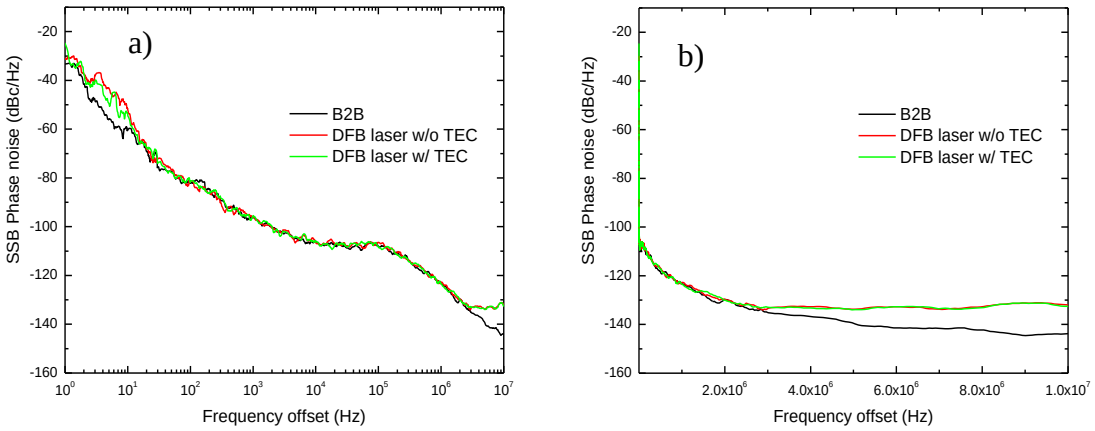

Figure 8.4: the SSB phase noise of DFB laser with and without TEC as a function of a) log offset frequency b) offset frequency away from carrier

The phase noise of the signal generator is -108.13 dBc/Hz at 10 kHz frequency offset. The corresponding RMS jitter is 439.10 fs. At low frequency offset (close to the carrier), adding temperature control reduces the phase noise of the distribution link as seen in figure. 8.4. Between 100 Hz and 1.2 MHz the laser and photodiode noise contribution does not affect the RF reference signal significantly. At 10 kHz frequency offset the phase noise is -95.49 dBc/Hz for laser with temperature control with 682.54 fs RMS jitter compared to 735.25 fs when operated without TEC. Adding a temperature control helped smooth the spurious noise peak at offset close to the carrier. The VSCEL is unstable compared to the DFB laser, this can be associated with the narrow linewidth of DFB laser relative to VCSEL. Temperature stabilization helps reduce frequency fluctuation, resulting in less random noise contribution from the semiconductor laser assuming the photodiode noise is insignificant.

The optical power output of the DFB laser was 4.08 dBm at 55 mA bias current as measured by the power metre, as seen in figure 8.1. The modulation with a 10 GHz RF signal increases the optical power output to 5.33 dBm. The RF power is obtained from the spectrum analyzer, at the central frequency the power of the signal generator is 8.77 dBm. Upon adding a DFB laser and PIN photodiode to the distribution link to generate optical clock signal, the central frequency power drops to -5.41 dBm. Adding a temperature control does not affect the main signal power of the DFB laser as seen in figure. 8.3 a) since it is already stable. The linewidth of the DFB laser is narrow compared to the VCSEL. From the power spectrum the VCSEL displays discrete peaks close to the main power peak. The optical power output of the VCSEL was -6.23 dBm at 5.5 mA bias current, as measured by the power meter. The modulation with 10 GHz RF signal with 61.87 mV RMS level corresponding to the peak to peak current of 3.5 mA for a 50 Ω load, the optical power output changes to a mere -6.40 dBm. The RF power is obtained from the spectrum analyzer, at the central frequency the power of the signal generator is 6.14 dBm. Upon adding a VCSEL and PIN photodiode to the distribution link to generate the optical clock signal, the central frequency power drops to -24.82 dBm.

8.2 Noise contribution of VCSEL vs DFB laser

In this section the noise contribution of different semiconductor lasers is compared. The affect they have on the frequency instability of a clock signal is studied in an attempt to optimize the distribution system. The DFB laser emits an elliptical cone shape optical beam parallel to the wafer surface cleaved into laser bars, a processes not needed on the circular optical beam emitting VCSEL[165]. The VCSEL has low-cost fabrication and can be tested without waiting until the end of the production process. The DFB laser radiation is more concentrated compared to the vertical cavity surface-emitting laser. VCSEL has a low threshold current of 2 mA at room temperature. This is due to its small volume, providing lower power consumption and wide temperature range [166]. The physical size of a DFB laser is large and is the main reason for its larger current threshold (10 times more than the VCSEL) and power consumption. The DFB laser has diffractive optical grating structure inside the resonator which helps with wavelength selection, the resonator of a VCSEL is short in length thus it uses the vertical lasing axis in its cavity[167]. VCSELs are not suitable for high power applications. Both lasers operate in a single longitudinal mode, with the DFB laser having a narrow-spectral width, this allows it to stay in a single mode even in high speed modulation [168]. DFB laser is ideal for high capacity, long distance optical distribution systems. The lasers were both operated with TEC, to provide temperature stabilization reducing frequency fluctuations which may result in random noise contribution.

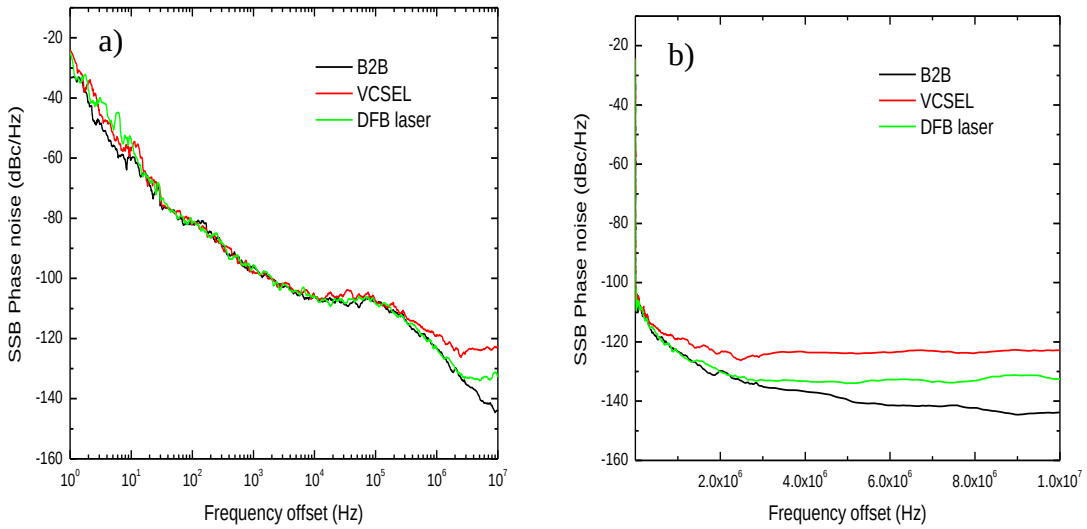

Figure 8.5: the SSB phase noise of VCSEL and DFB laser as a function of a) log offset frequency b) offset frequency away from carrier

The VCSEL has a broader linewidth and lower optical power output compared to the DFB laser. Both lasers maintain the same shape at the noise floor. At offset frequencies close to the carrier the VCSEL is compatible with the DFB laser, even outperforming it in some instances below 10 Hz offset frequency as seen in figure. 8.5 a). At high offset frequencies the DFB laser additive SSB phase noise is less than that of the VCSEL, contributing a lower effect to the clock instability. The SBB phase noise of the DFB laser with PIN PD is -108.25 dBc/Hz and -107.53 dBc/Hz for VCSEL at 10 kHz offset frequency. The RMS jitter of the RF reference signal is degraded due to DFB laser and VSCEL by 243.44 and 296.44 fs, respectively. The results are within the clock stability requirement for successful operation of the MeerKAT telescope. Though the VCSEL is small and cost effective, for highly stable RF signal distribution the DFB laser would maintain purity of time and frequency reference stability as it contributes less noise to the clock signal. Over long distance distribution of the optical clock signal over optical fibre the DFB laser would maintain spectral purity of the reference signal at a level within the clock stability budget. VCSEL can be used for short length optical fibre distribution system if the stability requirements are satisfied and the optical power output is within the sensitivity of the photodiode.

8.3 Noise Contribution of PIN vs APD Photodiode

In this section an evaluation and comparison between the PIN and APD photodiodes is conducted based on the functional parameters as a means to characterize and analyze the performance in terms of phase noise measurements. A photodiode converts an optical signal to an electrical signal for easier information extraction. When photons of energy equal to or higher than the band gap illuminate the photodiode, electrons carried by the absorbed photon move from the valance band to the conduction band. The number of electron-hole pairs created is relative to the absorbed light. The junction capacity and transit time limit the responsivity of the photodiode, improved by increasing the reverse bias voltage. The PIN intrinsic layer width is optimized to maximize the performance of the device at the recommended reverse bias voltage. APD is a refinement of the PIN, the internal gain multiplies electrons by the avalanche effect on the intrinsic layer[67].

Random intrinsic fluctuations generate photodiode noise, which degrades the stability of the signal, imposing difficulties in information extraction at the photodiode output. The photocurrent generated through the photon to electron-hole pair conversion is used to measure the noise. The photodiode noise is a sum of thermal and shot noise. Thermal noise is derived from the shunt resistance (photodiode load resistor) the cause thermal agitation of electrons affecting responsivity, this type of noise is dominant in the PIN photodiode. Shot noise is associated with the dark current and the photocurrent, arises due to the optical power fluctuations of light made up of a discrete number of photons[169]. Photodiode is required to have low sensitivity and high responsivity at the wavelength of interest, high bandwidth, fast response time and temperature variation insensitivity, amongst other things. The photodiode absorption coefficient is related to the temperature; temperature variation affects the sensitivity and dark current[170]. Electrons in the valance band are excited by increasing temperature, pulling them to the conduction band[171].

The APD gain factor improves the lowest detection limits, resisting thermal noise through avalanche processes giving rise to quantum noise. The excess noise is generated by the current statistical fluctuation associated with the process of ionization by impact

affecting response time. The gain increases until the shot noise and thermal noise reach a level of equilibrium, making both noise types significant in the APD. The avalanche photodiode has an internal gain making it a good candidate for long haul communication, where a signal from central point to remote location is reliably transmitted over long distance. APD needs a high reverse bias voltage corresponding to the high electric field that energizes the photo-generated electrons. PIN is easier and cheaper to fabricate[172]. The optical input power threshold for the APD is 3 dBm; since the directly modulated DFB laser has an optical power output of 5.33 dBm a 3 dB attenuator was added bringing the power to 2.75 dBm. Figure 8.5 shows the power spectrum of the APD for the different multiplication gain tuned by changing the bias voltage of the amplification stage between 24 V and 35.6 V.

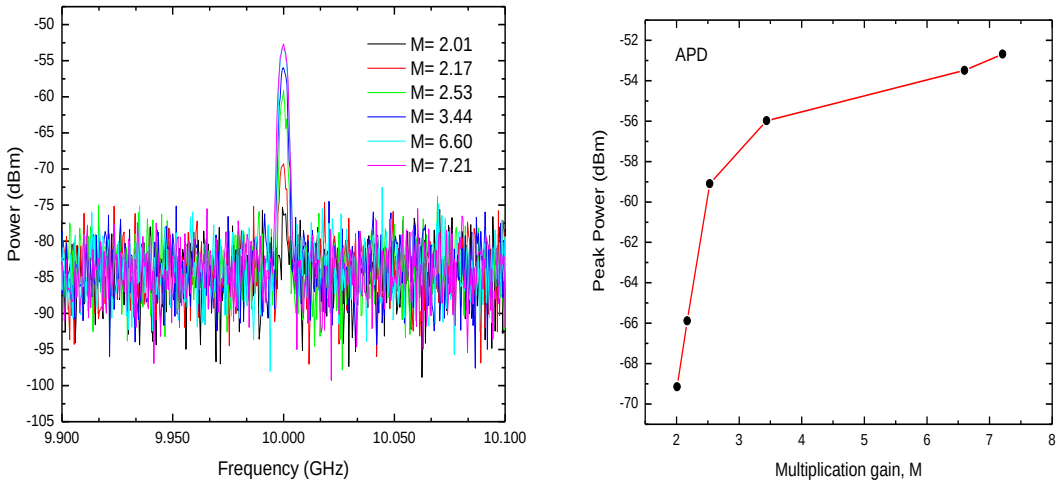

Figure 8.6: Power spectrum as a function of frequency for APD photodiode at different multiplication gain

The central frequency power peak increases with the multiplication gain M as seen in figure 8.6. For M= 2.01 the central peak is lost within the noise with RF power of -69.15 dBm, improving to -52.68 dBm for M= 7.21 at bias voltage of 35.6 V closely related to the -53.49 dBm at M= 6.60 at 34 V. The SSB phase noise is dependent on the power of the carrier.

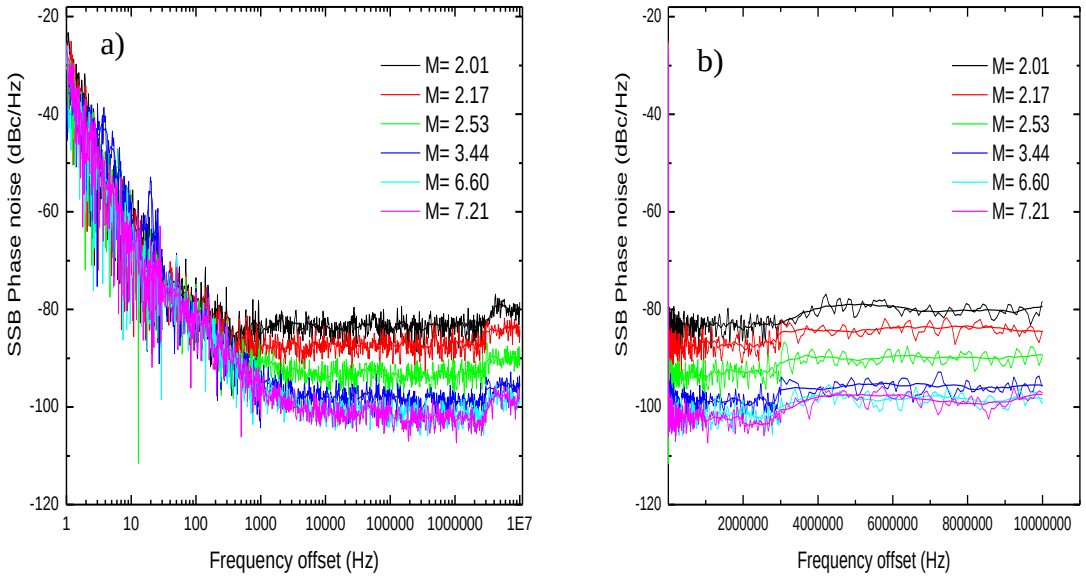

Figure 8.7: the SSB phase noise of APD photodiode as a function of a) log offset frequency b) offset frequency away from carrier

At offset frequencies close to the carrier, the noise contribution is relatively similar with no spurious noise with the exception at M=3.44 possessing a discrete peak at offset frequency around 10 Hz. At far offset the larger multiplication gain has lower noise contribution reaching equilibrium at M=6.60 and M=7.21. The RMS jitter is 6.62 ps for M= 2.01 compared to 915.34 fs at M= 7.21. The APD had a fan attached to it to maintain temperature stability and avoid over heating with time.

The 10 Gb/s APD has an ultra-high sensitivity of -26 dBm and 0.7 A/W responsivity at 1550 nm. It contributes a group delay deviation of 15 ps. The PIN photodiode optical sensitivity is -19 dBm with a typical responsivity of 0.8 A/W at 1550 nm. It has a group delay deviation of 10 ps. The optical input power damage threshold for a PIN photodiode is 8 dBm. Figure 8.8 displays the power spectrum of both photodiodes against the signal generator (back to back) measurement. The 10 GHz RF clock tone from the signal generator was used to intensity modulate a DFB laser generating an optical clock signal with 5.33 dBm optical output power. This is the optical input power sent into the PIN photodiode.

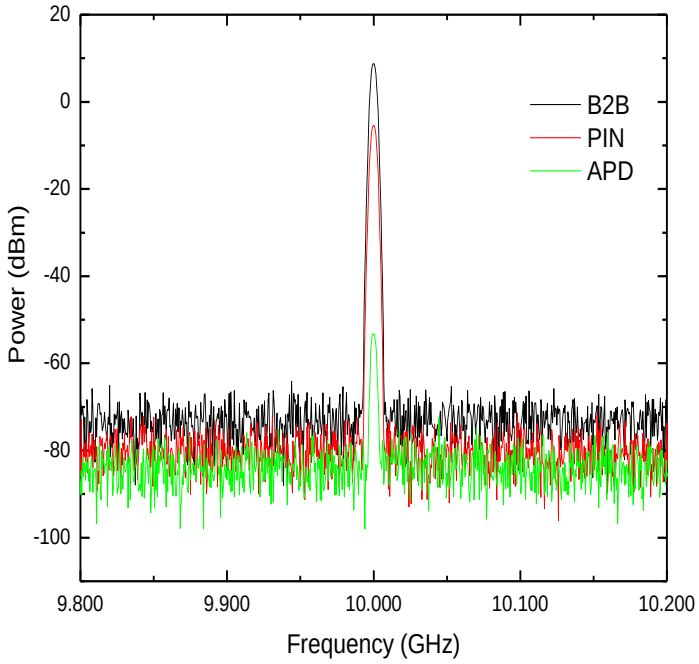

Figure 8.8: Power spectrum as a function of frequency for PIN and APD photodiode

The APD peak is low in power as the input power was attenuated using a 3 dB attenuator to satisfy the optical input power damage threshold. The optical input power sent into the APD is 2.67 dBm. The peak appears narrower. The bandwidth of APD is typically 7 GHz with that of the PIN being 10 GHz with wavelength response range of 950-1650 nm and 800-1650 nm respectively. Both photodiodes have a transimpendance of 500 Ω. The thermal noise of the PIN photodiode is more dominant as it has a higher bandwidth for the same resistance and temperature conditions. To ensure temperature stability, both photodiodes were operated with a fan to mitigate the effect of temperature variation.

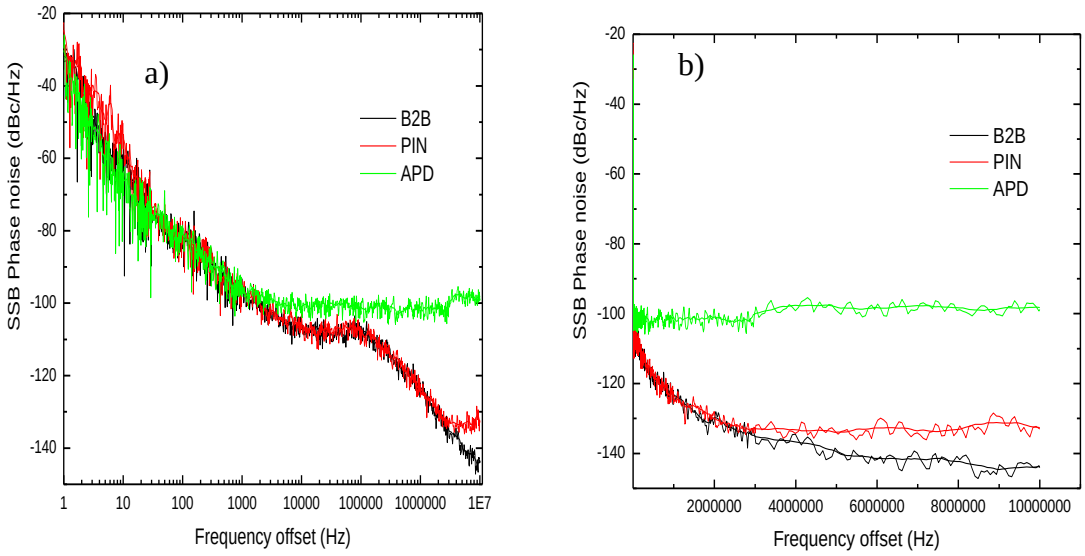

Figure 8.9: the SSB phase noise of PIN and APD photodiode as a function of a) log offset frequency b) offset frequency away from carrier

At offset frequencies close to the carrier, the APD does not degrade the stability of the signal, it follows the same trace as the clock tone at the same SSB phase noise level. At offset above 100 kHz the phase noise flattens with the photodiode noise contribution highly noticeable as seen in figure 8.9. The PIN deviates from the back to back trace at offset frequencies above 3 MHz. The RMS jitter contributed by using the APD to convert the optical signal to electrical is 915.34 fs which drops to 682.54 fs when PIN photodiode is used. Both photodiodes would be useful for the successful operation of the MeerKAT telescope but the PIN would optimize the link stability. For low optical power signal detection and long haul communication APD would be ideal as it has a lower detection limit and an internal gain to increase the electrical signal power that corresponds to the incident optical power.

8.4 Cabling Effect on the Different Types of Optical Fibre

Radio frequency (RF) signals transmission from a centralized clock to remotely located antennas interlinked by optical fibre forms the backbone of telescope networks. The time and frequency reference signal is disseminated via a buried fibre to every digitizer to ensure they are synchronized to the same clock tone for proper alignment and later correlation. The correlator is situated inside the Karoo Array Processing building (KAPB) with a maximum of 12 km length of fibre between it and any single antenna [173]. For thermal stability the optical fibre cable runs through a conduit buried 1m below the ground. In this section the cabling effect of optical fibre with different profile on the clock tone stability is studied. A 23.5 km low water peak non zero dispersion-shifted fiber (ITU-T G.652.C- compliant) with 10.5 µm mode field diameter offers low attenuation around the OH peak. The corresponding effective area is 52 μm^2. It has a cutoff wavelength ≤1260 nm and is optimized for transmission systems that occur across a broad range of wavelengths from 1285 nm to 1625 nm. For short, unamplified metro and access networks the G.652 fiber offers excellent capability with a dispersion limit distance of 60 km at 10 Gb/s without dispersion compensation. For transmission at 1550 nm the dispersion is 16.34 ps/nm*km[24].

The G.652.C optical fibre used in the NMMU lab has customized cabling with thermal protection tape, loose fibre sealed with moisture-proof gel and laid around a non-metallic stress member. It is rolled up into a spool with a bigger radius compared to G.655 whose optical fibre is just a core and cladding. G.652.C frequency and amplitude is fairly kept constant with deterministic phase shift[174]. A 24.8 km nonzero dispersion shifted fiber (ITU-T G.655) has a mode field diameter of 8.3 µm with 80 μm^2 corresponding effective area. At 1550 nm the chromatic dispersion is roughly 3.65 ps/nm*km. G.655 fiber is more suitable for long distance transmission and high capacity WDM (wavelength division multiplexing) system[10]. WDM systems are optimized at conventional C-band (1530-1565 nm) and long wavelength L- band (1565-1625 nm) with less attenuation

compared to original O-band (1260-1360 nm). G.655 fiber suppress the growth of four-wave mixing by moving the zero-dispersion wavelength outside the 1550-nm operating window .The limited distance at 10 Gb/s without any dispersion compensation is 260 km. The channel spacing is ≤0.8 compared to the G.652 ≥0.8 nm.

A 10 GHz RF clock signal was used to intensity modulate a 1550 nm DFB laser. The generated optical clock signal of 5.33 dBm optical output power was transmitted over different types of optical fibre with under different cabling conditions. A 24.8 km G.655 optical fibre spool was used to distribute the optical signal and the effect it has on the phase stability of the clock was studied. This was compared to transmission over a specially cabled 22.3 km G.652.C optical fibre.

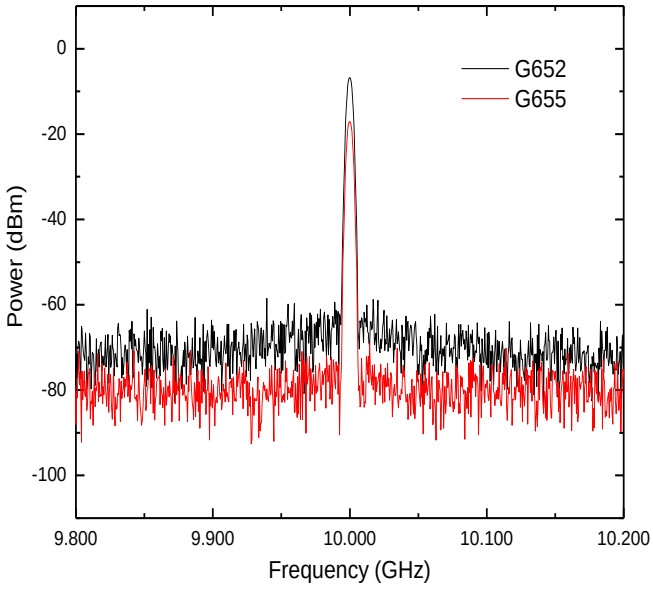

Figure 8.10: Power spectrum as a function of frequency for different fibre at 1550 nm detected by PIN photodiode

Both fibers have the same ≤1260 nm cut off wavelength. The attenuation is 0.2 dB/km with a typical less than 0.1 ps/km PMD parameter in both cases. Upon transmission over the G.655 optical fiber the RF power of the central peak is -17.09 dBm with a lower noise floor compared to the G.652.C optical fiber as seen in figure 8.10.

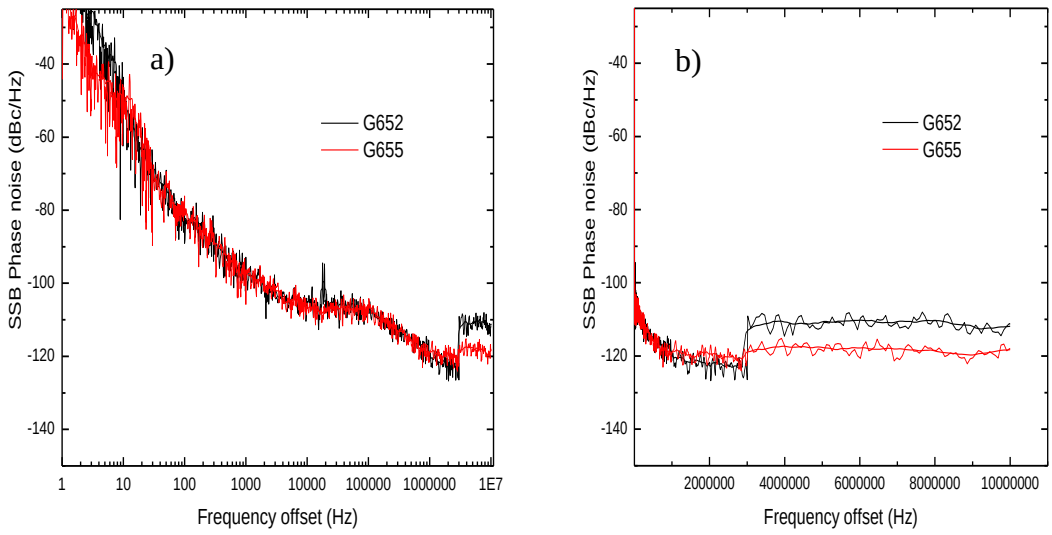

Figure 8.11: the SSB phase noise for different fibre at 1550 nm detected by PIN photodiode as a function of a) log offset frequency b) offset frequency away from carrier

A complex interaction of parameters of the fiber induces the nonlinear effect. This effect is directly proportional to the reciprocal of the effective area. The higher effective area of the G.655 mitigates the nonlinear effect meaning it has less noise contributing factors. At offset frequencies lower than 10 Hz the SSB phase noise of the G.655 optical fibre is lower than the G.652.C and again at values greater than 1 MHz. the G.652.C fibre has a spurious noise peak at offset frequency close to 10 kHz as seen in figure 8.11, this affects the overall RMS jitter of the transmission link. The RF clock signal distribution system has a RMS jitter of 1.37 ps short-term instability when 10 GHz is transmitted via 24.8 km G.655 optical fiber. The lower dispersion of the G.655 fiber makes it highly dispersion tolerant for the cost effective direct modulation of DFB laser. It is ideal for long haul high capacity systems. Erbium Doped Fiber Amplifier (EDFA) can be used to boost the optical signals in C-band capability before transmission.

For any given signal the PMD is unstable, and unpredictable and must be measured. Unpolarized light is represented at the centre of the Poincaré sphere. Linear states lie in the equator. Elliptically polarized state are found everywhere on the surface[28], [41]. The north and south pole represent the right and left circular states respectively.

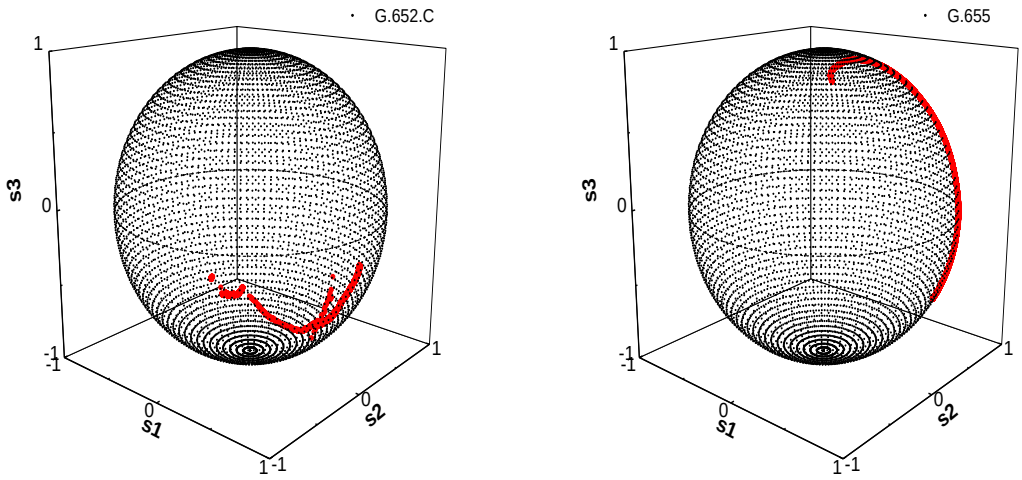

Figure 8.12: PMD vector on a Poincaré sphere for G.652.C and G.655 fibre

The PMD vectors for an optical clock signal were observed over 24 hours; the phase shifts due to the state of polarization shift from SOP to another is represented on the Poincaré sphere. Figure 8.12 shows a continuous evolution of SOP for G.655 transmitted optical clock signal, the light moves from one orthogonal state to another. The fibre birefringence is temperature dependent, with phase and group delay changing with temperature variation. Cabling fibre ensures thermal stability and reduced fibre noise contribution and frequency instability on the RF clock signal. The G.652.C optical fibre has customized cabling with thermal protection tape, loose fibre sealed with moisture-proof gel and laid around a non-metallic stress member. It is rolled up into a spool with a bigger radius compared to G.655 whose optical fibre is just a core and cladding. G.652.C frequency and amplitude is fairly kept constant with deterministic phase shift.

The SKA requirement for frequency stability to ensure successful is at least 1.30×10^{-14} for 100 s averaging time distributed over 8-12 km optical fibre. This is for distribution of precise time and frequency reference signal from a centralized processing station to remote antenna array interlinked by optical fibre. The optical fibre is superior to coaxial fibre as it is immune to radio frequency and magnetic interferences and can transmit high frequency signals over tens of kilometers without the use of O-E-O repeaters

(regenerators). The optical fibre group delay variation imposes difficulties in ultra-stable frequency signal distribution. This results in the RF clock signal being offset by an amount proportional to the rate of change, frequency fluctuations.

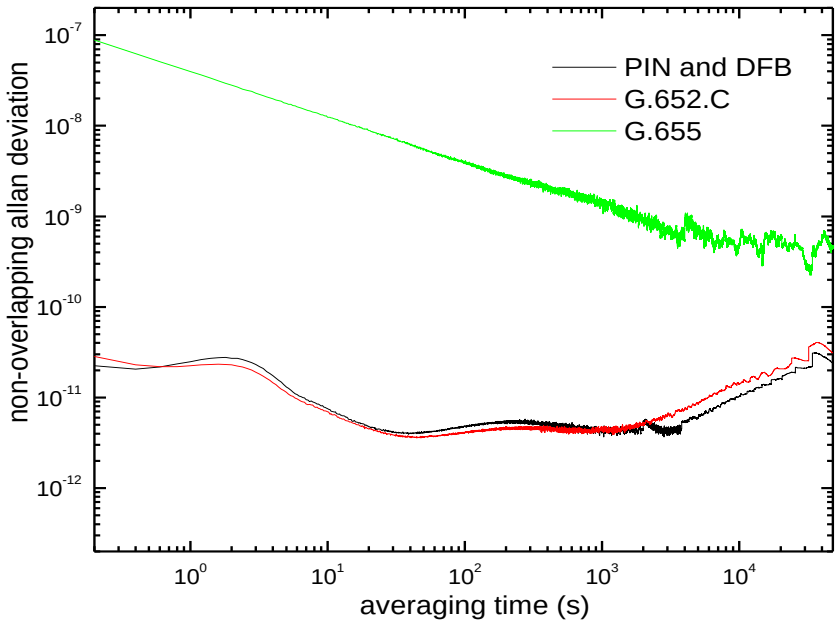

Figure 8.13: non-overlapping Allan deviation as a function of tau log-log plot

The instantaneous frequency of the optical signal was observed for 6 hours at 0.2 seconds sampling time interval. The frequency instability of the RF reference clock signal from a 10 GHz signal generator transmitted over a 22.3 km G.652.C optical fibre follows an unlocked system pattern with stability degradation over time. The frequency instability was measured and expressed as a non-overlapping (standard) Allan deviation to be 4.12×10^{-9} for 100 s averaging time. The optical clock signal after transmision through a 24.8 km G.655 optical fibre has a locked system pattern. The Allan deviation is of the expected $\frac{1}{\tau}$ slope. This can be used to predict the stability of the system over time and the amount of drift in the clock. The frequency instability is 4.08×10^{-9} for 100 s averaging time.

In this chapter a distribution system similar to the MeerKAT telescope was developed. The noise contribution of different components that make up the transmission link was studied, analyzing how each affects the stability of the frequency reference clock signal. The comparison was made between VCSEL and DFB laser, PIN and APD photodiode, and between G.655 and G.652.C under different cabling conditions. The noise contribution was demonstrated as the short-term instability characterized as the single sideband phase noise as measured by the spectrum analyzer direct method. The results were used to hand pick optical components for the distribution system design that would reduce the additive noise contribution and optimize the performance of the RF clock stability. Furthermore, the optimized distribution system will be used to study the additive noise contribution of an optical amplifier, with focus on the position to place the device along the transmission link for reduced noise.

Chapter 9

Environmental variation induced noise and amplifier additive noise

In this chapter the effect of the environmental variation in the surrounding areas of an optical fibre was studied. The optical fibre length changes with varying temperature introduce group delay variation. Birefringence of the optical fibre introduces phase instability in the clock signal. The thermally induced signal instability was analyzed in the time domain and characterized in terms of Allan deviation as measured by the spectrum analyzer direct method. Furthermore, the method was used to measure the additive noise of an optical amplifier at different positions along the optical fibre link.

9.1 Effect of Temperature Variation on the Transmission Link

Optical fibre is the perfect choice for RF clock distribution at high frequency with high precision; additive timing jitter is expected to be low, and there is a demand for long-term stability over short distance and low frequency capable coaxial cable. A one-way transfer is used to distribute a centralized frequency reference signal to the remote site (antennas) over optical fibre. The phase and frequency fluctuation of the RF clock signal over optical fibre limits the performance of the telescope network. The transmission line instability degrades the optical signal (laser cavity gets broadened)[175], contributing a significant fraction to the overall deviation of highly stable and precise RF clock signal required for successful operation of the telescope. The noise in the optical fibre link results from noise contribution from multiple sources. The waveguide phase noise contribution appears at the receiver. The temperature and mechanical variations in the surrounding areas of optical fibre translate to phase noise, which will need to be considered in the network design[47].

These environmental perturbations introduce group delay variation on the optical fibre. In unidirectional (one-way) frequency distribution the temperature effect on the optical fibre propagation variation results in: thermal induce change of the refractive index, physical length of the fibre variation with temperature fluctuation and the interaction between the thermal induced laser wavelength shift and the fibre chromatic dispersion [176]. The rapid changes in the optical fibre group delay cause the frequency and phase of the transferred RF clock tone to shift. The temperature variation of fibre is 6.6 ppm/℃[87]. For a 20 km long optical fibre, 10 ℃ temperature change in the surrounding areas of the fibre constitutes a 1.32 m length increase equivalent to 6.38 ns change in phase as seen in figure 9.1

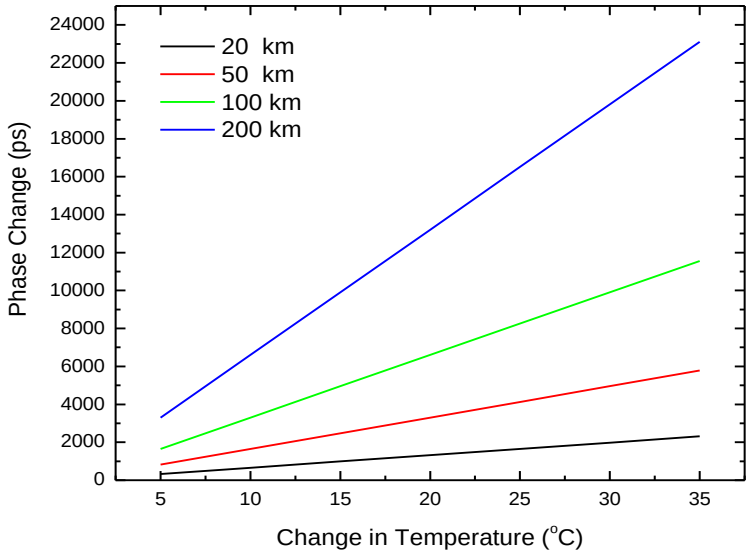

Figure 9.1: phase change in difference fibre lengths as a function of temperature variation

For monochromatic light (single mode frequency signal) the noise accumulates along the length of the transmission medium[177]–[179].The laser wavelength shift can be reduced by thermal stabilization of the laser, achieved by using a temperature controller. This variation in the propagation delay affects the stability and precision of the time and frequency reference signal. The RF frequency remains more stable over environmental isolated fibre (the variation is slow in thermal stabilized optical fibre) compared to overhead path, this is more apparent in short-term characterization [175][179].

The fibre is cabled and buried 1 m under the earth's surface to reduce temperature and vibration fluctuations, the unidirectional optical fibre transfer of the RF clock signal is suitable for short distance 8-12 km distances between any antenna and the central building for the MeerKAT telescope[84], [85], [87]. Shielding the optical fibre helps compensate for the environmental induced noise. To achieve an Allan deviation in the 10^{-15} range at 24 hour duration distributed over a $\sim$12 km link, the delay variation should be within the picosecond range. In this section the temperature induced group delay variation on a frequency reference optical clock signal distribution system using standard available telecommunication components is studied. The measurements were performed on an optical fibre on a spool, exposed to daily temperature changes and subjected to drastic temperature changes.

9.1.1 Experimental Setup

A G.655 optical fibre on a spool of 23.8 km length was used to transfer an optical clock signal. The signal is generated by the intensity modulation of a C-band thermally stabilized 1550 nm DFB laser using a highly stable 10 GHz RF clock tone from the signal generator. The optical fibre was subjected to harsh temperature variations, regularly inserted inside a fridge to lower the surrounding temperature (simulating the late night levels in the Karroo) and was also left out in the open exposing it to daily temperature variations. The temperature variation was done at random times for different time intervals, enough to change the temperature from cold to warm with the range of 7 ℃ to 25 ℃. The optical clock signal is recovered at the receiver end, PIN photodiode converting it from optical to electrical signal before inserting it to the electrical spectrum analyzer for slow variation analysis. A Rubidium clock was attached to the spectrum analyzer and was used as an internal reference signal (local oscillator) of the measuring instrument, tracking how the phase of an optical clock signal changes with time. The single mode fibre dependence on temperature was measured and characterized in the frequency domain as well as the time domain in terms of phase noise and Allan deviation, respectively. The experimental set up used is shown in figure 9.2.

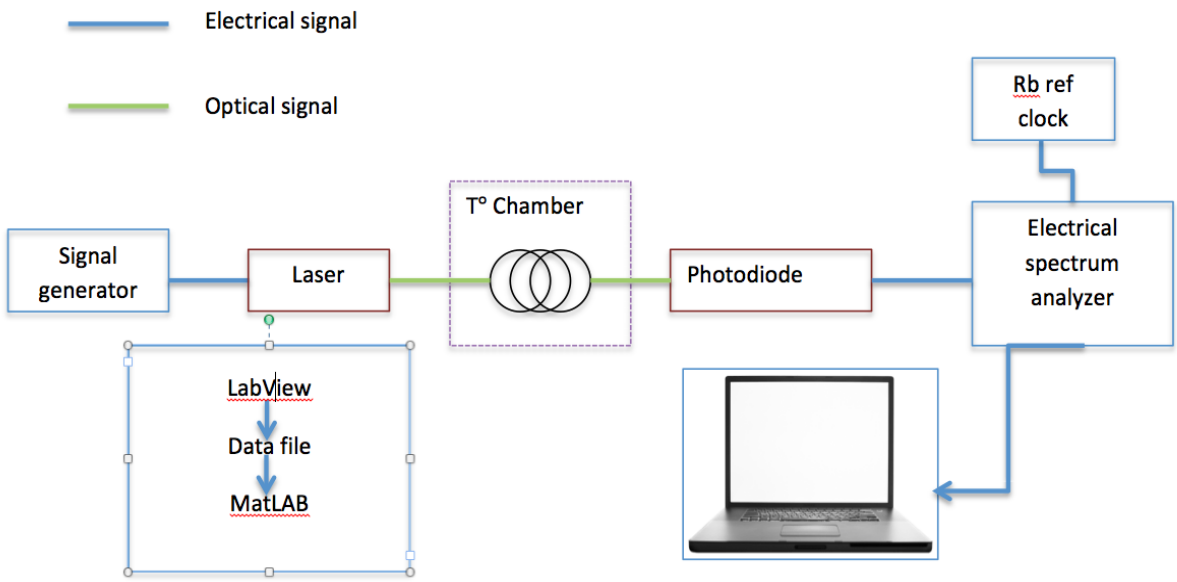

Figure 9.2: experimental setup measuring the frequency instability effect of temperature variation on optical fibre transmitting 10 GHz RF clock tone from the signal generator in the frequency and time domain

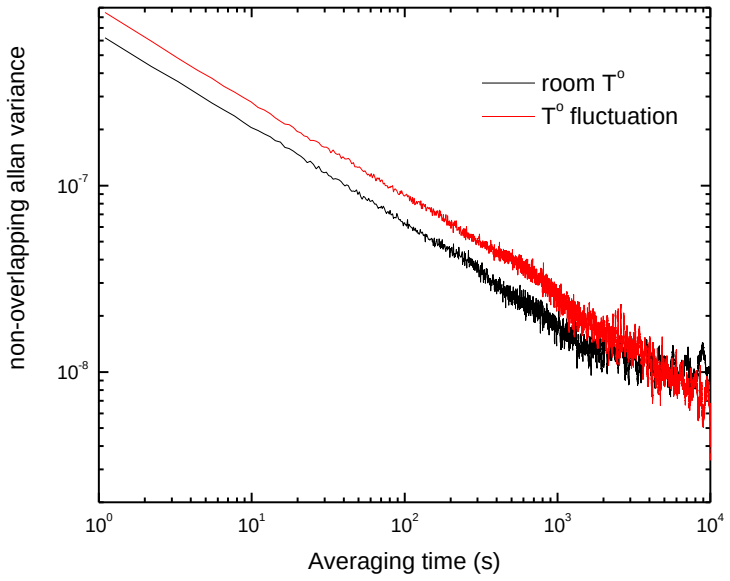

Figure 9.3: frequency instability of optical fibre with temperature fluctuating conditions in the time domain characterized as log-log plot non-overlapping Allan deviation as a function of averaging time

The phase fluctuates due to temperature expansion of the fibre and the thermal by induced changes in the refractive index. Figure 9.3 shows the effects of temperature

fluctuation on a G.655 fibre, degrading the frequency stability of RF signal from 4.08E-09 non-overlapping Allan deviation averaged over 100 s to 7.8E-08. The measurement was taken over 2.7 hrs with the temperature variation between 7 and 25 ℃. For an optical fibre kept at room temperature an Allan deviation of 6.31E-08 averaged over 100s was measured. At short time scale the environment perturbation couples to optical fibre and causes the physical length of fibre to change.

The RF clock tone is transfer based on the group delay for propagation of the single mode optical fibre, this is expressed as group velocity for 1550 nm at 23.8 km. the group delay depends on the refractive index which is affected by the environmental conditions (temperature fluctuations, atmospheric pressure change and bending in the optical fibre) with a significant contribution being from temperature variation effects on the frequency stability transmitted through the optical fibre. For MeerKAT telescope networks the optical fibre is buried 1 m underground to shield the optical fibre from temperature fluctuations, thus the process will be slow and will mostly be affected by the diurnal and seasonal temperature cycles.

9.2 The Optical Amplifier Residual Phase Noise

A classical optical fibre link (modulator, laser, optical fibre, and photodiode) signal is weak and results in a strongly degraded RF reference signal, especially in short-term characterization in the frequency domain where the phase noise is related to the power of the signal. The use of optical amplifiers in transmission links overcomes the distance limitation imposed by optical fibre attenuation, assisting in the retrieval of high power signal on the photodiode. An optical amplifier allows for direct optical signal amplification with high capacity WDM transmission over ultra-long haul. Passing the signal through the optical amplifier lowers the optical SNR, linearly adding amplitude spontaneous emission to the signal resulting in amplitude noise[78]. The non-linear interaction between the electrical spectrum analyzer (ESA) from optical amplifier and the signal under test results in phase noise. The amplifier additive phase noise contributed to the phase noise close and far away from the carrier frequency of the RF signal. The main types of phase noise that originate inside an amplifier are white noise and flicker noise,

these are responsible for the short-term phase fluctuation of the signal. The white noise is produced by the random motion of electrons, adding random noise to the RF frequency signal power spectral density[77][180]. Flicker phase noise is formed at offset Fourier frequency close to the carrier. Independent of the signal, the noise contribution by optical amplifier is constant. The amplifier can be specified by its noise figure/noise factor, which is a measure of the noise out of the two-port as a function of inverse gain. An ideal amplifier noise factor is 0 dB, with low noise amplifiers ranging between 0.5 and 2 dB[79][181]. Amplifier additive noise is low and is measured as a contribution to the absolute phase noise measurement of the system.

9.2.1 Measurement Setup

For this study an Erbium Doped Fibre Amplifier (EDFA) was used in the linear regime operation condition. The device was used to amplify an optical clock signal generated by intensity modulation 1550 nm DFB laser by a 10 GHz RF clock tone distributed over a 23.8 km G.655 optical fibre kept at room temperature. Upon amplification the optical signal is converted to electrical signal by a PIN photodiode before being sent to the electrical spectrum analyzer for instability measurement using direct method as shown in figure 9.4. The residual phase noise measurements were done relative to the signal gain of the amplifier. The amplifier is necessary for bringing the amplitude of the signal to a usable power level. The amplifier added phase noise contribution is distinguished from the other optical link components added noise by comparing the classical optical fibre link (pre-amplified) noise floor measurement to the amplified signal.

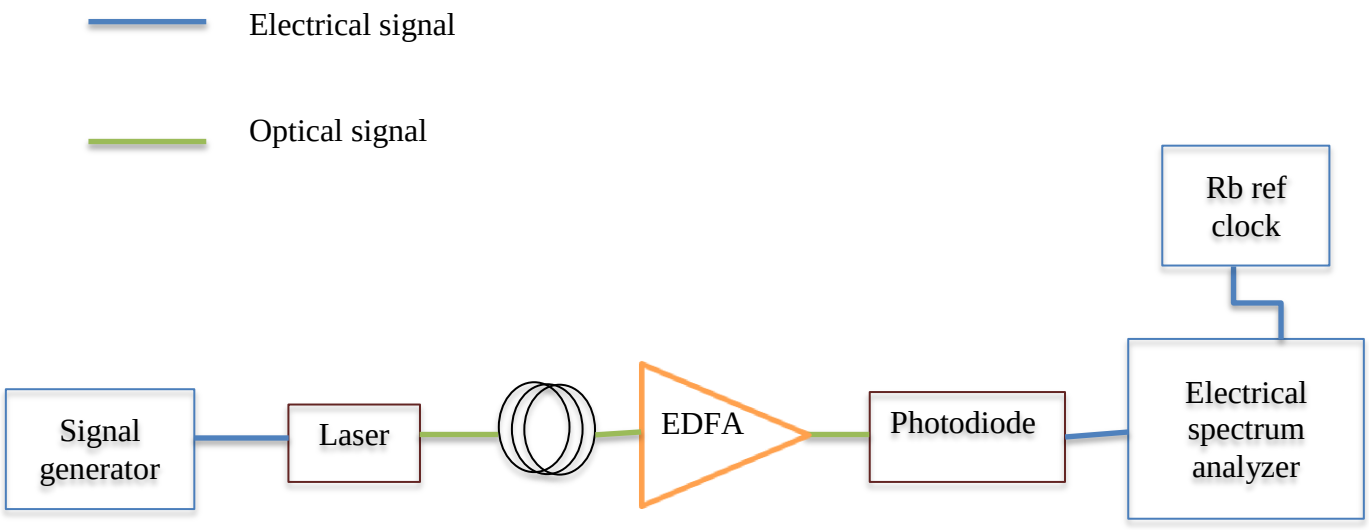

Figure 9.4: experimental setup measuring the frequency instability of the temperature variation on optical fibre 10 GHz RF clock clock tone from the signal generator in the frequency domain

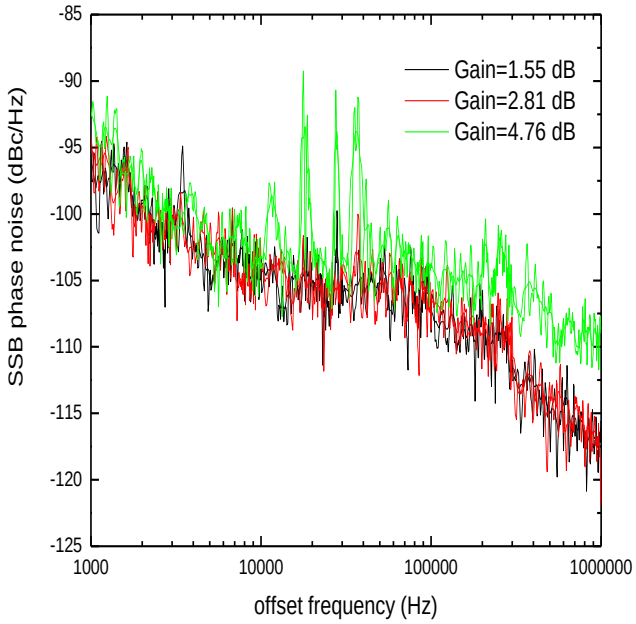

Figure 9.5: SSB phase noise as a function of Fourier frequency for different amplifier gains

The power spectral density of the EDFA at different gain is shown in figure 9.5. In the linear regime, the gain corresponds to small signal gain. The additive phase noise increases with increasing gain. The flicker phase noise is independent of the power. Flicker phase noise is represented by $1/f^2$ slope on the single sideband phase noise plot. This type of noise is introduced to the clock signal by noisy electronic devices such as amplifiers. At 4.76 dB gain the noise floor is reduced and there is multiple spurious noise peaks, discrete phase noise. The noise floor for the EDFA at 1.55 dB gain is ~ -115 dBc/Hz compared to the ~ -109 dBc/Hz for 4.76 dB. The phase noise floor changes with changing gain. The amplifier gain is directly proportional to the amount of additive noise; the maximum amplifier phase noise contribution occurs at maximum signal gain.

The optical amplifier is commonly placed at the end of the optical fibre span to boost the power of the transmitted signal to compensate for the attenuation. The cumulative noise induced by the amplifier is a function of gain. To ensure minimalistic noise contribution and reduced frequency/phase instability of the link, the EDFA should be operated at high optical input. This can be achieved by placing the optical amplifier close to the transmitter.

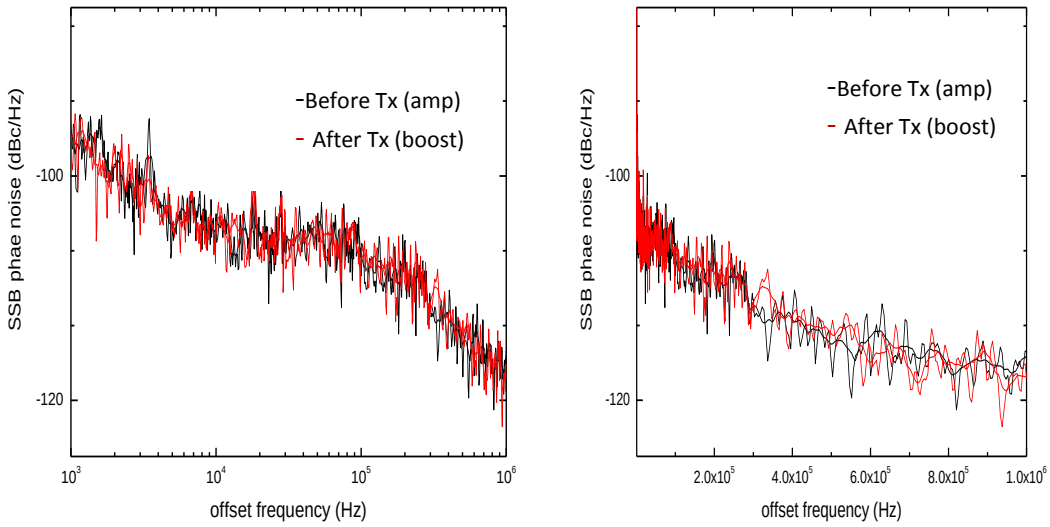

Figure 9.6: Optical amplifier additive SSB phase noise on RF clock signal as a function of a) log offset frequency (close to carrier) b) offset frequency (far away from carrier) at different position of the transmission link

The short-term instability of the RF time and frequency reference signal is affected by the additive noise contribution of an optical amplifier to the transmission link. The effects of placing the amplifier close to the transmitter or after the signal has been transferred (just before the receiver) does not have a drastic/significant change to the overall frequency instability in the frequency domain as seen in figure 9.6. Increasing the input power to the EDFA results in lower EDFA gain and the additive phase noise decreases as the EDFA gain decreases.

The long-term frequency instability for a clock tone signal transferred over an optical fibre transmission link was measured. The additive noise contribution of the optical amplifier was studied as a function of power, moving the amplifier close to the transmitter (amp) and at the end of the transmission link (boost) to observe the frequency drift as a function of time.

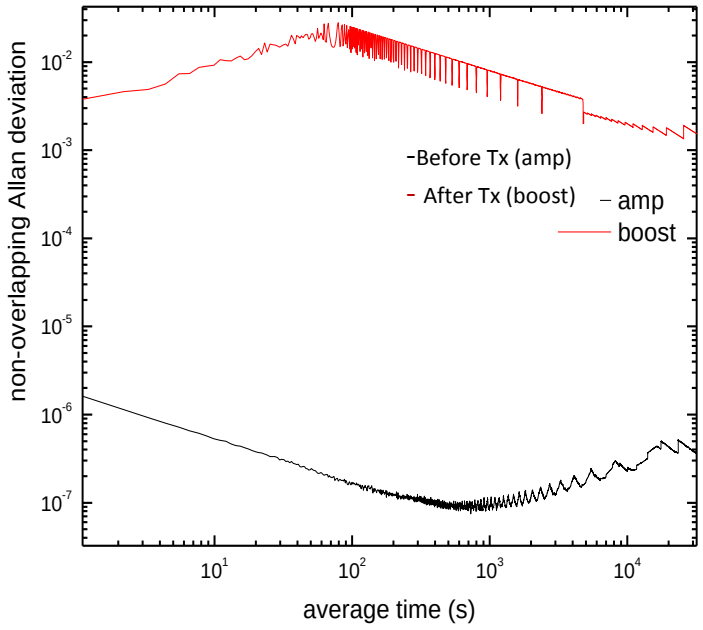

Figure 9.7: frequency instability of RF clock signal transferred through amplifier containing transmission link in the time domain characterized as non-overlapping Allan deviation as a function of averaging time (log-log plot)

The instantaneous frequency instability of the system was observed for 27 hours at 0.1 seconds sampling time. The data collected was used to calculate the Allan deviation at different averaging times as seen in figure 9.7. From the results the noise contribution of the amplifier and the improvement associated with the placement is evident. The frequency instability of the G.655 at 100 s averaging time is 6.31×10^{-8} as represented by Allan deviation. Upon amplification the ASE reduce the phase stability to 1.65×10^{-7} and 2.00×10^{-2} at 100 s averaging time for amp and boost respectively. The position of the amplifier on the optical fibre link leads to different phase noise contributions, placing the amplifier close as possible to the transmitter a higher input power is achieved. Placing the amplifier close to the transmitter is not always the best solution (especially for fixed output amplifiers), as inputting high power signals into the optical fibre lead to nonlinear effects burning the optical fibre.

In this chapter the direct method of electrical spectrum analyzer was used to measure and analyze the effects of environmental variation in the surrounding areas of optical fibre on the phase stability of an optical clock signal. The instability was characterized in the frequency domain as well as the time domain in terms of phase noise and Allan deviation, respectively. Furthermore the technique was used to investigate the additive phase noise of an optical amplifier as a function of gain. The amplifier was placed at different positions along the RF clock signal distribution system over an optical fibre kept at room temperature.

Chapter 10

Conclusion

The direct method of spectrum analyzer is a common technique for measuring signal instability. The technique does not require a lot of components, making it easy to setup and calibrate. In this work, a direct method was used to formulate and implement a suite of measuring tools for complete characterization of fibre-based clock tone distribution systems used in the MeerKAT and SKA telescope networks. The suite was used to measure the signal instability of a RF frequency reference clock signal and the noise induced by the components making up the optical fibre transmission link. The signal instability was measured and analyzed at 1 Hz and above offset frequency away from the carrier using phase noise. The signal instability was also measured at offset less than 1 Hz away from carrier using the Allan Deviation. This was the first time that these measurements were conducted at the Nelson Mandela Metropolitan University, Centre for Broadband Communication. The MeerKAT and SKA RF clock stability requirements for successful operation were used as a guideline for a detailed study of signal instability. The short-term instability was characterized in the time domain as phase noise and spurious noise. Long-term instabilities such as aging and frequency drift were analyzed in the frequency domain.

A spectrum analyzer was used to measure the phase and frequency fluctuations at a given time instance. Labview code was developed to log the instantaneous frequency values as measured by the signal counter built into the Rhode and Schwarz electrical spectrum analyzer. The data points were recorded at fixed time intervals equal to or larger than the signal counter resolution (100ms) for a desired observation time period. The finite number of data points was loaded to Matlab code developed to statistically estimate the frequency drift at different averaging time based on the observed frequency fluctuation.

The estimation is taken as the two-sample variance of instantaneous frequency from its nominal value and was analyzed as non-overlapping Allan Deviation. The suite is capable of measuring the amount of instability, the type of noise and the source of the noise. These include the birefringence of optical fibre induced instabilities in the RF clock phase as the polarization of lightwave fluctuates.

For a telescope network such as the MeerKAT and SKA, the RF clock is the heartbeat and optical fibre forms the backbone of this scientific project. The stable clock is distributed over optical fibre from the central processing site to each antenna of the radio telescope array. The clock is used to trigger the digitizers in the antennas and to time-stamp the captured data. When a stable RF frequency reference clock tone is used to directly modulate a coherent source for distribution over optical fibre to the receiver, instabilities may arise due to the components that make up the optical transmission link, the operation parameters of the devices and the environmental conditions in the surroundings of the components. The effects of environmental conditions (especial temperature variations) on the optical fibre is of great importance because of the harsh temperature conditions in the Karoo.

In chapter 6 the direct method was used to measure and analyze the inherent noise of the RF clock tone as generated by the signal generator. A back-to-back phase noise measurement was performed for a 10 GHz clock signal with 6.14 dBm power. The phase noise spectrum spanned over an offset frequency range from 1 Hz to 1 MHz. At 10 kHz offset frequency the phase noise was recorded as –104.62 dBc/Hz. The signal instability of 501.99 fs phase jitter was recorded for the clock and used as a noise floor to extract the additive phase noise contributed by the components making up the optical link of the distribution system. For the MeerKAT telescope the clock tone will be distributed to antennas positioned at 8- 12 km away from the central processing building. A signal propagating through optical fibre is attenuated and distorted as a function of wavelength. In chapter 6 the effect of optical fibre length on RF clock tone stability was studied. The 10 GHz frequency reference signal was used to directly modulate a 1550 nm DFB laser transmitted over a 11 km and 22 km G.652. C fibre kept under the same environmental

conditions. At 10 kHz offset frequency the phase noise was measured as - 105.98 dBc/Hz and – 105.35 dBc/Hz for an optical clock signal transmitted over an 11 km and 22 km optical fibre, respectively. The phase noise contribution was found to increase with increasing fibre length. For a 22 km distribution link the signal was severely distorted, as shown by the presence of spurious noise. The phase noise proved useful for demonstrating the effect of fibre length on the short-term signal instability.

The reference frequency signal generated by the clock randomly fluctuates and with time starts to drift from its nominal value as demonstrated in chapter 7. A 10 GHz RF signal was observed for 24 hours recording the instantaneous frequency every 0.2 s for the non-overlapping Allan Deviation computation at different averaging time ranging from 1s to 10 hours. An Allan deviation value of 4.08×10^{-9} was recorded for the RF signal at 100 s averaging time. The log-log plot of the non-overlapping Allan Deviation as a function averaging time revealed that the clock exhibits different types of noise including white/flicker phase noise, flicker frequency noise and random-walk frequency. The RF reference clock signal displayed a relatively similar trace as the Allan deviation requirements for the MeerKAT/SKA telescope. The Allan variance proved to be a useful method for long-term signal instability analysis. The RF clock tone Allan deviation plot was used as a reference to observe how the long term stability is affected by the optical link components of the distribution system.

There are a number of optical components commercially available, each having advantages and disadvantages. For optical transmission link performance to be optimized the selection of components should be done with precision based on the requirements of application. In chapter 8 components for the distribution system were selected based on their additive phase noise contribution. A phase noise contribution of -97.61 dBc/Hz at 10 kHz frequency offset was measured for a VCSEL operated with temperature controller. The phase noise was integrated over the offset range from 1 Hz to 10 MHz to give an RMS jitter. For a VCSEL laser operated without a TEC the RMS jitter was measured to be 847.42 fs compared to 798.43 fs for a laser operated with TEC. The noise

contribution of the laser was reduced by adding a temperature controller to the light source, this compensated for the thermal induced phase/frequency fluctuation.

In chapter 9, a 23.8 km G.655 optical fibre was subjected to temperature variation prone to change the physical length of the fibre, thus leading to change in the time delay. The optical fibre was kept in an environment where the temperature was fluctuated randomly between 7 ℃ and 25 ℃. The long-term instability of an RF clock signal distribution over optical fibre was measured in the time domain and characterized in terms of Allan deviation. At room temperature the Allan deviation at 100 s averaging time was measured at 6.31E-08. For an optical fibre subjected to temperature fluctuation the Allan deviation of 7.8E-08 at 100 s averaging time was measured. The phase fluctuation due to temperature expansion of the fibre and the thermal induced changes in the refractive index resulted in an added phase noise further degrading the RF clock tone stability as compared to a distribution system where the fibre was kept at relatively stable conditions such as room temperature.

A light pulse propagating through an optical fibre is attenuated as a function of wavelength. A 10 GHz clock tone was used to directly modulate a 1550 nm DFB laser to generate an optical clock signal distributed over a 23.8 km G.655 optical fibre with 0.2 dB/km attenuation. This effect can be compensated by adding an amplifier to the transmission link. Amplifier introduces noise that degrades the RF reference signal stability. In chapter 9 the additive noise of an Erbium Doped Fibre Amplifier (EDFA) operating in the linear regime was measured and analyzed at different gains. The noise contribution of the amplifier was found to increase with gain. Phase noise is related to the power input; in theory, the additive phase noise of an amplifier could be reduced by operating it at high optical power. In this work, this was achieved by placing the amplifier closer to the transmitter as opposed to the end of the transmission link (close to the receiver) to avoid amplifying both the intended and accidental modulated signal.

In this work, a direct method was used to formulate and implement a suite of measurement tools complete for short and long-term characterization of RF clock tone

distribution system over optical fibre, similar to the MeerKAT and SKA radio telescope network. The characterization of the signal instability was done in the frequency and time domain as phase noise and non-overlapping Allan deviation, respectively. The technique proved useful for measuring and analyzing the stability of RF frequency reference clock tone and signal instability effects that different components of an optical transmission link impose on the under different environmental conditions, and operating parameters.

The techniques developed in this thesis are of crucial importance for distribution system design, power budgeting and optimizing the optical transmission link based on the additive noise contribution of components and stability requirement of different time and synchronization application.

APPENDIX I

Instantaneous Frequency Logging

In chapter 7 the RF clock tone long-term instability measurement in the time domain in terms of Allan deviation was discussed. A suite of measurement tools was established using the frequency counter built into the electrical spectrum analyzer. The direct method of the incorporated Labview code was used to log the data samples, measuring the instantaneous frequency of the clock signal of desired frequency at fixed time interval, as shown in figure A.1.1.

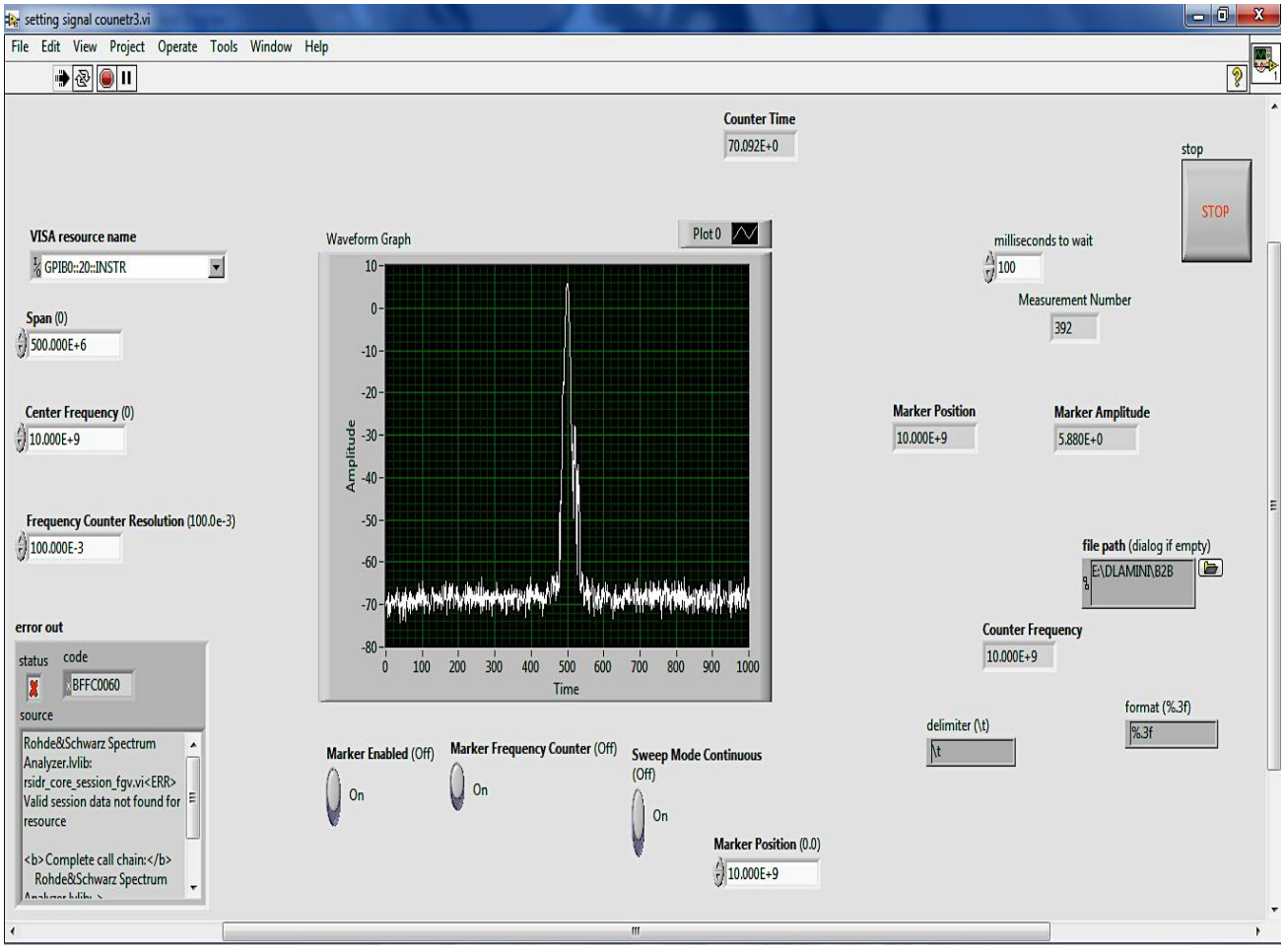

Figure A.1.1: Labview electrical spectrum analyzer signal counter

The signal counter function originating from the Rohde & Schwarz FWS signal and spectrum analyzer was used and coupled, with Labview mainly incorporated for data handling. Parameters such as span, center frequency, frequency counter resolution, sampling time interval and marker position are set on Labview to resemble those of the spectrum analyzer signal counter. The computer running the Labview code is connected to the electrical spectrum analyzer by a GPIB cable for remote control operation. Once all the relevant parameters have been set, the program may start by clicking the run button. The RF clock instantaneous frequency is then recorded at every defined sampling time interval defined as milliseconds to wait in the program, and will track the sample number and the observation time defined as counter time on the program. After reaching the desired observation period the program may be ended by clicking the stop button. The data file (labeled on file path) from labview is then used to compute the Allan deviation at different averaging times, as earlier discussed in chapter 7.

APPENDIX II

Research outputs

Dlamini P.P., Gibbon, T.G., Gamatham, R.G.G., Leitch, A.W.R. (2015), " Phase Noise Analysis for 1.7-14.5 GHz Clock Signal Transmission over 12km Telescope Network Optical Fibre", *South African Institution of Physics (SAIP) 60th annual conference proceedings 2015*
[Proceeding, poster]

Dlamini P.P., Gibbon, T.G., Gamatham, R.G.G., Leitch, A.W.R. (2015), "Phase Noise Reduction of Optical Fibre Link by Changing Operation Conditions of Amplifier" *South African Telecommunication Networks and Application Conference 2015 (SATNAC 2015)*

[Proceeding, Oral]

Dlamini P.P., Gibbon, T.G., Gamatham, R.G.G., Leitch, A.W.R. (2015), "Characterization of Clock Tone for Distribution over Optical Fibre Link", *The South African Square Kilometre Array Project Postgraduate Bursary Conference 2015*
[Proceeding, poster]

Dlamini P.P., Boiyo D., Gibbon, T.G., Gamatham, R.G.G., Leitch, A.W.R. (2016), "Laser Effect on the RF Signal Stability for Clock Signal Distribution over Optical Fibre", *South African Institution of Physics (SAIP) 61st annual conference proceedings 2016*

[Proceeding, Oral]

Dlamini P.P., Gibbon, T.G., Gamatham, R.G.G., Leitch, A.W.R. (2016), " Stability Budget of Optical Clock Signal Stability Transmitted over Single Mode Optical Fibre" *South African Telecommunication Networks and Application Conference 2016, pp. 166-170 (SATNAC 2016)*
[Proceeding, Oral]

Dlamini P.P., Gibbon, T.G., Gamatham, R.G.G., Leitch, A.W.R. (2016), "Characterization of Clock Tone for Distribution over Optical Fibre Link", *The South African Square Kilometre Array Project Postgraduate Bursary Conference 2016*

[Proceeding, Oral]

References

[1] "http://abyss.uoregon.edu/~js/ast121/lectures/lec02.html."

[2] "A short history of telescopes and astronomy: Galileo to the TMT." www.keckobservatory.org/images/files/podcast/Bolte_Hawaii09.pdf

[3] "http://www.space.com/21950-who-invented-the-telescope.html."

[4] W. Sie-Hilland and K. Mogk "RadioAstronomyTimeline." www.physics.umanitoba.ca/undergraduate/.../2070/.../RadioAstronomyTimeline.pptx

[5] "http://www.haystack.edu/edu/undergrad/materials/tut3.html."

[6] "https://www.skatelescope.org/signal-processing/."

[7] "http://www.photonics.com/EDU/Handbook.aspx?AID=42279."

[8] "https://www.boundless.com/physics/textbooks/boundless-physics-textbook/geometric-optics-24/reflection-refraction-and-dispersion-169/total-internal-reflection-and-fiber-optics-609-6258/." [Online]. Available: https://www.mendeley.com/library/.

[9] "http://www.ni.com/cms/images/devzone/tut/shmxvbep3658135761405291971.gif." [Online]. Available: https://www.mendeley.com/library/.

[10] Newport, "Fiber Optics : Fiber Basics."

[11] B. Saleh, B. Teich, "Fibre Optic." Fundamentals of Photonics,1991

[12] Z. Yasin, "Optical Fiber Communication," Technical Publications Pune, 2003.

[13] R. French and R. Abou-Rahme, "Absorption Edge and Band Gap of SiO~ 2 Fused Silica Glass," *Ceramic Transactions*, vol. 28. pp. 63–81, 1992.

[14] G. P. Pal and M. Gupta, "Signal degradation in optical fibers 1,2," vol. 1, no. 1, pp. 15–19, 2014.

[15] N. Massa, "Fiber Optic Telecommunication," *Fundam. Photonics*, pp. 293–347, 2008.

[16] A. E. Awad, "Basics of Fiber Optics," *Fiber Opt. Tech. Man.*, pp. 17–34, 2006.

[17] S. Savović, A. Djordjevich, B. Drljača, and M. S. Kovačević, "Comparison of methods for calculating coupling length in step-index optical fibers," *Acta Phys. Pol. A*, vol. 116, no. 4, pp. 652–654, 2009.

[18] "Dispersion in Optical Fibres." applied optoelectronic centre [online] available:

http://course.ee.ust.hk/elec509/notes/Lect12-photodiode%20detectors.pdf

[19] T. Torounidis, "Fiber optic parametric amplifiers in single and multi wavelength applications," *Doktorsavhandlingar vid Chalmers Tek. Hogsk.*, no. 2499, pp. 1–91, 2006.

[20] B. E. A. Saleh and M. C. Teich, *Fiber optics*, vol. 5. 1991.

[21] V. Wongpaibool, "Optical Fiber Characteristics And System," https://theses.lib.vt.edu/theses/available/etd-02042003-164941/.../02_Ch2.pdf,pp. 23–45.

[22] "Fiber_Types @ www.olson-technology.com." .

[23] Sivanantha Raja, A.Selvendran, S.Priya, R.Mahendran, C., "An optimized design for non-zero dispersion shifted fiber with reduced nonlinear effects for future optical networks," Optica Applicata vol.44 April 2015, 2014.

[24] International Telecommunication Union, "Recommendation ITU-T G.652 (11/2009)," *Networks*, p. 22, 2009.

[25] IEC, "Polarization Mode Dispersion Definition," *Engineering*.

[26] "17a5cd7d15bff637db1ba9e7bc8b4ab2342e541c @ www.tuhh.de." .

[27] L. E. Nelson and R. M. Jopson, "Introduction to polarization mode dispersion in optical systems," vol. 344, pp. 312–344, 2004.

[28] B. G. Lietaert and J. P. Manager, "Testing Polarization Mode Dispersion (PMD) in the Field Testing Polarization Mode Dispersion (PMD) in the Field," vol. 9114.

[29] C. Paper, "Fibre-to-the-telescope : MeerKAT , the South African precursor to Square Kilometre telescope Array (SKA)," no. November 2016, pp. 0–13, 2013.

[30] "http://www.timbercon.com/history-of-fiber-optics/." [Online]. Available: about:blank.

[31] "https://www.miniphysics.com/optical-fibres.html." [Online]. Available: about:blank.

[32] International Telecommunications Union, "Optical Fibres, Cables and Systems," pp. 144–147, 2009.

[33] "Chapter 13 Maxwell ' s Equations and Electromagnetic Waves," pp. 0–58.

[34] S. Errede, "Lecture notes: Electromagnetic Theory and Maxwell's Equations," p. 33, 2011.

[35] E. Hecht, "Mathematical representation of light (EM waves)," no. 1, pp. 1–9.

[36] T. Chapter, “Chapter 2 Introduction to polarization of light,” pp. 5–20.

[37] D. R. Tobergte and S. Curtis, *Polarization in Optical Fibers*, vol. 53, no. 9. 2013.

[38] “http://www.intechopen.com/source/html/47749/media/image8.png.” [Online]. Available: about:blank.

[39] T. P. Ellipse, “P457 : Wave Polarisation and Stokes Parameters,” vol. 1, no. 3, pp. 1–14, 2000.

[40] N. I. T. Calicut and I. I. T. Madras, “B.Tech.”

[41] N. Fressengeas, N. Fressengeas, P. Optics, and D. E. A. Universit, “Polarization Optics UE SPM-PHY-S07-101,” 2014.

[42] G. Interpretation and T. Stokes, “The Poincaré Sphere.,” *Changes*, no. L, pp. 2–3, 1999.

[43] " Polarized Light And The Stokes Parameters" http://astrowww.phys.uvic.ca/~tatum/physopt/physopt4.pdf

[44] “http://course.ee.ust.hk/elec509/notes/Lect12-photodiode%20detectors.pdf” .

[45] J. Kim, D. Wu, G. Marra, D. J. Richardson, and R. Slavík, “Stability Characterization of an Optical Injection Phase Locked Loop for Optical Frequency Transfer Applications,” *2014 CLEO Sci. Innov.*, vol. 1, pp. 9–10, 2014.

[46] “Contenu_05 @ www.optique-ingenieur.org.” .

[47] R. Dahlgren, “Noise in fiber optic communication links,” *Signal, 2, 2*, 2000.

[48] K. Volyanskiy, Y. K. Chembo, L. Larger, and E. Rubiola, “Contribution of laser frequency and power fluctuations to the microwave phase noise of optoelectronic oscillators,” *J. Light. Technol.*, vol. 28, no. 18, pp. 2730–2735, 2010.

[49] P. Wang, J. Xiong, T. Zhang, D. Chen, P. Xiang, J. Zheng, Y. Zhang, R. Li, L. Huang, T. Pu, and X. Chen, “Frequency tunable optoelectronic oscillator based on a directly modulated DFB semiconductor laser under optical injection,” *Opt. Express*, vol. 23, no. 16, p. 20450, 2015.

[50] Agilent, “Digital Communication Analyzer (DCA), Measure Relative Intensity Noise (RIN),” *Prod. Note 86100-7*.

[51] J. A. Taylor, F. Quinlan, A. Hati, C. Nelson, S. A. Diddams, S. Datta, and A. Joshi, “Phase noise in the photodetection of ultrashort optical pulses,” *Freq. Control Symp. {(FCS)}, 2010 IEEE Int.*, pp. 684–688, 2010.

[52] X. Pang, A. Lebedev, J. J. Vegas Olmos, I. Tafur Monroy, M. Beltrán, and R.

Llorente, “Performance evaluation for DFB and VCSEL-based 60 GHz radio-over-fiber system,” *2013 17th Int. Conf. Opt. Netw. Des. Model. ONDM 2013*, no. February 2016, pp. 252–256, 2013.

[53] S. Azaizia, K. Saleh, O. Llopis, and A. Rissons, “Evaluation of low cost solutions for the transmission through optical fiber of low phase noise OCXO signals,” *2012 IEEE Int. Freq. Control Symp. IFCS 2012, Proc.*, 2012.

[54] N. Y. Voo, P. Horak, M. Ibsen, and W. H. Loh, “Linewidth and Phase Noise Characteristics of DFB Fibre Lasers,” pp. 2–9.

[55] J. B. Jensen, R. Rodes, A. Caballero, and N. Cheng, “VCSEL Based Coherent PONs,” vol. 32, no. 8, pp. 1423–1433, 2014.

[56] P. Krehlik, “Characterization of semiconductor laser frequency chirp based on signal distortion in dispersive optical fiber,” vol. 14, no. 2, pp. 123–128, 2006.

[57] B. Onillon, B. B??nazet, and O. Llopis, “Advanced microwave optical links for LO distribution in satellite payloads,” *2006 Int. Top. Meet. Microw. Photonics, MWP*, pp. 1–4, 2006.

[58] J. Liu, “Photonic Devices” Cambridge University Press, 2005 ISBN-13 978-0-521-55195-3, Pages: 1104

[59] C. Studies, O. Links, and B. Nikolic, “Advanced Topics in Circuit Design High-Speed Electrical Interfaces Fiber optic transcievers,” pp. 4–5, 2004.

[60] W. Wang, “Optical Detectors.” University of washington [online] avilable: http://depts.washington.edu/mictech/optics/sensors/detector.pdf

[61] Thorlabs “Photodiode Saturation and Noise Floor,” pp. 1–12, 2015.

[62] J. Taylor, S. Member, S. Datta, A. Hati, C. Nelson, F. Quinlan, A. Joshi, S. Diddams, and P. Photodiodes, “Characterization of Power-to-Phase Conversion in High-Speed P-I-N Photodiodes Characterization of Power-to-Phase,” vol. 3, no. 1, 2011.

[63] J. Taylor, S. Member, F. Quinlan, and S. A. Diddams, “Noise Floor Reduction of an Er : Fiber Laser-Based Photonic Microwave Generator Noise Floor Reduction of an Er : Fiber Laser-Based Photonic,” vol. 3, no. 6, 2011.

[64] H. Tian, B. Fowler, and A. El Gamal, “Analysis of Temporal Noise in CMOS Photodiode Active Pixel Sensor,” vol. 36, no. 1, pp. 92–101, 2001.

[65] U. Avalanche, “Avalanche photodiode A User Guide.”

[66] Optical Fibres and Telecommunications; Detection and Noise, [online] available: https://www.st-andrews.ac.uk/~ctab/MSc_Oft/Lecture_Notes/lecture_10.pdf

[67] A. Boudkhil, "Analysis of Fundamental Photodetection Noises and Evaluation of PIN and APD Photodiodes Performances using an Optical High Debit Transmission Chain Simulated by Optisystem," vol. 115, no. 18, pp. 21–29, 2015.

[68] E. Rubiola, E. Salik, N. Yu, and L. Maleki, "Flicker Noise in High-Speed p-i-n Photodiodes," vol. 54, no. 2, pp. 816–820, 2006.

[69] T. Information, "Characteristics and use of Si APD (Avalanche Photodiode)."

[70] R. J. Mcintyre and J. Conradi, "Silicon Avalanche Photodiodes," 1974.

[71] N. Shafi and P. G. Gokul, "Performance Analysis of Photodetectors and Effect of Photodetection Noises in Optical," pp. 1631–1637, 2016.

[72] T. Note, "Avalanche Photodiode Receiver Performance Metrics."

[73] "MILCOM06-presentation-final (4)." .

[74] E. Rubiola, "Phase noise and frequency stability in oscillators", Cambridge University Press, Nov. 2008, ISBN 978-0-521-88677-2

[75] Y. Kaneda"Optical Amplifiers", [online] available: http://www2.engr.arizona.edu/~ece487/opamp1.pdf

[76] "edfa @ www.cables-solutions.com." .

[77] R. Boudot and E. Rubiola, "[1001.2047] Phase Noise in RF and Microwave Amplifiers," vol. 59, no. 12, p. 22, 2010.

[78] V. Auroux, A. Fernandez, O. Llopis, P. H. Merrer, and A. Vouzellaud, "Microwave phase noise properties of optical links involving small signal and gain saturated optical amplifiers," *2014 Eur. Freq. Time Forum, EFTF 2014*, pp. 381–383, 2015.

[79] M. Bury, Y. Yashchyshyn, and J. Modelski, "F Requency D Omain M Easurements for an," *Time*, no. June, pp. 4–7, 2008.

[80] B. N. Corporation, "Berkeley Nucleonics Corporation," pp. 1–7.

[81] M. Shadaram, P. Cotae, J. Summerfield, J. Bratton, and S. Antonio, "Y (f) ZMkN (f-kfo)."

[82] M. Shadaram, C. Thomas, J. Summerfield, and P. Chennu, "RF Phase Noise in WDM Fiber Optic Links," pp. 401–404, 2005.

[83] "http://www.ska.ac.za/science-engineering/meerkat/ citations into your library

using the Mendeley Web Importer | Mendeley." [Online]. Available: https://www.mendeley.com/import/.

[84] D. S. S. Tech-, "Ska sadt technical development plan," 2013.

[85] B. P. E. Dewdney, P. J. Hall, R. T. Schilizzi, and T. J. L. W. Lazio, "The Square Kilometre Array," vol. 97, no. 8, 2009.

[86] "36c975bf77614197d9bc50a04e3fcb704ac8b7be @ www.ska.ac.za." .

[87] R. Spencer, C. Shenton, and M. Bentley, "Concept Description For Synchronisation " 2011.

[88] "vlbi @ www.cpi.com." .

[89] B. Wang, C. Gao, W. L. Chen, J. Miao, Y. Bai, T. C. Li, and L. J. Wang, "Fiber-Based Time and Frequency Dissemination between THU and NIM," pp. 5–8, 2012.

[90] B. Wang, C. Gao, W. L. Chen, J. W. Zhang, Y. Y. Feng, and T. C. Li, "A 10 − 18 / day Fiber-Based RF Frequency Dissemination Chain," vol. 1, pp. 4–5, 2012.

[91] W. Riley, "W. Riley."

[92] G. Marra, S. Lea, H. Margolis, and P. Gill, "Fibre Transfer of High Stability Microwave References with Optical Frequency Combs," no. 2 m, pp. 2–3, 2008.

[93] G. Marra, S. Lea, H. Margolis, and P. Gill, "Microwave Frequency Transfer by Propagation of an Optical Frequency Comb over Optical Fibre," pp. 1–2, 2009.

[94] G. Marra, R. Slav, H. S. Margolis, S. N. Lea, P. Petropoulos, D. J. Richardson, and P. Gill, "High resolution microwave frequency transfer over a 86 km-long optical fiber network using an optical frequency comb," pp. 15–18, 2010.

[95] R. McCool "LO & Timing", square kilometre array Domain specialist in signal transport & networks- SPDO

[96] B. Shillue, S. Albanna, and L. D. Addario, "ALMA Memo # 483 The ALMA 1 st Local Oscillator Reference," no. Ml, 2004.

[97] P. Skads and J. B. Observatory, "Demonstration of a fibre-based round trip correction system for the distribution of local oscillator signals to outstations of a radio telescope," no. November, pp. 4–6, 2009.

[98] R. Mccool, M. Bentley, R. Spencer, S. Garrington, R. Davis, and B. Anderson, "Phase Transfer For Radio Astronomy Interferometers , Over Installed Fibre

Networks , Using A Round Trip Correction System .," p. 110.

[99] M. A. Lombardi, "Fundamentals of Time and Frequency," The Mechatronics Handbook 2002.

[100] Jacques Vanier and Michel TZtu, "Time Domain Measurement Of Frequency Stability," *Tenth Annu. Precise Time Time Interval Appl. Plan. Meet.*, 1978.

[101] J. Rutman and F. L. Walls, "Characterization of Frequency Stability in Precision Frequency Sources," *Proc. IEEE*, vol. 79, no. 7, pp. 952–960, 1991.

[102] A. Note, "Keysight Technologies Analyzing Frequency Stability in the Frequency and Time Domains."

[103] D. Howe, "No Title," pp. 1706–1720.

[104] F. Standards, "Jz (42)," pp. 470–475, 1991.

[105] S. R. Stein, "Frequency and Time - Their Measurement and Characterization," *Precision Frequency Control*, vol. 2. pp. 191–232, 1985.

[106] W. J. Riley and H. T. Services, "Methodologies For Time Domain Frequency Stability Measurement And Analysis."

[107] B. Lorbeer, "Phase noise measurements of the new master oscillator for TTF2," no. June, 2004.

[108] D. Support and T. Documents, "Random Noise Contribution to Timing Jitter — Theory and Practice Broadband Noise Contribution to Timing Jitter Jitter in Sinusoids," pp. 1–15, 2005.

[109] E. Rubiola, "Tutorial on the double balanced mixer arXiv : physics / 0608211v1 [physics . ins-det] 21 Aug 2006," 2008.

[110] "knowledgebase-05-time-vs-frequency @ www.erzetich-audio.com." .

[111] W. J. Riley, "Techniques for Frequency Stability Analysis," 2003.

[112] J. Alkemade, G. A. Goschloo, J. H. Sanders, C. Freed, F. L. Fork, M. A. Pollack, and N. Wax, "04 It can be written in the form," 1965.

[113] M. Clock and O. Frequency, "Clock Oscillator Stability," pp. 1–3.

[114] J. Stiles, "Oscillator Stability," pp. 1–3, 2005.

[115] S. A. Diddams, J. Ye, and L. Hollberg, " Femtosecond Lasers For Optical Clocks And Low Noise Frequency," 1990.

[116] "d9583bf07b10679232c0999088718550108c5d07 @ www.febo.com." .

[117] H. Fruehauf, “Understanding Oscillator Specs,” no. August, 2004.

[118] D. W. Allan, “National Bureau of Standards Time and Frequency Division The primary reasons for improved long-term stability in atomic clocks have been the study autonomy questions for GPS , maintaining syntonization for the of millisecond pulsar ~ l ’* ~], timing cent.”

[119] D. A. Howe and T. N. Tasset, “Theo1 : Characterization Of Very Long-Term Frequency Stability ∗.”

[120] W. Kester, “Converting Oscillator Phase Noise to Time Jitter MT-008,” pp. 1–10.

[121] C. Gao, B. Wang, X. Zhu, Y. B. Yuan, and L. J. Wang, “Dissemination stability and phase noise specification of fiber- cascaded RF frequency dissemination,” 1840.

[122] M. S. Mccorquodale, R. B. Brown, and A. O. Modeling, “On Modern and Historical Short-Term Frequency Stability Metrics for Frequency Sources,” no. 2, pp. 328–333, 2009.

[123] W. J. Riley, *Handbook of Frequency Stability Analysis*, vol. 31, no. 1. 1994.

[124] “news @ www.dataweek.co.za.” .

[125] G. Trudgen, “Phase Noise / Jitter In Crystal Oscillators,” no. July, pp. 1–4, 2009.

[126] S. Knappe, V. Shah, V. Gerginov, A. Brannon, L. Hollberg, and J. Kitching, “Long-Term Stability Of Nist Chip-Scale Atomic Clock Physics Packages,” pp. 241–250.

[127] M. Lessing “Ultra-Low-Noise Frequency Synthesis, Comparison And Dissemination Using Femtosecond Optical Frequency Combs,” University of St Andrews 2016.

[128] David W. Allan. John H. Shoaf. tand Donald Halford, " Statistics of Time and Frequency Data Analysis", Time and Frequency Division. Institute for Basic Standards. National Bureau of Standards Boulder. Colorado 80302, vol.54p, May 1971.

[129] D. Howe, "Frequency Stability", National Institute of Standards and Technology (NIST) Boulder, 1706–1720.

[130] B. T. Neu, “Clock jitter analyzed in the time domain , Part 1,” 2010.

[131] F. Ramian, “Time Domain Oscillator Stability Measurement Allan variance,”

Rohde Schwarz Appl. Note, pp. 1–16, 2012.

[132] C. A, “Characterization and measurement of time and frequency stability TN-171,” vol. 14, no. 4, pp. 521–539, 1979.

[133] Hewlett-Packard, “Phase Noise Characterization of Microwave Oscillators.” 2007.

[134] HP, “Phase Noise Measurement.”

[135] D. Owen, “Good Practice Guide to Phase Noise,” *Meas. good Pract. Guid.*, no. 68, 2004.

[136] A. Note, “Characterizing Phase Locked Loops Using Tektronix Real-Time Spectrum Analyzers.”

[137] U. L. Rohde, A. K. Poddar, and S. M. Corp, “Phase Noise Measurements and System Comparisons,” *Microw. J.*, no. April, pp. 1–13, 2013.

[138] K. Gheen, “Phase Noise Measurement Methods and Techniques,” pp. 1–48, 2012.

[139] K. Kundert, “Predicting the phase noise and jitter of PLL-based frequency synthesizers,” *Des. Guid.*, pp. 1–24, 2003.

[140] “Reviewing Phase Noise Measurement Methods | Military Defense Electronics content from Defense Electronics Magazine.” [Online]. Available: http://defenseelectronicsmag.com/military-defense-electronics/reviewing-phase-noise-measurement-methods.

[141] O. Rajala, “Oscillator Phase Noise Measurements using the Phase Lock Method,” p. 57, 2010.

[142] “Optimum PLL settings for Phase Noise Measurements with the R&S ® FSUP.pdf.”

[143] H. Gheidi and A. Banai, “Phase-noise measurement of microwave oscillators using phase-shifterless delay-line discriminator,” *IEEE Trans. Microw. Theory Tech.*, vol. 58, no. 2, pp. 468–477, 2010.

[144] P. Lemut, B. Batagelj, M. Leskovec, J. Tratnik, and S. Zorzut, “Evaluation Of Short And Long-Term Stability Of The 2998 Mhz Reference-Clock Transfer System,” no. 1, pp. 2–4.

[145] J. H. S. David W . Allan and D. Halford, “Statistics of Time and Frequency Data Analysis,” , vol. 54p, no. May 1971, p. N-N, 1973.

[146] A. Devices and R. B. Park, “A Comparison Of Two Delay Line Discriminator

Implementations For Low Cost Phase Noise 1 . Introduction and Background 2 . Phase Noise Measurement," pp. 1–11.

[147] "Phase Nosie Characterization of Microwave Oscillator.Pdf." .

[148] Johannes Jacobus Grobbelaar, "Phase Noise Measurement Techniques," Stellenbosch University, 2011.

[149] S. T. Dawkins, J. J. McFerran, and A. N. Luiten, "Considerations on the measurement of the stability of oscillators with frequency counters," *Proc. IEEE Int. Freq. Control Symp. Expo.*, vol. 54, no. 5, pp. 759–764, 2007.

[150] S. Johansson, "New frequency counting principle improves resolution," *Proc. IEEE Int. Freq. Control Symp. Expo.*, vol. 2005, pp. 628–635, 2005.

[151] Rohde & Schwarz, "Phase Noise Measurement Techniques," *Rohde Schwarz Webinar*, no. March, p. 43, 2015.

[152] "Phase Noise Basic." [Online]. Available: http://hpmemoryproject.org/technics/bench/3048/basic_01.htm.

[153] S. Instructions, O. E. Dut, S. Rf, and V. Mode, "Phase Noise Meas . and the 89441a," vol. 1.

[154] "R & S ® FSW Signal and Spectrum Analyzer Setting standards in RF performance and usability R & S ® FSW Signal and Spectrum Analyzer At a glance."

[155] W. Drive, "R & S ® SMB100A Signal Generator Setting standards in the mid-range," vol. 44, no. 0.

[156] S. Manual, "FS725 Rubidium Frequency Standard Operation and Service Manual," vol. 3, no. 408, 2015.

[157] O. Manual and L. D. Controller, "LDC2xx," 2004.

[158] G. Grosche, O. Terra, K. Predehl, R. Holzwarth, B. Lipphardt, F. Vogt, and U. Sterr, "Relative Accuracy," pp. 1–12.

[159] T. Temperature, "Controller TED200C Operation Manual," 2016.

[160] S. Temperature and R. Temperature, "1550 nm Vertical-Cavity Surface-Emitting Laser," pp. 1550–1551.

[161] "NLK5C5EBKA," no. 1112, p. 2005, 2005.

[162] "DSCR603 @ www.discoverysemi.com." .

[163] L. a Johnson, “Controlling temperatures of diode lasers and detectors thermoelectrically,” *Las. & Optron.*, vol. april, 109, p. N-N, 1988.

[164] N. Yulianto, B. Widiyatmoko, and P. S. Priambodo, “Temperature Effect towards DFB Laser Wavelength on Microwave Generation Based on Two Optical Wave Mixing,” vol. 5, no. 2, pp. 21–27, 2015.

[165] “Chapter 3: Category of Laser Diode | Laser Diode Selection.” [Online]. Available: http://ldselection.com/tutorial/category-of-laser-diode/chapter3-category-of-laser-diode/.

[166] “Introduction & Benefits | Vertilas.” [Online]. Available: http://www.vertilas.com/content/introduction-benefits.

[167] and G. X. S. C. Du1, J. Yuan1, “Comparison of FP , VCSEL and DFB laser diode in optical transmission for MR RF coil array Introduction : Methods :,” vol. 411, no. 2005, p. 7170, 2007.

[168] C. Law, “Semiconductor Laser Device-Level Characteristics,” California Polytechnic State University, May 2011.

[169] A. Technology and D. Group, “Getting the best out of photodiode detectors,” *Cancer*, pp. 1–6, 2005.

[170] X.Fernando, “Optical Receivers Theory and Operation.” Ryerson Communications Lab.

[171] Hamamatsu, “Photodiode Technical Information,” pp. 1–18, 2007.

[172] O. Kharraz and D. Forsyth, “Performance comparisons between PIN and APD photodetectors for use in optical communication systems,” *Optik (Stuttg).*, vol. 124, no. 13, pp. 1493–1498, 2013.

[173] “MeerKAT – SKA SA.” [Online]. Available: https://www.ska.ac.za/science-engineering/meerkat/.

[174] J. Tratnik, P. Lemut, U. Dragonja, B. Batagelj, and M. Vidmar, “Distribution of RF-clock signal over single optical fiber with temperature-drift and vibration compensation,” *2013 IEEE Int. Top. Meet. Microw. Photonics, MWP 2013*, pp. 162–165, 2013.

[175] J. Ye, J.-L. Peng, R. J. Jones, K. W. Holman, J. L. Hall, D. J. Jones, S. a. Diddams, J. Kitching, S. Bize, J. C. Bergquist, L. W. Hollberg, L. Robertsson, and L.-S. Ma,

"Delivery of high-stability optical and microwave frequency standards over an optical fiber network," *J. Opt. Soc. Am. B*, vol. 20, no. 7, p. 1459, 2003.

[176] A. Czubla, "Stabilization Of The Propagation Delay In Fiber Optics In A Frequency Distribution Link Using Electronic Delay," 42nd Annual Precise Time and Time Interval (PTTI) Meeting, pp. 389–396.

[177] Ł. Śliwczyński, P. Krehlik, and M. Lipiński, "Optical fibers in time and frequency transfer," *Meas. Sci. Technol.*, vol. 21, no. 7, p. 75302, 2010.

[178] S. Preutz, "Master Thesis Department of Atomic Physics Lund University - faculty of engineering , LTH Ultra-stable frequency transfer using optical fibers - Report - ," 2016.

[179] T. J. Pinkert, O. Boll, L. Willmann, G. S. M. Jansen, E. A. Dijck, B. Groeneveld, R. Smets, F. C. Bosveld, W. Ubachs, K. Jungmann, K. S. E. Eikema, and J. C. J. Koelemeij, "Effect of soil temperature on optical frequency transfer through unidirectional dense-wavelength-division-multiplexing fiber-optic links," *Appl. Opt.*, vol. 54, no. 4, pp. 728–738, 2015.

[180] Pasquinelli, Ralph J., "Rf Systems," Fermilab, 2008.

[181] a. Hajimiri and T. H. Lee, "A general theory of phase noise in electrical oscillators," *IEEE J. Solid-State Circuits*, vol. 33, no. 2, pp. 179–194, 1998.